USAAVLABS TECHNICAL REPORT 66-4

HELICOPTER ROTOR NOISE GENERATION AND PROPAGATION

By

Robert Schlegel

Robert King

Harold Mull

October 1966

U. S. ARMY AVIATION MATERIEL LABORATORIES
FORT EUSTIS, VIRGINIA

CONTRACT DA 44-177-AMC-141(T)
SIKORSKY AIRCRAFT
DIVISION OF UNITED AIRCRAFT CORPORATION
STRATFORD, CONNECTICUT

Distribution of this document is unlimited

U. S. ARMY MATERIEL COMMAND

Disclaimers

Disposition Instructions

DEPARTMENT OF THE ARMY
U. S. ARMY AVIATION MATERIEL LABORATORIES
FORT EUSTIS, VIRGINIA 23604

This report has been reviewed by the U. S. Army Aviation Materiel Laboratories and is considered to be technically sound. This report is disseminated for the exchange of information and the stimulation of ideas.

Task 1P121401A14801

Contract DA 44-177-AMC-141 (T)
USAAVLABS Technical Report 66-4
October 1966

HELICOPTER ROTOR NOISE GENERATION AND PROPAGATION

by

RONALD SCHLEGEL
ROBERT KING
HAROLD MULL

Prepared by

Sikorsky Aircraft
Division of United Aircraft Corporation
Stratford, Connecticut

for

U. S. ARMY AVIATION MATERIEL LABORATORIES
FORT EUSTIS, VIRGINIA

Distribution of this document is unlimited

SUMMARY

An improved method is presented for calculating rotor system overall vortex noise and frequency spectra for stalled and unstalled rotors. Correlation of measured and predicted vortex noise was evaluated using two rotor systems operating over a wide range of speeds and thrusts. Correlation was found to be excellent. Blade tip planform studies revealed significant vortex noise reductions with tapered tips.

A new procedure is also derived for calculating near and far field rotor rotational noise with nonuniform inflow. The method extends the standard steady load method by including the effects of harmonic airloads. Correlation studies were conducted using an H-34 helicopter. Agreement between low frequency measured and predicted noise was good. However, correlation with high harmonic rotational noise was poor. This is probably due to inadequate definition of high harmonic airloads.

Presented results establish the importance of high harmonic rotational noise for detectability and loudness, and further work is recommended to more accurately define high harmonic blade loading. Since an airload measurement program is being conducted on the NH-3A, it is recommended that a correlation program be conducted to more fully evaluate the accuracy of the presented noise analysis program using the NH-3A airload results.

This study was performed for single rotor systems only, and in its present form is not directly applicable to systems with multiple rotors in juxtaposition.

FOREWORD

The program was conducted by Sikorsky Aircraft Division of United Aircraft Corporation under Contract DA 44-177-AMC-141 (T). USAAVLABS Project Engineer was Mr. J. McGarvey. The task was begun on 28 May 1964 and completed on 31 August 1965.

Acknowledgement is hereby made of the flight test data supplied by NASA Langley Research Center which supplement that published in NASA TM X-952. Personnel associated with the program were: Messrs. Kenneth C. Mard, Ronald G. Schlegel, Robert J. King, David C. Carmichael, Edward R. Wood, A. Charles Buffalano and Victor Berecz of Sikorsky Aircraft and Mr. H. R. Mull of H. R. Mull and Associates.

CONTENTS

CONTENTS (Con't)

ILLUSTRATIONS

ILLUSTRATIONS (Con't)

ILLUSTRATIONS (Con't)

ILLUSTRATIONS (Con't)

TABLES

TABLES | PAGE

LIST OF SYMBOLS

A_B	blade area, square feet
a	blade chord, feet
b	blade thickness, feet
C_α	form drag coefficient
C_L	coefficient of lift
c	speed of sound, feet per second
d	diameter, feet
db	decibel
$\vec{F}$	force vector, pounds
$\vec{f'}$	arbitrary force per unit volume
f	frequency, cycles per second
g	Fourier coefficient
h	altitude, positive above rotor, feet
h'	projected blade thickness, feet
L	blade section loading, pounds per inch
M	Mach number
M_T	tip Mach number
m	order of harmonic
n	number of blades
P	pressure, pounds per square inch
p	sound pressure, pounds per square inch
p_m	sound pressure for mth harmonic, pounds per square inch

LIST OF SYMBOLS (Con't)

Q	torque, pound-feet
R	distance from center of rotor head to field point, feet
r	distance from center of rotor head to source point in rotor disk, feet
r_T	tip radius, feet
r_o	distance from center of rotor head to the point on the rotor blade where twist begins, feet
S	distance from source point on rotor disk to field point, feet
SPL	sound pressure level, decibels
S_t	constant of value 0.28, Strouhal Number
T	thrust, pounds
t	time, seconds
Δt	time increment, seconds
u	phase angle, radians
V	velocity, feet per second
V_T	velocity at tip, feet per second
W_α	acoustic power, watts per square centimeter
x, y, z	Cartesian coordinates (fixed system)
x_1, y_1, z_1	Cartesian coordinates in rotor system
α	angle of attack, degrees
α_T	angle of attack of tip, degrees
β	blade pitch angle, radians
β_o	blade steady pitch angle at rotor head corresponding to collective pitch, radians

LIST OF SYMBOLS (Con't)

β_1	cosine component of cyclic pitch (ref: ψ = 0), radians
$\overline{\beta_1}$	sine component of cyclic pitch (ref: ψ = 0), radians
γ	blade twist rate, radians per inch
θ	field point azimuth angle, degrees
ζ	blade chord location, feet
σ	angle between rotor plane and field point - positive upward, degrees
ψ	azimuth angle in rotor plane, degrees
Ω	rotor rotational speed, radians per second

PHASE I

MAIN ROTOR VORTEX NOISE DURING UNIFORM INFLOW

INTRODUCTION

The task of Phase I was to develop an improved procedure for predicting single rotor helicopter main rotor vortex noise under conditions of uniform inflow. This task was accomplished by a review of vortex noise theory, development of a formula and a program of rotor stand measurements. Although the proposed work covered only the testing of one main rotor system under three conditions each of disk loading and rotor tip speed, the availability of another rotor system provided an opportunity to check analytical accuracy.

Previous studies of vortex noise generation by helicopter rotor systems have been limited to prediction of the overall levels for systems operating out of stall. Very little has been reported on prediction of the frequency spectrum for conditions either in or below stall. However, the importance of the spectral distribution of the noise in assessing the effects of rotor design on such psycho-acoustic factors as detectability and hearing damage requires the estimation of the spectrum shape. Consequently, the individual spectra were studied in detail.

This report presents the results of this study including an improved method of calculation of the noise levels and normalized spectra for operation in and out of stall. Sample spectra are given for both conditions. The improved method consists of corrections to Harvey Hubbard's formula (Reference 16) to account for changes in lift coefficient. The lift coefficient is now a variable, and the actual blade area is used rather than a calculated effective blade area. The coefficients to be used in this formula have been established empirically from CH-3C and CH-53A rotor test stand data.

VORTEX NOISE GENERATION

The subject of sound generation by fluid flow has been studied intensively by a number of investigators. Recent advances in the understanding of how sound is generated and propagated by unsteady aerodynamic phenomena such as vortices have permitted rigorous mathematical treatment. Reference 26 contains a complete physical and mathematical description of the phenomena of vortex sound.

Briefly, vortex sound is generated by the fluid force on an object arising from the formation and shedding of vortices in the flow past it. This results in a dipole form of radiation in which the strength of the source is proportional to the sixth power of the free-stream velocity.

For a rod or bluff body operating at low Reynolds numbers, the vortices are shed alternately from each side of the rod in regular vortex shedding. The shedding of vortices causes fluctuating lift and drag. The sound associated with the fluctuating drag is much weaker and is double the frequency of that associated with lift.

In the usual range of Reynolds numbers (approximately 5 x 10^6) associated with a rotating wing, the sound frequency is given by

$$f = S_t \frac{V}{d} \tag{1}$$

where V is the free-stream velocity and d is the thickness of the rod or bluff body. The Strouhal number, S_t, has been experimentally determined to have a value of 0.28 (Reference 28). Since there is a different velocity associated with each station over the span, there is a broad band of frequencies. However, the intensity of sound is proportional to the sixth power of the velocity V, so that the frequencies of interest are associated with the area near the tip where the velocity is highest. Table I shows the calculated frequencies and their relative intensity for the CH-53A rotor blade. From Table I, it can be seen that the most intense sound appears in the octave from 300 to 600 cps. For the purposes of this report, all of the sound from 150 to 9600 cps was considered to be vortex sound.

Although vortex sound is the principal source of medium and high frequency noise, boundary layer turbulence and noise from blade irregularities can contribute to the overall noise. Turbulence on the blade is another source of frequency broadening. The turbulence causes an irregular rate of shedding. If the blade is operating in a region beyond the onset of tip stall, there is a sharp rise in the 1200-to 2400-cps octave band associated with the flow separation in the region near the tip. This flow separation can be associated with blade slap as shown in Phase III.

CALCULATION OF VORTEX NOISE

Overall Level

A theory of vortex sound was first presented by E. Y. Yudin (Reference 33). Yudin's theory for the radiation of vortex sound from rotating rods was based on a dimensional analysis of the flow parameters around the rods. In developing his theory, Yudin assumed that a rigid body in a moving fluid has forces impressed upon it due to the shedding of vortices. The sound radiation is the same in this case as that from equal but opposite forces acting directly on an otherwise still fluid.

Curle (Reference 4), in his analysis of the influence of solid boundaries on aerodynamic sound, showed that Yudin's result could be obtained formally from Lighthill's theory (Reference 19) in which the total fluid stress is associated with the local dipole strength. Curle has thus shown that Yudin's relationship was correct. Yudin's result can be written as follows:

$$W_{\alpha} = \text{const.} \frac{\rho}{c^3} (C_{\alpha}^2 S_t)^2 V_T^6 \, r h' \tag{2}$$

In using equation 2 to calculate vortex noise from rotating wings, some of the terms can be considered to be constant because their range of permissible values is too small to affect the results appreciably. These are ρ, c, C_{α} and S_t. Although C_{α}, the form drag coefficient, appears in the equation to the fourth power, the range in lift between an unloaded aircraft and a fully loaded aircraft is small enough to accept an average value for C_{α} for approximate calculations. Lumping the constant terms then gives the following:

$$W_{\alpha} = \text{const.} V_T^6 \, r h' \tag{3}$$

The two helicopter rotor systems tested had untapered 0012 airfoils. Therefore, a constant proportion exists between the chord and the thickness h'. Thus, the sound power is proportional to the chord length times the blade length r, or blade area. Furthermore, since the noise from each blade is additive, the total sound power will be proportional to the blade area of the rotor system. This simplifies the equation to the following:

$$W_{\alpha} = \text{const.} A_B V_T^6 \tag{4}$$

Equation 4 can now be compared directly to Hubbard's formula (Reference 16) which was used to calculate the sound pressure level of the vortex noise from propellers, which is as follows:

$$SPL = 10 \log \left\{ \frac{K A_B (V_{0.7})^6}{10^{-16}} \right\} \tag{5}$$

Hubbard's measurements were made at a distance of 300 feet and an angle of 105° from the axis of rotation. The constant K in equation 5 was determined empirically for the measurement position. The terms

10 log and 10^{-16} give the sound pressure level in decibels.

Hubbard's formula is based on $C_L = 0.4$. He adjusts the formula for other values of C_L by using an effective blade area, A_B. Intensive analysis of experimental rotor test data indicated that greater accuracy could be attained by using the actual blade area and coefficient of lift. The test data yielded a value of 6.1×10^{-27} for the constant K of equation 5 for use in a modified equation. Variations in lift for the modified equation are accounted for by addition of the term 20 log $C_L/0.4$ where the 0.4 is the coefficient of lift used by Hubbard in equation 5. The resulting equation is as follows:

$$SPL = 10 \log \frac{6.1 \times 10^{-27} A_B (V_{0.7})^6}{10^{-16}} + 20 \log \frac{C_L}{0.4} \qquad (6a)$$

This equation may be rewritten in a more convenient form for sea level 70°F conditions as follows:

$$SPL = 10\{2 \log V_{0.7} + 2 \log T - \log A_B - 3.57\} \qquad (6b)$$

Overall vortex noise levels were calculated for the CH-3C and CH-53A rotor systems by means of equations 5 and 6. The results of these calculations are shown in Table II. All numbers have been rounded off to the nearest db. As can be seen in Table II, the calculated levels agree with the measured levels within 2 db. Also, it can be seen that equation 5 is sufficiently accurate for all but the most stringent requirements.

Since equations 5 and 6 are for a distance of 300 feet from the center of rotation, the calculated values in Table II have been increased by 2.6 db to correct for the distance of 225 feet to the point of measurement. The usual distance corrections (20 log $300/R$) can be made for distances other than 300 feet. *

Spectrum Shape

The spectrum shape of a blade operating out of stall is shown in Figure 19. This condition is present at low angles of attack at the tip. The peak frequency is determined by the Strouhal number which is defined as follows:

$$S_t = \frac{f h'}{V_{0.7}} \qquad (7)$$

In the usual range of Reynolds numbers for a helicopter rotor, the Strouhal number is 0.28. In keeping with Yudin's "round rod" approach,

* A sample calculation is shown in Appendix I.

the projected blade thickness h' is defined by the following equation:

$$h' = b\cos\alpha + a\sin\alpha \tag{8}$$

where b is the blade thickness, a the chord length and α the angle of attack.

Tip Stall

When unsteady aerodynamic forces appear near the tip of a blade due to the occurrence of either stall or drag divergence, there is a definite change in the shape of the vortex noise level frequency spectrum. A portion of the rotor test data acquired was taken while portions of the blades were experiencing drag divergence (and probably stall as well), and the general spectrum obtained is shown in Figure 20. Compare this spectrum with that of Figure 19 where no separated flow is present and it is evident that the separated flow has caused a rise in the levels of the octaves above the peak octave. Using these curves (Figures 19 and 20), one may determine whether stall or drag divergence is present in a measured vortex noise spectrum. For prediction purposes, the proper spectrum may be selected on the basis of aerodynamic stall and drag-divergence criteria.

The exact point where tip stall begins is difficult to determine accurately. At that point, however, there is a deterioration of the lift/drag ratio. Figure 21 is a drag-divergence curve for the CH-3C blade. The experimental data points plotted indicated that some of the Mach number-angle of attack combinations are in the region of drag divergence.

In Figure 22 the difference between the 300 to 600 octave levels and the 1200 to 2400 octave levels is plotted against the blade tip pitch for the same data points of Figure 21. The rise of the 1200-to 2400-cps octave relative to the 300 to 600 octave corresponds with the data points that lie above the drag-divergence curves. The rise appears less abrupt for the high Mach numbers.

EXPERIMENTAL TEST PROGRAM

General

The object of the test program was to measure the vortex noise radiated by the rotor system over a range of speeds and loads. Two rotor systems were measured at three different speeds each and at several different thrusts at each speed. Test instrumentation is described in Appendix II.

Description of Rotor Systems

Both of the two systems tested used untapered 0012 airfoils and had square tips. The CH-3C system had five rotor blades and a diameter of 62 feet. The CH-53A system had six blades and a diameter of 72 feet. Although the program originally called for tests of only one rotor system, the opportunity to check the results with another quite different arrangement was valuable. The physical characteristics of each system are shown in Table III.

Acoustical Measurements

The rotors were tested on a whirl stand approximately 70 feet above the ground. Figure 1 shows the test arrangement. The ground plane around the test stand was covered with heavily matted dry grass except for a roadway. The microphone was mounted on a wire fence 225 feet to the east of the stand and about six feet above the ground.

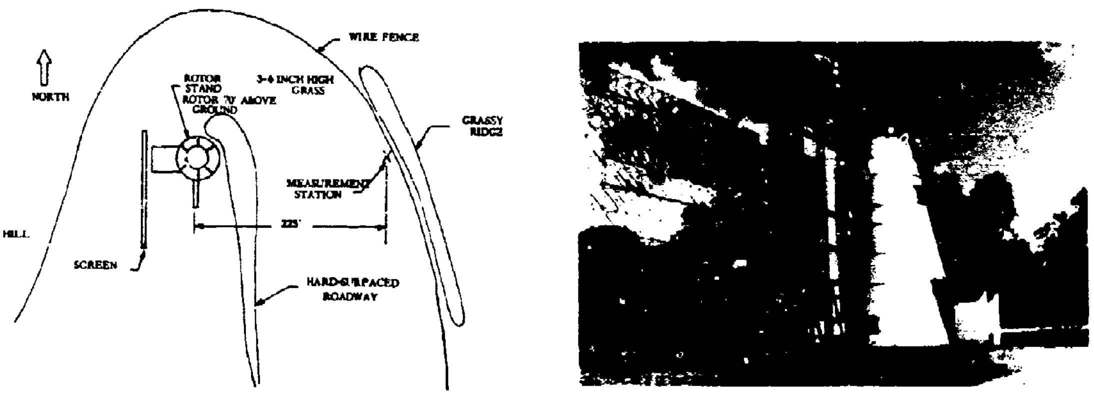

Figure 1. Vortex Noise Test Arrangement and Rotor Test Stand

There was a grassy ridge beyond the fence and a wooded hill to the west of the stand. All measurements were made at the same microphone position. It is assumed that the measurements were the direct field from the test rotor because (1) the portion of the spectrum of interest was above 150 cps, (2) the test rotor was 70 feet above the ground, and (3) the ground was covered with an absorbent grass cover.

Since the sound fields are strongly affected by winds, measurements were made when the ambient wind was below 5 knots. Thus the measured data should closely approximate free field conditions unaffected by non-uniform inflow.

PHASE II

HELICOPTER ROTATIONAL NOISE UNDER CONDITIONS OF NONUNIFORM INFLOW

INTRODUCTION

Rotational noise, which is comprised of discrete frequencies at multiples of the blade passage frequency, as opposed to vortex noise, which is broad-band random noise centered about the Strouhal frequency, was first defined by Gutin (Reference 11) in 1948. Since the establishment by Gutin's theory, there have been a number of outstanding studies (References 1, 7, 14, 17, 30, 34) involving propeller rotational noise generation and propagation. These studies have extended the rotational noise theory developed by Gutin to account for noise in the near field, thickness noise, and noise field distortion due to source translational motion. It is desirable to make use of the techniques developed through these studies to obtain increased accuracy where Gutin's model is found to be inadequate.

The study undertaken here has followed along the lines of those mentioned above in that it seeks to extend Gutin's basic theory for noise generated by a particular type of propeller, in this case the helicopter rotor. Gutin's theory is still commonly used for propeller noise prediction but is subject to the following limitations:

1. Uniform axial inflow is maintained throughout the propeller disk.
2. Field points, at least 5 diameters from the hub, are calculated (far field).
3. Only first harmonic noise is calculated.
4. Propeller speed normal to the axis is held below approximately Mach 0.3.

In the case of the helicopters, the inadequacy of Gutin's theory is obvious; diameters are large and inflow is nonuniform because of predominantly nonaxial translational motion. Most rotor noise field points of interest fall within the "near field", and generally the first rotational noise harmonic falls below the audible frequency range, making it less important than its harmonics.

In general, the intensity of these harmonics cannot be predicted accurately. This report represents a newly developed mathematical theory which removed the limitations of Gutin's theory as applied to the rotational noise of single rotor helicopters.

The prediction method utilizes blade section loading, both steady and varying at integral multiples of the main rotor rotational speed, as a function of radius and azimuth. The solution describes as many harmonics of rotational noise as the input data allows in both the near and far field. The periodically varying blade loading comprises the variable inflow condition. This solution has been programmed by Sikorsky Aircraft as an IBM-7094 procedure.

DERIVATION OF VARIABLE INFLOW ROTATIONAL NOISE SOLUTION

The rotor system noise source will be represented by a surface of stationary dipole radiators which simulate the normal pressure distribution in the rotor disk. Shear forces as well as thickness effects are ignored. It can be shown (References 7 and 18) that for sound sources in rectilinear motion, the acoustic pressure in the sound field can be exactly represented by the sum of pressure from stationary sound sources placed in the path of the moving source which radiate only when the moving source passes by. In this case the stationary sound sources are the dipoles in the rotor disk which radiate only when a blade (corresponding to the moving source) passes by.

Solution of Wave Equation

For the range of rotational Mach numbers and sound frequencies considered here, the pressure field due to a rotating force is the sum of pressure fields from stationary dipoles, and the radiation from the stationary dipoles satisfies the nonhomogeneous wave equation

$$\nabla^2 p - \frac{1}{c^2}\left\{\frac{\partial^2 p}{\partial t^2}\right\} = \nabla \cdot \vec{f} \qquad (9)$$

where $\vec{f}$ is an arbitrary force per unit volume.

Since this wave equation is for radiation from a stationary force into a stationary medium, it is exact for only hover conditions. However, as long as the vehicle translational Mach number is below 0.3, the accuracy of the wave equation is considered adequate, as shown in Reference 23.

Figures 2 and 3 show the geometry of the rotor system used in the analysis and the sound field coordinate system. The force vectors $\vec{F}(r,\psi,t)$ are restricted to the region covered by the rotor disk, and the field point is outside of a sphere having the diameter of the rotor disk and centered at the rotor hub.

The solution to equation 9 for concentrated forces is given by

$$p(x,y,z,t) = -\frac{1}{4\pi}\, \text{div} \left[\frac{\vec{F}(S,\theta,\sigma,t-\frac{S}{c})}{S} \right] \tag{10}$$

where

$$S = \sqrt{(x-x_1)^2 + (y-y_1)^2 + (z-z_1)^2}$$

is the distance from the elemental source point to the field point.

Since the forces of interest here are harmonic at integral multiples of the rotor blade passage, the force vector may be represented by a Fourier series:

$$\vec{F}(r,\psi,t) = \sum_{m=1}^{\infty} \vec{g}_m(r,\psi)\, e^{imn\Omega t} \tag{11}$$

where the steady component is neglected because it is not an acoustic signal. The component of the vector $\vec{F}$ in the x direction is

$$F_x(r,\psi,t) = \sum_{m=1}^{\infty} g_{mx}(r,\psi)\, e^{imn\Omega t}$$

where $g_{mx}(r,\psi)$ is the component of $\vec{g}_m(r,\psi)$ in the x direction. Similar components exist in the y and z directions.

Using these expressions in equation 10 yields

$$p(x,y,z,t) = -\frac{1}{4\pi}\left\{ \frac{\partial}{\partial x}\frac{1}{S}\sum_{m=1}^{\infty} g_{mx}\, e^{i(mn\Omega t - mn\Omega\frac{S}{c})} + \right.$$

$$\frac{\partial}{\partial y}\frac{1}{S}\sum_{m=1}^{\infty} g_{my}\, e^{i(mn\Omega t - mn\Omega\frac{S}{c})} +$$

$$\left. \frac{\partial}{\partial z}\frac{1}{S}\sum_{m=1}^{\infty} g_{mz}\, e^{i(mn\Omega t - mn\Omega\frac{S}{c})} \right\} \tag{12}$$

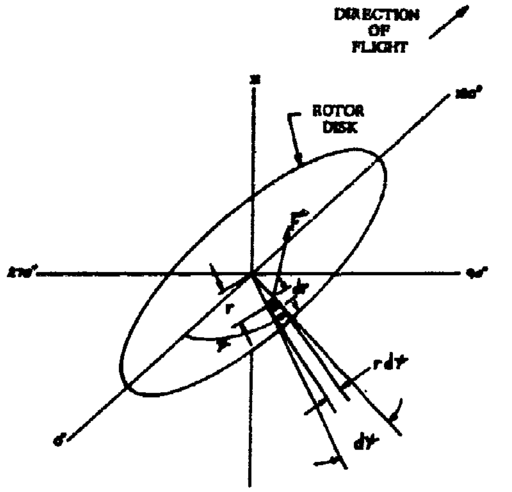

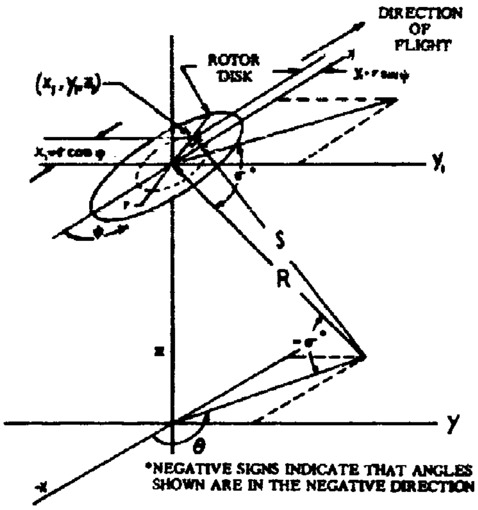

Figure 2. Rotor System Geometry   Figure 3. Field Point Location

which reduces to

$$p(x,y,z,t) = -\frac{1}{4\pi} \sum_{m=1}^{\infty} e^{imn\Omega t} \left\{ g_{mx}\left(\frac{\partial S}{\partial x}\right) + g_{my}\left(\frac{\partial S}{\partial y}\right) + g_{mz}\left(\frac{\partial S}{\partial z}\right) \right\} \frac{\partial}{\partial S} \left(\frac{e^{-imn\Omega \frac{S}{c}}}{S} \right) \tag{13}$$

This expression describes the sound pressure $p(x,y,z,t)$ at the field point x, y, z at time t due to the force components g_{mx}, g_{my}, g_{mz} acting at the point r, ψ in the rotor disk. Now the components of equation 13 are defined.

As previously defined

$$S = \sqrt{(x-x_1)^2 + (y-y_1)^2 + (z-z_1)^2}$$

which in spherical coordinates (Figure 3) is

$$S = \sqrt{(-R\cos\sigma\cos\theta + r\cos\psi)^2 + (R\cos\sigma\sin\theta - r\sin\psi)^2 + (R\sin\sigma)^2}$$

which reduces to

$$S=\sqrt{R^2+r^2-2rR\cos\sigma\cos(\theta-\psi)} \tag{14}$$

This is an exact representation and holds for both near and far field. From Appendix III

$$\frac{\partial S}{\partial x} \approx \frac{-R}{S}\cos\sigma\cos\theta$$

$$\frac{\partial S}{\partial y} \approx \frac{R}{S}\cos\sigma\sin\theta$$

$$\frac{\partial S}{\partial z} \approx \frac{R}{S}\sin\sigma \tag{15}$$

Equation 15 is valid outside of one rotor diameter from the hub.

The differential

$$\frac{\partial}{\partial S}\left\{\frac{e^{-imn\Omega\frac{S}{c}}}{S}\right\}$$

becomes

$$-\left\{\frac{1}{S}+\frac{imn\Omega}{c}\right\}\frac{e^{-imn\Omega\frac{S}{c}}}{S} \tag{16}$$

Placing equations 15 and 16 into equation 13 yields for the harmonic m

$$p_m(x,y,z,t)=\frac{R}{4\pi S^2}\,e^{imn\Omega(t-\frac{S}{c})}\left\{-g_{mx}\cos\sigma\cos\theta+\right.$$

$$\left.g_{my}\cos\sigma\sin\theta+g_{mz}\sin\sigma\right\}\left\{\frac{imn\Omega}{c}+\frac{1}{S}\right\} \tag{17}$$

Now the forces g_{mx}, g_{my}, g_{mz} acting on the rotor blade remain to be determined.

<u>Blade Aerodynamic Loads</u>

Blade pressures for this study were obtained from flight test measurements taken on a Sikorsky S-58 (Army CH-34) at NASA, Langley Field, Virginia (Reference 29). This data consists of differential pressure measurements made on one main rotor blade during various flight conditions. Data was recorded at several chordal stations and integrated over the chord at 15-degree azimuth intervals, yielding section loadings at these points. This was done at several blade spanwise stations. At each station, a harmonic analysis was performed on the section loading-azimuth position curve resulting in a steady plus 10 harmonics of the loading. This harmonic blade loading data is utilized for the present study.

Transformation of Rotating Concentrated Forces to Stationary Forces

Consider a rotating blade with a normal differential pressure distribution given by $\Delta P(r,\zeta,t)$ and located as shown in Figure 4.

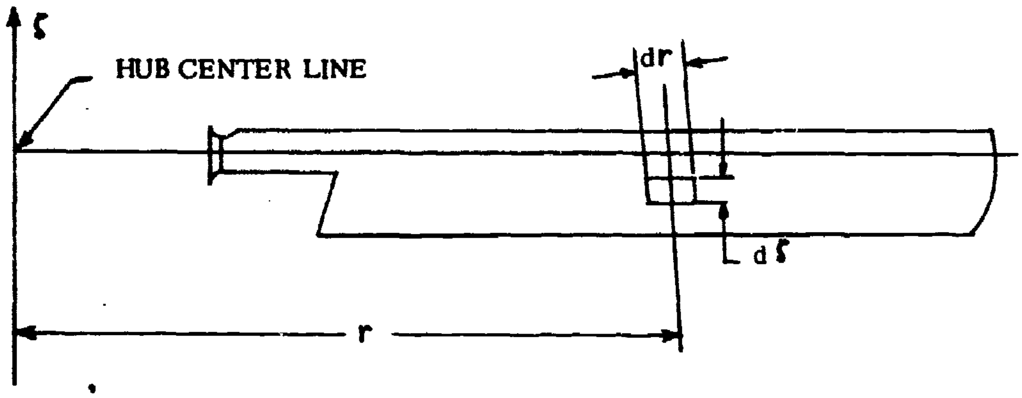

Figure 4. Blade Normal Differential Pressure Location

The force acting on a small blade area is $\Delta P d\zeta dr$ and is considered to be concentrated force when $d\zeta dr$ is very small. This same force will be considered to be acting on a differential area at the rotor disk $r dr d\psi$ when the blade area is covering the rotor disk area (Figure 2). The time history of pressure as two blades pass over the area $r dr d\psi$ is shown in Figure 5.

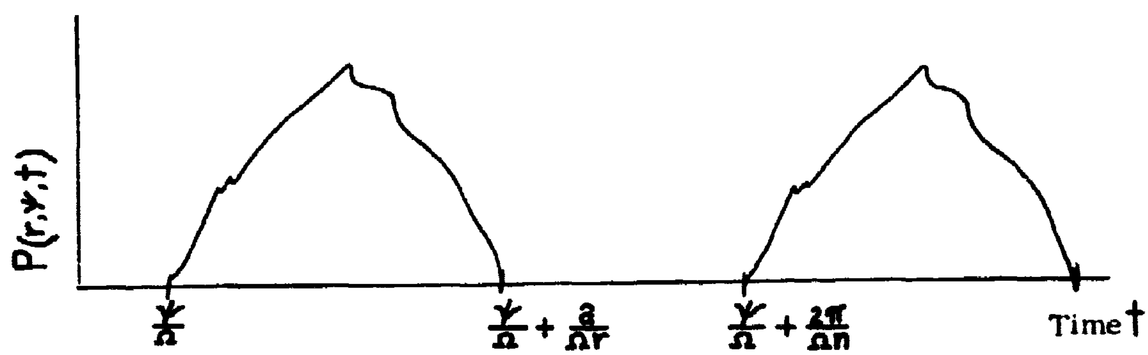

Figure 5. Pressure Time History of Blade Passing Over an Elemental Disk Area

Note that the only time a pressure exists is when a blade covers the area. The amount of time an elemental area is covered is finite and equal to the time it takes for the blade to pass a given point. That is $\Delta\tau = a/\Omega r$. The time between blades is equal to the time required for a blade to traverse $2\pi/n$ radians or $\Delta T = 2\pi/n\Omega$. The magnitude of the force acting on the rotor disk is $\Delta P r\,dr\,d\psi$ and its direction is normal to the chord. After shifting scale and approximating the chordwise pressure distribution as a step function (see Appendix IV), the function of Figure 6 is obtained.

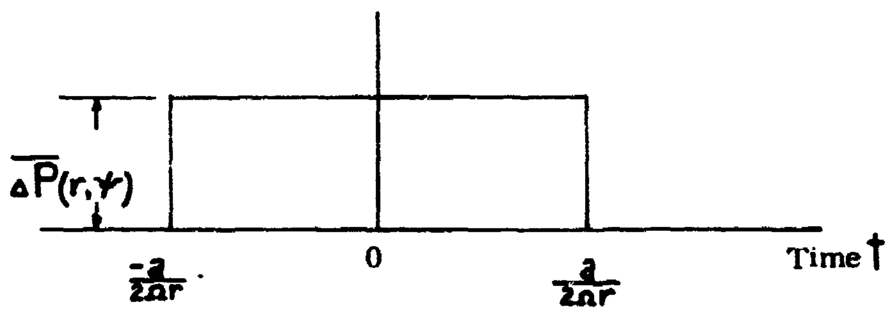

Figure 6. Step Function

The cosine series expansion of this function is

$$\Delta P(r,\psi,t) = \sum_{m=1}^{\infty} a_m \cos\left(mn\Omega t - mn\psi - \frac{man}{2r}\right) \qquad (18)$$

where

$$a_m = \frac{2}{m\pi} \sin\left(\frac{man}{2r}\right) \overline{\Delta P}(r,\psi) \qquad (19)$$

and $\overline{\Delta P}$ is the average chordal pressure on the blade.

Since average pressure data is available (Reference 29) as blade loading data $L(r,\psi)$ and

$$L(r,\psi) = a\,\overline{\Delta P}$$

equation 19 becomes

$$a_m = \frac{2}{m\pi a} \sin\left(\frac{man}{2r}\right) L(r,\psi) \qquad (20)$$

Substituting 20 into 18 yields:

$$\Delta P(r,\psi,t) = \sum_{m=1}^{\infty} \frac{2}{m\pi a} \sin\left(\frac{man}{2r}\right) L(r,\psi) \cos\left(mn\Omega t - mn\psi - \frac{man}{2r}\right) \tag{21}$$

Putting this into complex form and multiplying by $r\,dr\,d\psi$ to change to force yields

$$F(r,\psi,t) = \sum_{m=1}^{\infty} \frac{2}{m\pi a} \sin\left(\frac{man}{2r}\right) L(r,\psi)\, e^{i\left(mn\Omega t - mn\psi - \frac{man}{2r}\right)}\, r\,dr\,d\psi \tag{22a}$$

and from Equation 11

$$g_m = \frac{2}{m\pi a} \sin\left(\frac{man}{2r}\right) L(r,\psi)\, e^{-imn\left(\psi + \frac{a}{2r}\right)}\, r\,dr\,d\psi \tag{22b}$$

Equation 22 corresponds to the force exerted on the rotor disk by a passing blade in the direction normal to the blade chord. From Figure 7, note that the out-of-plane component of $\vec{g}_m$ is

$$g_{mz} = g_m \cos\beta \tag{23a}$$

and from Figures 2 and 7 the in-plane components are

$$-g_{mx} = g_m \sin\beta \sin\psi \tag{23b}$$

$$-g_{my} = g_m \sin\beta \cos\psi \tag{23c}$$

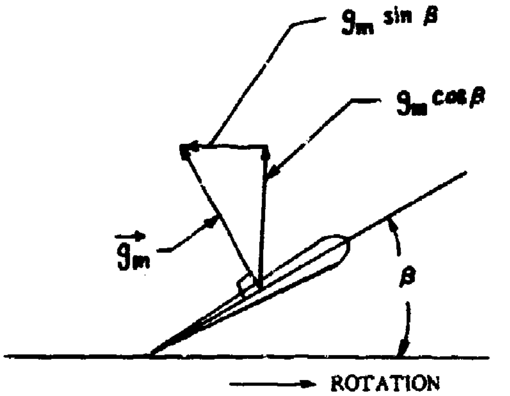

Figure 7. Aerodynamic Forces Generated by a Blade

where

$$\beta = \beta_0 - \gamma(r - r_0) + \beta_1 \cos\psi + \bar{\beta}_1 \sin\psi$$

as derived in Appendix V.

Substituting equation 22 into equation 23 and substituting the result in equation 17 gives

$$p_m(x,y,z,t) = e^{imn\Omega t}\left\{\frac{R}{2\pi^2 am}\,\frac{L(r,\psi)}{S^2}\sin\left(\frac{man}{2r}\right)\right\} e^{-imn\left(\frac{\Omega S}{c} + \psi + \frac{a}{2r}\right)} \tag{24}$$

$$\left\{\frac{imn\Omega}{c} + \frac{1}{S}\right\}\left\{\sin\beta \sin\psi \cos\theta \cos\sigma - \sin\beta \cos\psi \cos\sigma \sin\theta + \cos\beta \sin\sigma\; r\,dr\,d\psi\right\}$$

This expression after integrating, transforming to the uniform disk loading case, and introducing the small angle assumptions made in References 11 and 7, reduces to the sum of equations 21 and 22 of Reference 7 for Mach zero. It represents the sound pressure at a point x, y, z, at time t of the m'th harmonic of rotational noise due to the blade section loading $L(r,\psi)$ on the radius r of the blade when the blade is at azimuth location ψ. The equation may be integrated over the rotor disk to account for all sources and the root mean square (rms) value of the pressure with respect to time may be taken to correlate with sound pressure measurements. These operations result in the following solution:

$$P_{rms} = \frac{1}{\sqrt{2}} |P_m| = \frac{1}{\sqrt{2}} \left\{ P_{re}^2 + P_{im}^2 \right\}^{\frac{1}{2}} \tag{25}$$

$$P_{rms} = \frac{R}{2\sqrt{2}\,\pi^2 a} \left\{ (P_{re'})^2 + (P_{im'})^2 \right\}^{\frac{1}{2}} \tag{26a}$$

where

$$P_{re'} = \int_0^{2\pi}\int_0^{r_t} \frac{L(r,\psi)}{mS^2} \sin\left(\frac{man}{2r}\right) \left\{ \frac{mn\Omega}{c} \sin u + \frac{\cos u}{S} \right\} \left\{ \sin\beta \cos\sigma \sin(\psi-\theta) + \cos\beta \sin\sigma \right\} r\, dr\, d\psi \tag{26b}$$

$$P_{im'} = \int_0^{2\pi}\int_0^{r_t} \frac{L(r,\psi)}{mS^2} \sin\left(\frac{man}{2r}\right) \left\{ \frac{mn\Omega}{c} \cos u - \frac{\sin u}{S} \right\} \left\{ \sin\beta \cos\sigma \sin(\psi-\theta) + \cos\beta \sin\sigma \right\} r\, dr\, d\psi \tag{26c}$$

for which

$$u = mn\left\{ \frac{\Omega S}{c} + \frac{a}{2r} + \psi \right\}$$

This integral solution (equation 26) represents the rms sound pressure at a point x, y, z for rotational noise at the m'th harmonic of blade passage. This solution may be used for calculating the rms sound pressure at any point in the near or far field one diameter or more from the rotor hub. The number of harmonics which may be calculated accurately is limited only by the detail of the available blade loading data. The solution's accuracy decreases with increasing rotor system translational speed up to Mach 0.3, which is the practical limit for accuracy.

The solution has been programed as an IBM-7094 procedure to facilitate calculation. The program is described in Appendix VI.

A trial case was run with steady loads only placed about the 0.8 radius point of the rotor as assumed in Gutin's derivation (Reference 11).

Using relationships between blade pitch, loading, radius, etc., the torque and thrust for this case were calculated for the S-58 rotor system. The derivation is explained and parameters for the example are given in Appendix VII. Calculations of first harmonic noise were made at a 320-foot radius by both the Sikorsky program and by Gutin's equation for various elevation angles. The results of these calculations are tabulated in Table IV and shown in Figure 8.

Agreement between the two solutions is excellent except for the point where σ is -30 degrees. At this spatial point, Gutin's solution involves a small difference between two large numbers, and the number of significant digits used in the hand calculation was not sufficient to define the true magnitude.

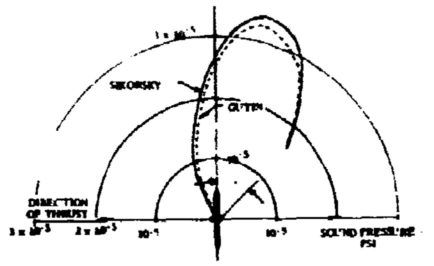

Figure 8. Comparison of Sikorsky Program and Gutin Equation Results at 320-Foot Radius

To further check the solution's validity, a similar calculation was made comparing the program output with the near field case (Figure 4 of Garrick and Watkins, Reference 7). The comparison is shown in Figure 9 for zero Mach number.

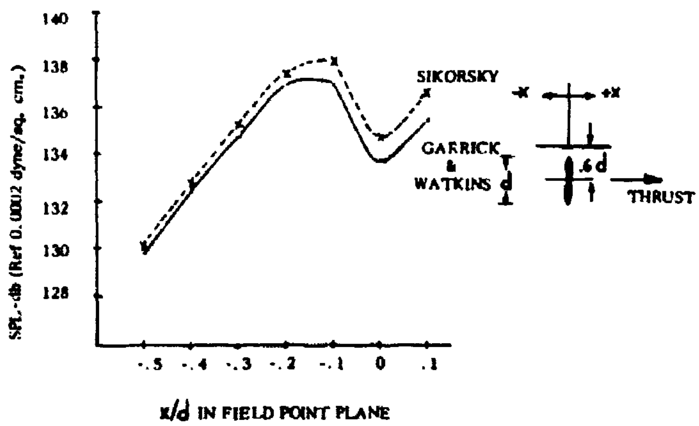

Figure 9. Comparison of Results From Developed Solution and Garrick and Watkins' Results

The agreement between the calculated values and those of Garrick and Watkins is excellent, the maximum deviation being 1 db up to 1/2 diameter downstream of the propeller.

EXPERIMENTAL TEST PROGRAM

General

Measurements of rotational noise from an S-58 (CH-34) helicopter were made at Bridgeport Airport in Stratford, Connecticut, on April 5, 1965. Physical and test parameters of the aircraft are listed in Table V. Instrumentation is described in Appendix VIII. The purpose of the test was to provide data for comparison with the calculated data of Phase II. It was found during testing that although rotor noise harmonics up to the tenth were sometimes distinguishable above background noise, harmonics above the fourth (approximately 60 cps) were generally masked by engine and tail rotor noise.

Description of Test Helicopter

The S-58 (Figure 10) is a single main rotor reciprocating engine helicopter in the 13,000-pound weight class. The main rotor is 4 bladed, with 0012 airfoil shape and untapered square tip blades.

Figure 10. S-58 Helicopter

Acoustical Measurements

The test layout is shown in Figure 1.

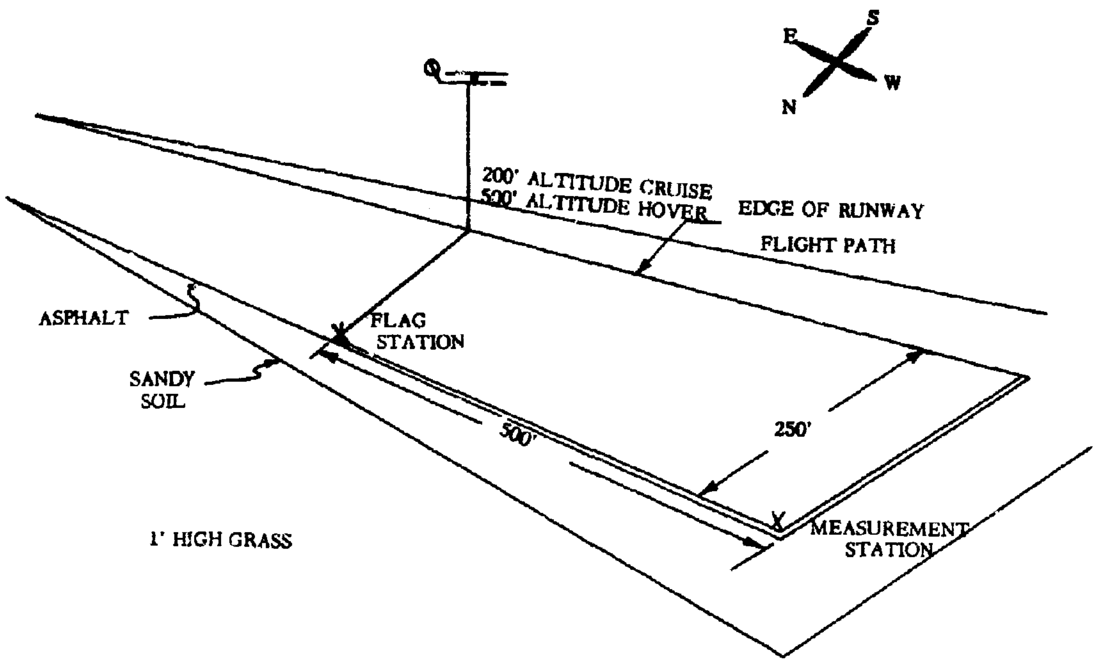

Figure 11. Rotational Noise Test Layout

The ambient wind was northeasterly at approximately 4 miles per hour, gusting occasionally to 10 miles per hour. The flight path for cruise measurements was from east to west directly over the south edge of the runway. The ship's altitude was 200 feet for all cruise and transient measurements.

For a time and location reference, a flag was dropped as the ship passed the flag station, signalling the measurement station to put a short-duration 400-cycle-per-second signal tone on the recording tape. Using the aircraft's indicated airspeed, its position was calculated from this signal. One-third-octave band analysis was used and the frequencies under study went only up to 60 cps, thereby eliminating the possibility of the 400-cps tone interfering with the records.

Because the noise was a series of pure tones, actual bandwidth was not important in determining levels. One-third-octave filters were used so as to define the individual harmonics and to accommodate the doppler shift for the flyby conditions.

Because of safety regulations, hover measurements were made at an altitude of 500 feet. The hover location was above the south edge of the runway.

Data was recorded with the microphone held approximately three feet above the ground. The runway between the aircraft and microphone was hard-surfaced. In the frequency range of interest, 15 to 60 cps, the wavelength of 75 to 18 feet precluded interference or reinforcement between the incident and reflected waves.

Noise data was recorded for hover; 40-knot, 80-knot, and 110-knot cruise; and 70-knot cyclic pullout. These conditions correspond to the blade loading data of Reference 28 (Tables 4, 8, 13, 19, and 111, respectively).

CORRELATION OF MEASURED AND CALCULATED ROTATIONAL NOISE

Correlation of measured and calculated rotational noise levels is summarized for the first harmonic in Table VI. The calculated levels shown are the maximum attained for flybys using NASA (Reference 29) blade loading data. The measured levels are the corresponding maximums for the test flybys. The blade loading tables from Reference 29 which were used are listed in Table VII. The spread of data for the measured hover condition is due to time variation. Levels calculated by Gutin's equation, using thrusts and torques as shown for the S-58, are included for reference. Note that the calculated and measured levels agree within 3 db, while Gutin's equation gives levels as much as 19 db low. Gutin's method is most nearly accurate (3 db low) during hover where the inflow is almost uniform. Obviously, nonuniform inflow has a significant effect on rotor first harmonic noise levels. The effect of nonuniform inflow is even more pronounced for the higher noise harmonics. The conclusion is that Gutin's equation is not an adequate method of predicting rotor noise levels during nonuniform inflow.

Figure 23 shows calculated and measured levels for a 500-foot hover. The program calculated the measured data much more closely than Gutin's equation, which predicts a rapid dropoff in level with increasing harmonic.

It is felt that the agreement between the calculated and measured levels for the higher harmonics would have been closer than that shown if the flight test conditions under which the noise measurements were made were identical with those for which the blade loading data was taken. According to Reference 29, the blade loading test aircraft was "hovering in light wind", which implies slight, relatively steady wind conditions, while during the noise measurement test, winds ranged from 4 to 10 knots. The lack of agreement between the measured and calculated levels for the higher harmonics can be attributed partly to the uncertainty in blade loading harmonics caused by the variable wind velocity.

Levels for the cruise and transient flybys are shown in Figures 24 through 27. As shown, the data is 1-1/2 db low at the plus 250-foot and minus 250-foot points. This error results from the frequency change due to doppler effects reaching the band limits of the one-third-octave filter used in the analysis. Correlation of measured and calculated data is good for the first two harmonics. It appears for some of the cases that the distance scale is shifted. This may be attributed partially to lag in the time reference system used in the test and partially to uncertainty as to the test aircraft's ground speed.

Agreement between the third and fourth harmonics, and presumably for all higher harmonics, is poor. This can be attributed to differences in flight conditions between blade loading test and noise test, as mentioned earlier, and to the lack of sufficient higher harmonic content in the NASA blade loading data (Reference 29). Blade loading containing a greater proportion of higher harmonics would yield more nearly accurate higher harmonics of noise as explained in Phase III.

The observed chordal loading distribution for the data used in this report conforms to the general shape of Figure 12, which yields a harmonic level distribution similar to that of the rectangular distribution used. It should be noted that if the blade chordal pressure distribution had exhibited the form of the one shown in Figure 13, the rectangular chordal pressure distribution used in the program would yield much lower noise harmonic levels than actually exist. For all common cases of propeller or rotor loading where forces on the disk act in one direction, the assumption of uniform loading over the chord should yield realistic values for calculated noise. The effects of variation in chordal loading are treated in detail in Reference 31.

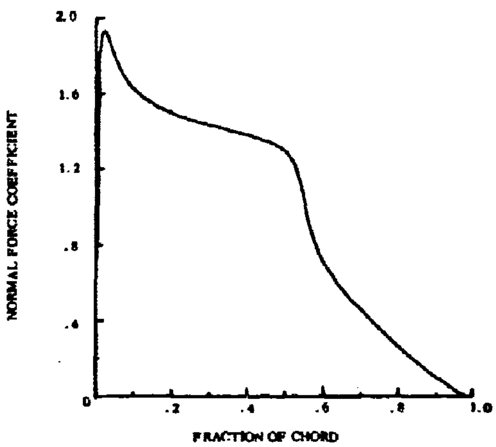

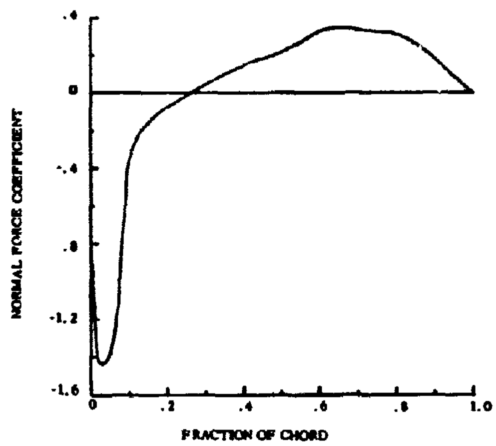

Figure 12. Chordwise Normal Force Distribution

Figure 13. Chordwise Normal Force Distribution With Reverse Flow

APPLICATIONS OF THE ROTATIONAL NOISE SOLUTION

The theory derived here for rotational noise generation lends itself to the evaluation of rotor design parameters better than the classical theory (Reference 11) for conditions of uniform inflow. For the more significant condition of nonuniform inflow it becomes a unique tool for study. The drawback is that the correct harmonic blade loading is required as input, and this is not available for harmonics above the fifth. Analysis (References 8 and 32) is available to calculate these blade loadings; however, the rotor inflow (References 21, 24, and 25) is not known in sufficient detail to allow the calculations to be made. Lack of information regarding blade wake geometry is the problem in predicting rotor inflow characteristics. The importance of the need for higher harmonic blade loading cannot be overemphasized, as the usefulness of the rotational noise solution depends on further progress in this area. In the case where some blade loading harmonics are known, even if only hand calculated steady loads, the distortion of the classical propeller noise field (Reference 11) due to planform, twist, blade collective, and cyclic pitch can be calculated in both the near and far fields. The effects of any other parameter changes are easily dealt with if blade loadings are known. Note that the solution, in its present form, is not directly applicable to systems with multiple rotors in juxtaposition.

PHASE III

ROTOR DESIGN TECHNIQUES FOR ALLEVIATION OF NOISE

VORTEX NOISE REDUCTION

The research in Phase I has shown how rotor vortex noise is generated and propagated. The theory developed permits accurate prediction of the noise amplitude and frequency spectrum directly from operational and physical parameters of the rotor system. In this section, the theory and test data of Phase I are used to evaluate the amount of noise reduction that can be achieved through the proper choice of rotor system design parameters. The formulas are valid for the conventional square-tipped blade with uniform inflow.

The work in Phase I has pointed out the importance of tip speed and aerodynamic conditions at the tip in noise generation. The intensity of the tip vortex and unstable flow near the tip also affect rotor aerodynamic efficiency. A company-sponsored research program to improve rotor efficiency by modification of the tip planform achieved increases in efficiency and reductions in noise. Reduction of tip vortex induced velocity, by approximating an elliptical load distribution, was effective in reducing noise.

Effect of Blade Area, Tip Speed and Lift Coefficient

The theoretical and experimental results of Phase I have shown that the most important parameters governing noise generation are blade area, tip speed and lift coefficient (or angle of attack). The relationship can be formalized as follows:

$$I = \frac{\rho V}{\rho c} K (V_T)^6 A_B (C_L)^2 \tag{27}$$

The parameters V_T, C_L, and A_B also govern the thrust of the rotor system, as can be seen from the following basic relationship:

$$T = \frac{1}{2} \rho V^2 C_L A_B \tag{28}$$

Although the above equation assumes a two-dimensional section with velocity V for the purpose of noise estimation, we can let the velocity V be that at the 0.7 radius and assume that C_L is the lift coefficient at a mean angle of attack.

Since the same three basic parameters appear in the equations for noise generation and lift, trade-offs between these parameters for noise control will directly affect lift. However, the appearance of blade velocity, V, to the sixth power in the noise equation allows for limited reduction of tip speed without sacrificing lift.

In Figure 28, calculated overall vortex noise levels are shown for a range of tip speeds with corresponding blade areas to maintain lift. The curves shown are for coefficients of lift of 0.4 and 0.2. These curves are for thrust of 20,000 pounds. The effect on vehicle weight of the changes in blade areas necessary for practical rotor system designs was not considered.

The curves show that sharp decreases in overall vortex noise can be achieved by reduction of the tip Mach number. However, as mentioned above, the larger and heavier blade systems have to produce more thrust to maintain the same payload. The noise associated with the increased thrust partially offsets the reduction shown in Figure 28.

The effect of thrust on the overall vortex noise is shown in Figures 29 and 30. The slope of the curves is approximately 20 times the log of the thrust ratio. Because of the wider variation in tip speeds, the CH-53A system curves show more clearly that tip speed is more important than angle of attack in reducing the vortex noise. For equal thrusts and blade area, reducing the tip speed necessitates increasing the angle of attack. However, the reduction in noise level due to lowering tip speed from 800 to 630 feet per second is about 5 db, even with this compensating increase in angle of attack.

Similar curves can be constructed for any desired thrust by using the vortex noise equation developed in Phase I (equation 6). Selection of rotor design parameters can be made with respect to noise and reconciled with other mission requirements.

Elliptical Tip Loading

Although a limited amount of vortex noise reduction can be achieved by trade-offs between tip speed, blade area and thrust coefficient, a more fruitful area of noise reduction was discovered during tests of blades having elliptical blade loading at the tip. Figure 31 shows the planform for a trapezoidal tip and the standard square-tipped blades studied in the remainder of this report. The trapezoidal shape was adopted as an approximation of the elliptical blade loading. It was expected that elliptical loading would reduce the induced velocity of the tip vortex and thereby increase lifting efficiency.

At the onset of the program it was anticipated that some noise reduction would result. The noise reduction proved to be substantial and appeared to be directly related to increased efficiency.

In Figure 32, the overall vortex level is plotted against load for three tip speeds. The tip speeds are the same as those in Figure 29. Except for the tip change, the rotor system is identical to that plotted in Figure 29. The reference line from Figure 29 is repeated to allow direct comparison of the levels. It is interesting to note that the greatest difference between the square and elliptical tip noise levels is at low thrust. The sound pressure levels of the elliptical tips increase more rapidly with increased thrust. At high thrust the difference between the two designs is much smaller. At the normal disk loading of about 19,000 pounds for this size rotor, the reduction in overall noise is about 7 db.

Figure 33 shows the spectra for both square and trapezoidal tip blades at the extremes of the usual range of angles of attack. The spectra for the trapezoidal tips show much less noise in the octave containing the Strouhal frequencies. Each of the elliptical spectra showed a rise in the last octave which is unexplained. The square-tipped blade in Figure 33 is evidently experiencing stall, as discussed in Phase I, because of the secondary peak in the 1200 to 2400 octave. For the same pitch angle the trapezoidal tip still appears to be below the onset of stall.

Figure 34 shows the relative levels of the 300 to 600 octave which contains the Strouhal frequencies over a range of loads. The reduction in the vortex noise at the Strouhal frequencies is obvious. Also it can be seen that above 19,000 pounds the noise in this key octave increases more rapidly with load for the trapezoidal tip.

The reduction in tip vortex strength deduced from the reduction of Strouhal frequency noise is also demonstrated by less modulation of the noise amplitude as shown in Table VIII. Modulation, which results from movement of the source relative to the point of observation, depends on the strength of the moving source. If the moving source is much stronger than the average over the field, the modulation is greater.

Recommendations

Main rotor vortex noise can be reduced by reducing rotor tip speed and by improving load distribution at the tip. It is recommended that minimum tip speed consistent with good aerodynamic design be used. In addition, reduction of the induced velocity of the tip vortex (core thickening) will result in substantial vortex noise reduction without loss in efficiency. Vortex noise reductions of from 7 to 10 db have been achieved with this approach. Since vortex noise falls in a frequency range for which hearing acuity is high, it can be important in determining detectability, as can be seen in Figure 35. The tactical potential of good blade tip design is therefore apparent.

ROTATIONAL NOISE REDUCTION

Reduction of Noise Due to Steady Blade Loadings

Far field rotational noise due to steady blade loading and its relationship to the physical parameters of propeller systems are described mathematically by Gutin (Reference 11). This relationship has been put into graphic and tabular form (References 3, 15, and 16) which, in combination with aerodynamic and weight considerations, makes the matter of parameter selection for low noise straightforward. Additional investigations (References 12, 13, and 27) have defined the trade-offs necessary to obtain lower noise levels. These studies, in many cases, have concentrated on the propeller noise as it affects aircraft detectability. Aircraft detectability relates noise generated by an aircraft to the ability of a human to detect its presence audibly. Detectability is extremely important in military applications, as an aircraft's acoustic detectability is a factor in determining combat effectiveness and probability of survival. The concept of detectability will be used as a basis for evaluation of rotor noise alleviation techniques.

Figure 35 from Reference 20 shows the minimum detectable level of aircraft noise in a low noise background. The level up to approximately 250 cps is the threshold of hearing (Reference 6). Compare this with an S-58 helicopter noise spectrum shown in Figure 36. It is obvious that the fundamental (normally between 15 and 20 cps) of the main rotor blade passage noise would have to be at a much higher level than the higher harmonics in order to determine detectability. In general, the fundamental component of rotor rotational noise is below audible level and is not heard. Instead, blade passage harmonics and modulated vortex frequency noise are heard and incorrectly identified as blade passage frequency noise. It is recognized then that the fundamental of rotational noise of helicopter rotor systems is not important in determining detectability. While Gutin theory does not accurately predict the level of the harmonics, it is adequate for estimating the relative effect of design parameters.

Reduction of Noise from Nonuniform Rotor Loading

This study is based on the assumption that first harmonic rotational noise is not significant in judging loudness, and that harmonic levels resulting from steady inflow to the rotor will vary directly as the fundamental for which noise control methods are already known. To minimize the acoustic signature of a helicopter, techniques must be developed to reduce the harmonic content of rotational noise.

According to Gutin, the noise level of the individual harmonics decreases rapidly with harmonic number, as shown in curve A of Figure 37. Gutin's equation assumes that all blade loading is concentrated at a single point on the blade. This loading is simulated in curve A. When the concentrated loading is spread out over a larger segment of the blade, the upper harmonics increase in level. This implies that concentration of blade loading over a smaller disk area, which might be accomplished by reducing the diameter, for example, results in lower harmonic noise levels. This relationship cannot be utilized, however, because the harmonic dropoff gained by concentrating the load would be more than offset by the increase in overall noise level from the higher blade loading.

The fact that redistribution of steady blade loadings cannot be utilized to reduce harmonic noise levels leaves nonuniform loading as the controlling factor in determining harmonic level.

The influence of steady plus 4-per-rev blade loading on harmonic noise levels is shown in Figure 38. Three different levels of 4-per-rev plus steady loading were used to calculate the harmonic noise levels for the S-58 rotor system. The levels were calculated by the methods of Phase II. The rotor system parameters and loads for this hypothetical system are presented in Appendix IX. The harmonic dropoff is substantially affected by the addition of the variable blade loading. For example, the second noise harmonic is now higher than the fundamental and all the levels of the harmonics are increased over those generated by the steady loading.

The 4-per-rev loading contributes more to the level of the higher harmonics than the fundamental does. Calculations were made to determine whether a pattern exists which describes relationship between blade loading and rotational noise levels. The results are shown in Figures 39 to 45, which represent the same information as Figure 38 except that the noise due to steady loading has been removed to show only the result of harmonic loading. The increase in sound pressure level caused by doubling the harmonic loading (from 1/4 to 1/2 of the steady loading amplitude) is not always the 6 db which would result from interaction between the harmonic and the steady loadings. The shapes of the curves change considerably between one blade loading harmonic and the next. The higher blade loading harmonics have a greater effect on the higher noise harmonics and less effect on the lower noise harmonics. Notice that as the blade loading harmonic increases, the noise produced by a given level of loading greatly increases. In other words, the efficiency of conversion from blade loading to noise increases with blade loading harmonic. This effect is shown for blade loadings up to 10-per-rev in Figures 46 and 47, where noise level is plotted against rotational noise harmonic for several harmonic blade loading conditions. This is done for a harmonic loading level of one-quarter the amplitude of the steady component plus the steady loading, but with the noise attributed to the steady load omitted.

To get a better idea of how the noise producing efficiency of blade loading varies with noise and loading, the data of Figures 46 and 47 is cross plotted in Figure 48. The fact that certain blade loading harmonics generate noise most efficiently at certain noise harmonic frequencies is clearly shown here. Again the harmonic blade loading level used here is 1/4 that of the steady loading and the noise attributed to the steady loading itself has been removed. Even when the noise levels due to the steady loading are added to those of Figure 48, as shown in Figure 49, it is quite easy to produce a spectrum where many harmonic levels are higher than the fundamental. The acoustical efficiency of the many blade loading harmonics is the cause of the high levels of rotor and propeller noise harmonics.

If a helicopter is being designed for low detectability, it is essential to control the harmonics of blade loading. The more uniform the inflow, the lower are the blade loading harmonics. Although rotor system dynamics and aeroelastic characteristics play a role in determining the inflow pattern, the most important acoustic consideration is the presence or absence of wake interaction from other blades or rotor systems.

Quantitative analysis of the pressure field generated by a rotor and its blade loading is difficult. Improved correlation between measured and predicted blade loading has been obtained by replacing steady aerodynamic inflow theory with variable induced inflow theory (References 8 and 31). Further work is required, however, to generate harmonics of higher order analytically with any degree of accuracy. Figures 39 to 45 show the importance of the higher order blade loading harmonics in determining harmonics of rotational noise. As an example, Figure 46 shows that if a 2-per-rev blade loading, of 1/4 the amplitude of the steady, were present in addition to the steady, the fourth harmonic of rotational noise would be increased by 7 db. If there were a 5-per-rev blade loading of 1/4 the magnitude of the steady in addition to the 2-per-rev and steady loadings, the level of the fourth harmonic of rotational noise would be further increased by 41 db. For a rotor with n number of blades, it appears as though the mth harmonic of rotor noise is most sensitive to the $m(n-1)$ loading harmonic. To determine higher order noise harmonics accurately, it appears as though there is a need for loading data of much higher harmonic content than presently is available from measurements or analysis.

Design Recommendation

It is concluded from the Phase III study that it is necessary to control rotor harmonic loading in order to control rotational noise. Means are not presently available, however, to predict the nonuniform portion of rotor loading to the accuracy required for use in the rotor noise program. Gutin's theory of Reference 11 is adequate to predict trends only for first harmonic rotational noise under steady inflow conditions. The charts of References 3, 15, and 16 then become useful in determining the acoustic effect of blade parameter changes, but not the absolute level. For predicting rotational noise, for even relatively uniform inflow conditions, the analysis presented in Phase II should be used. The required input data for such predictions must include up to at least the m times n harmonic of blade loading. Here n is the number of blades and m is the desired harmonic of rotational noise. Since the state of the art does not allow prediction of higher than the fourth or fifth harmonic of blade loading, little can be concluded as to the parametric effects of design changes on harmonics of rotational noise.

In addition to the general requirements of low tip speed and blade loading, it is recommended that the blade tip be designed so that loading is distributed as evenly as possible and local turbulence is held to a minimum. This is the same requirement as that specified for vortex noise control and can be accomplished with tips such as the trapezoidal variety.

BLADE SLAP

Discussion

Blade slap is the sharp popping sound produced by a helicopter rotor during certain flight conditions. This characteristic was extensively investigated in this study to define the mechanism of blade slap and means of controlling it.

Results of this study and that described in Reference 2 indicated that blade slap consists of high-amplitude rotational noise plus highly modulated vortex frequency noise. The slapping or popping noise occurs when the blade has rotated approximately 270 degrees from the tail during forward flight. Reference 5 indicates that blade slap is due to amplitude modulation of broad-band noise during stall. It can be seen in Figure 33 and in Figure 2 of Reference 33 that vortex noise levels are a minimum of 7 db higher for the stalled (separated flow) condition than for the unstalled condition.

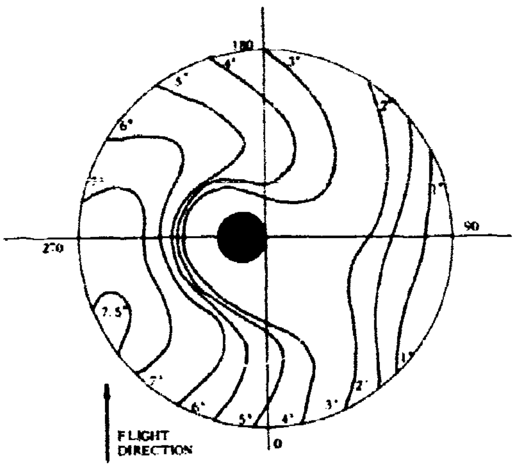

Figure 14. Single Rotor Helicopter Typical Angle of Attack Distribution

The contention that blade slap is associated with blade stall can be demonstrated as follows. Figure 14 shows the angles of attack around the disk of a single rotor helicopter during 100-knot forward flight. The maximum angle of attack occurs at an azimuth angle between 270 degrees and 360 degrees. As speed is increased, the angle of attack in this area is increased. Ultimately, stall will occur at the tip and will spread toward the rotor hub. The occurrences of stall and angle of attack change are explained quite clearly in Reference 9. These variations in angle of attack are typical for a single rotor helicopter. Experimental data from Reference 10 on a rotor system experiencing stall (Figure 15) shows that calculated results (dotted line) are reasonably accurate and that the region around 270 degrees is indeed the area which is most susceptible to stall during high speed flight. Since both blade slap and stall occur near the 270 degrees azimuth position, it can be concluded that slap is related to blade stall for this flight condition.

Pilot reports state that the blade slap occurs with high blade loading such as that encountered in high speed forward flight or in a heavily laden condition. They also report slap when making powered descent and in transition to autorotation. Where stall is imminent, a perturbation in the aerodynamic inflow, such as the downwash of another rotor or an encounter with a shed vortex from a preceding blade, may be sufficient to induce the stall.

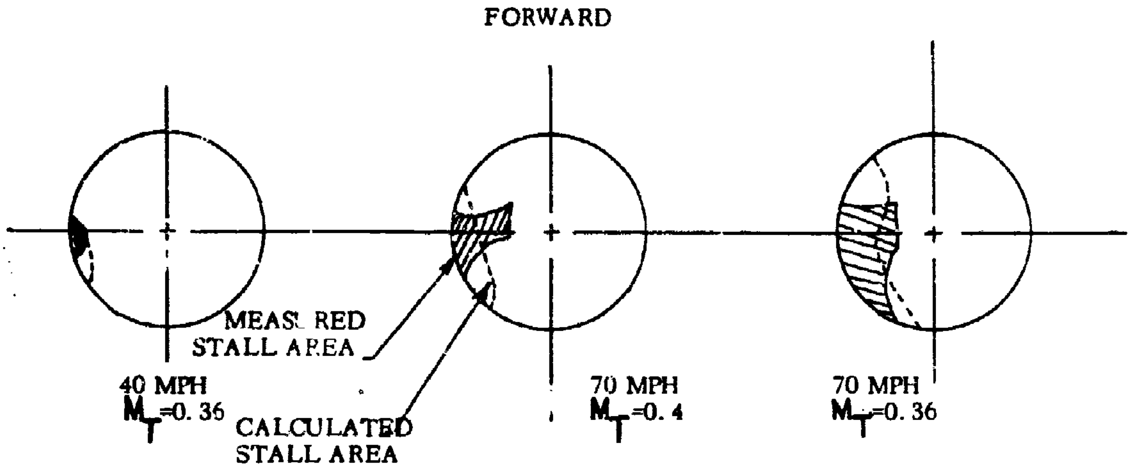

Figure 15. Occurrence of Stall in the Rotor Disk

With tandem rotor helicopters, the lower rotor encounters the downward induced flow along with shed vortices in a portion of its disk area. The intersection of these vortices and the resulting sudden change in angle of attack and flow separation cause nearly continuous slapping. A comparison of the levels of a single rotor (S-61) helicopter and a tandem rotor (V-107) helicopter during approach to landing is shown in Figure 16. The ships are of approximately 18,000-pound design gross weight and are performing the same maneuver. During the maneuver, both aircraft are producing impulse type noise.

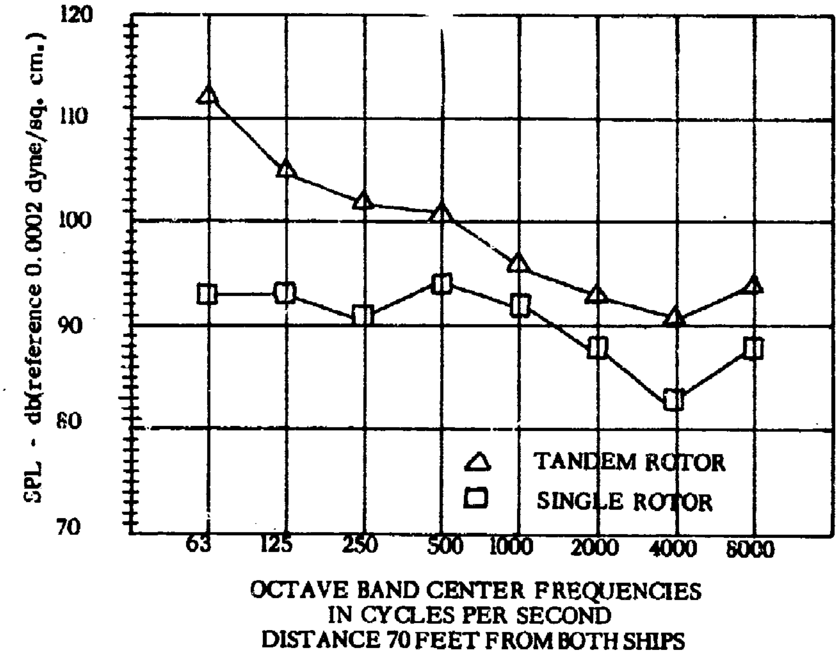

Figure 16. Single versus Tandem Rotor Noise in Approach (Reference 34)

The frequency content of the noise for the two helicopters is similar. The considerably higher noise in the 20-to 75-cps octave indicates that the tandem helicopter experiences corresponding changes in lift in the overlap region. As was shown in Phase II, the periodic change in lift or blade pressure causes high level noise at the blade passage frequency and its harmonics. Although momentary tip stall may occur on the single rotor ship, the fluctuation in lift is less intense. Consequently, it generates little more noise than in the unstalled condition.

Tests of blades with square and trapezoidal tips were made by Sikorsky Aircraft. The trapezoidal tips are designed to reduce the induced velocity of the tip vortex from that of the square-tipped blade. This lessens the depth of vortex noise modulation and also leaves less of a disturbance in the flow field to interact with the other blades. The differences between noise spectra of the two blade types are shown for various power and speed conditions in Figures 33 and 34. Details of the test are explained in Phase I.

The phenomenon of compressible drag divergence, which occurs with stall, is also related to blade slap. When drag divergence occurs, drag increases and power is consumed. The increase in drag is due to the unstable formation of local shock waves which transform energy into heat and pressure pulses. If sufficiently strong, these shock waves contribute to the blade slap noise.

The Phase II calculation procedure is completely general, and as such will predict the harmonic content of any condition, including blade slap. Blade slap was not detected during the measurement program. In order to determine whether blade slap could be predicted by the Phase II analysis, it was, therefore, necessary to simulate a blade loading condition which would induce blade slap. Since blade slap occurs during blade stall, blade pressure data recorded during the occurrence of blade stall was used as a basis for the harmonic loading input. Blade pressure time histories at 85 percent span for the 80-knot 1/2g turn are shown in Figure 17. From analysis of the pressure time history at the trailing edge, it was evident that stall was present. This trace was analyzed for harmonic content over one blade revolution. The resulting harmonics were used as blade loading for the entire chord at the 85 percent span of the rotor system and the noise harmonics were calculated. Noise levels were also calculated using only the steady component of the blade loading. The resulting harmonic distributions are shown in Figure 18 along with the harmonic distribution resulting from steady 80-knot flight on the same S-58. The steady loading spectrum exhibits the usual rapid dropoff in harmonic noise level associated with steady loads alone. The 80-knot cruise spectrum levels drop off also, although not so rapidly. Finally, the spectrum generated using the impulsive airloads experienced during blade stall shows extremely high harmonics.

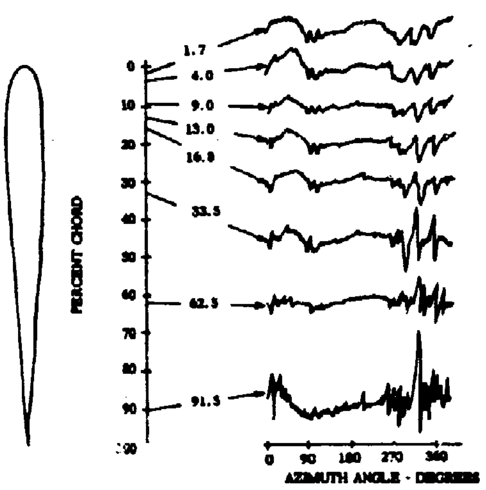

Figure 17. S-58 Blade Differential Pressure Time History During An 80-Knot, 1/2g Turn at 85 Percent Span - A Condition of Partial Blade Stall

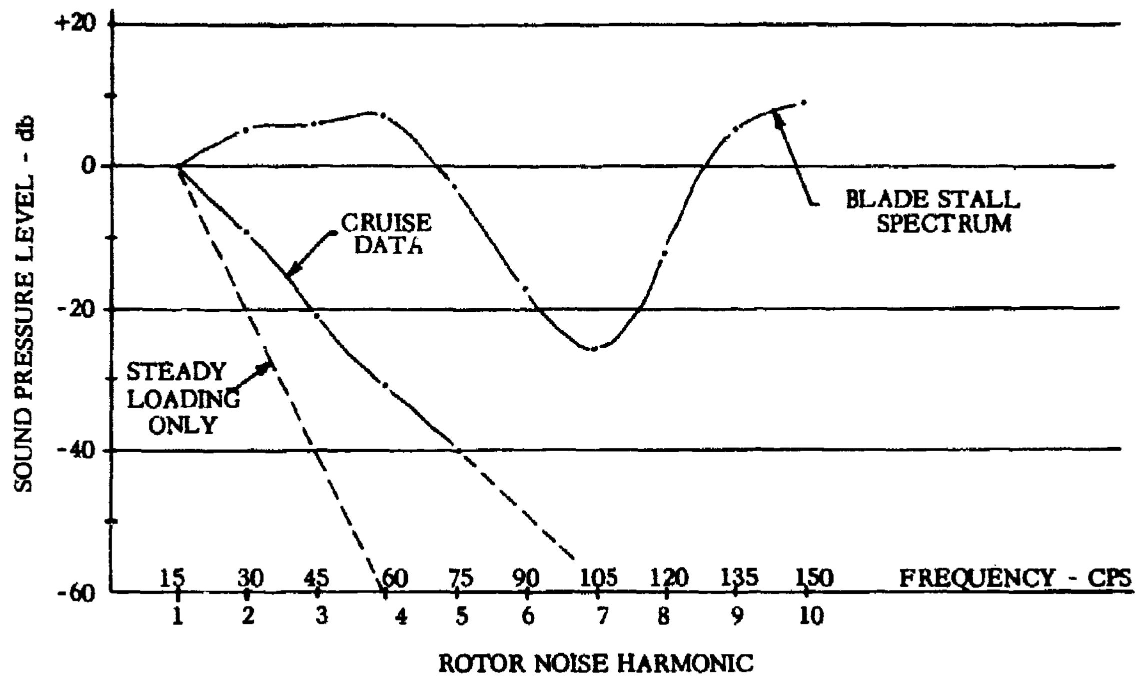

Figure 18. Rotational Noise Harmonic Content

This spectrum is similar in shape to the blade slap spectrum measured on an SH-3A helicopter during an abnormally rough flare from level flight to hover, at which time the blades were experiencing localized blade stall. Although the spectrum shown is limited to 150 cps, blade slap extends over a frequency range of 20 to over 1000 cps, and increases vortex noise levels as well as the rotational noise harmonic levels. Reference 1 also substantiates this point. Thus, if detailed blade surface pressures are available, the blade slap rotational harmonic spectrum can be predicted. As shown in Figure 17, stall can be a localized phenomenon, requiring detailed blade surface pressures to be described adequately. These prediction methods, however, are not presently available. It appears that the best basis upon which to judge the likelihood of blade slap occurrence is aerodynamic stall criteria.

Design Recommendations

For minimal rotational noise and blade slap, the obvious design guidelines are to use the lowest possible tip speed and to use shaped, twisted blades which distribute tip loading and substitute sheet vortices for the stronger tip vortices. Although blade stall appears to be the major cause of blade slap, compressible drag divergence, i.e., Mach effects, cannot be ignored. When blade elements are in stall, compressible drag divergence is also present. To make blade design recommendations for reduced blade slap strictly on the basis of reduced stall would be premature at this time, since blade design for reduced tendency to stall may well increase the extent of drag divergence. Further study is therefore needed to define the relationships between blade slap and the degree of stall, drag divergence, and tip vortex induced velocity if positive blade design recommendations are to be made.

TABLE I

CALCULATED VORTEX NOISE FREQUENCIES AND THEIR RELATIVE INTENSITY FOR THE CH-53A ROTOR BLADE AT 30,000 POUNDS THRUST

r/R	α (degrees)	M	V (ft. sec)	h' (ft)	f * (cps)	Down From Tip Level (db-db at Tip)
0.300	3.31	0.187	209	0.367	154	-31.3
0.450	3.54	0.280	313	0.375	225	-20.9
0.600	3.44	0.374	418	0.371	300	-13.3
0.700	3.30	0.436	487	0.366	360	- 9.3
0.750	3.20	0.467	522	0.362	390	- 7.5
0.800	3.10	0.499	556	0.359	420	- 5.9
0.850	3.00	0.530	591	0.355	450	- 4.3
0.900	2.84	0.561	626	0.349	480	- 2.8
0.950	2.64	0.592	661	0.341	520	- 1.3
0.975	2.45	0.608	679	0.334	550	- 0.7
1.000	0.00	0.624	696	0.000	-	0.0

* $f = \dfrac{S_t V}{h'}$

where $S_t = 0.28$

TABLE II
OVERALL VORTEX NOISE LEVELS

Rotor Speed (rpm)	Thrust (pounds)	SPL Calculated by Equation 6 (db*)	SPL Measured (db*)	SPL Calculated by Equation 5 (db*)
		CH-3C ROTOR SYSTEM		
183.0	13,400	78	76	79
	16,200	80	79	
	18,700	81	81	
	20,500	82	82	
203.0	16,300	82	81	82
	18,100	83	81	
	19,900	83	82	
	21,400	83	83	
213.0	14,500	81	81	83
	18,200	83	83	
	20,000	83	83	
		CH-53A ROTOR SYSTEM		
166.0	24,000	82	80	83
	28,400	83	81	
	32,000	84	83	
	36,200	85	83	
	39,000	86	85	
185.5	25,000	83	83	85
	30,100	85	83	
	36,200	86	85	
	41,600	87	87	
215.0	23,700	84	85	89
	29,600	86	86	
	37,900	88	89	
	43,520	89	90	

* Ref = 0.0002 dyne/sq. cm.

TABLE III

PHYSICAL CHARACTERISTICS OF TEST ROTOR SYSTEMS

	CH-3C	CH-53A
Number of blades	5	6
Diameter (feet)	62	72
Blade area (ft^2)	217	368
Solidity	0.078	0.115
Disk area (ft^2)	3020	4070
Airfoil	0012	0012 Modified
Chord (feet)	1.50	2.16
Rotor speed (RPM)	183	166.0
	203	185.5
	213	215.0
Tip speed (ft/sec)	595	625
	661	696
	692	810
Tip Mach number	0.532	0.591
	0.586	0.625
	0.613	0.726

TABLE IV

COMPARISON OF FIRST HARMONIC NOISE CALCULATIONS BY GUTIN'S EQUATION AND BY THE SIKORSKY PROGRAM

σ *	Sikorsky		Gutin	
(degrees)	Sound Pressure (psi)	SPL (db**)	Sound Pressure (psi)	SPL (db**)
-45	1.6×10^{-5}	74.8	1.58×10^{-5}	74.7
-30	2.92×10^{-5}	80.0	2.82×10^{-5}	79.8
-15	3.41×10^{-5}	81.4	3.29×10^{-5}	81.0
0	2.69×10^{-5}	79.3	2.58×10^{-5}	79.0
15	1.32×10^{5}	73.2	1.24×10^{-6}	72.6
30	3.39×10^{-6}	61.4	1.87×10^{-6}	56.2

* Elevation angle = 0° in rotor plane, positive above, negative below

** Ref = 0.0002 dyne/sq. cm.

TABLE V

FLIGHT TEST PARAMETERS

Test weight-pounds	approximately 12,000
Number of blades	4
Blade radius-feet	28
Blade twist-degrees	-8
Blade chord-feet	1.367
Test rotor speed-rpm	212
Test engine speed-rpm	2400
Test rotor-angular velocity-radians/second	22.2

TABLE VI

MEASURED AND CALCULATED FIRST HARMONIC NOISE LEVELS

Distance (Feet)	Speed (Kts)	Power (hp)	Torque (lb-in)	Thrust (lb)	Gutin Level (db)*	Program Level (db)*	Measured Level (db)*
300	40 (cruise)	651	192760	11761	71.8	91.0	91.0
300	80 (cruise)	647	180469	11769	71.7	89.0	88.0
300	110 (cruise)	1016	296530	11750	72.7	91.8	89.0
300	70 (pullout)	650 **	183000 **	11760 **	71.7	91.0	87.0
600	0 (hover)	1016 **	300000 **	12000 **	66.2	73.8	70.76

* Ref = 0.0002 dyne/sq. cm.

** Estimated

TABLE VII

BLADE LOADING TABLES USED IN PROGRAM

Blade Loading Data Table *	Noise Measurement Condition
4	Hover out of ground effect
8	40-Knot cruise
13	80-Knot cruise
19	110-Knot cruise
111	70-Knot cyclic pullout

* Reference 28

TABLE VIII

17-CYCLE-PER-SECOND AMPLITUDE MODULATION: COMPARISON OF CH-3C TRAPEZOIDAL TIP VERSUS SQUARE TIP BLADES

Average Depth of Modulation - db*

Octave	Square Tip	Trapezoidal Tip	Difference
150-300	8	5	3
300-600	10	6	4
600-1200	8	8	0
1200-2400	5	4	1
2400-4800	7	4	3
4800-9600	6	4	2
		6	13
		AVERAGE DIFFERENCE	2

* DEPTH OF MODULATION $= 20 \log \frac{a}{b}$

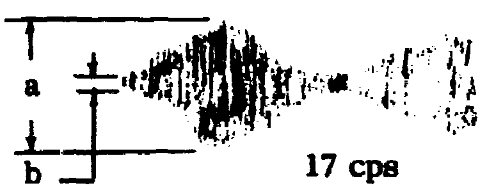

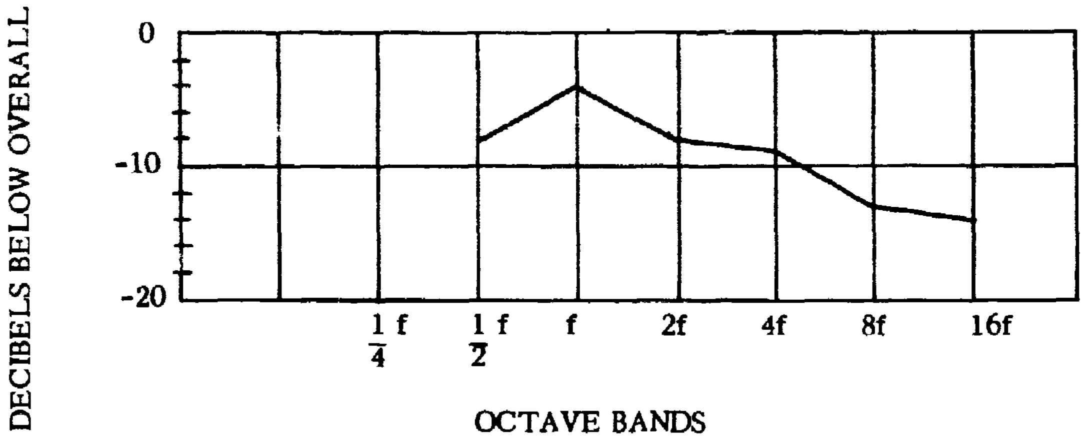

Figure 19. Spectrum Below Stall

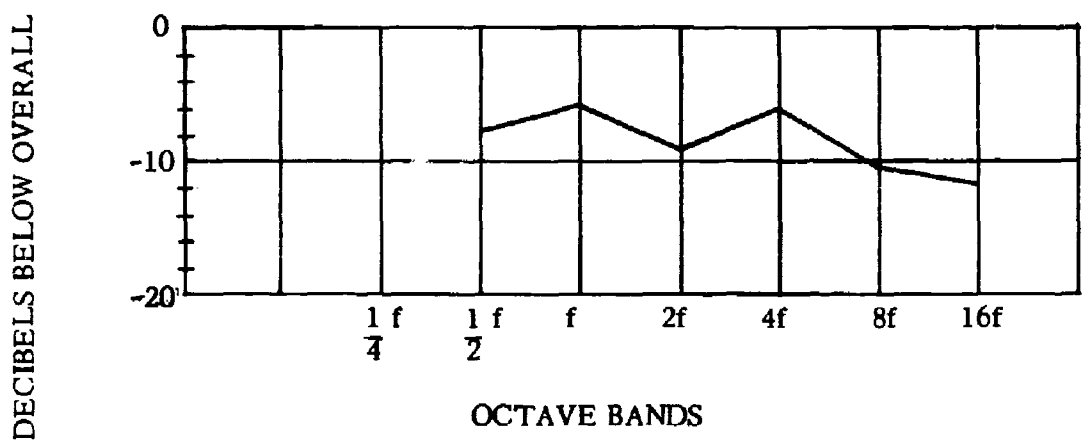

Figure 20. Spectrum Above Stall

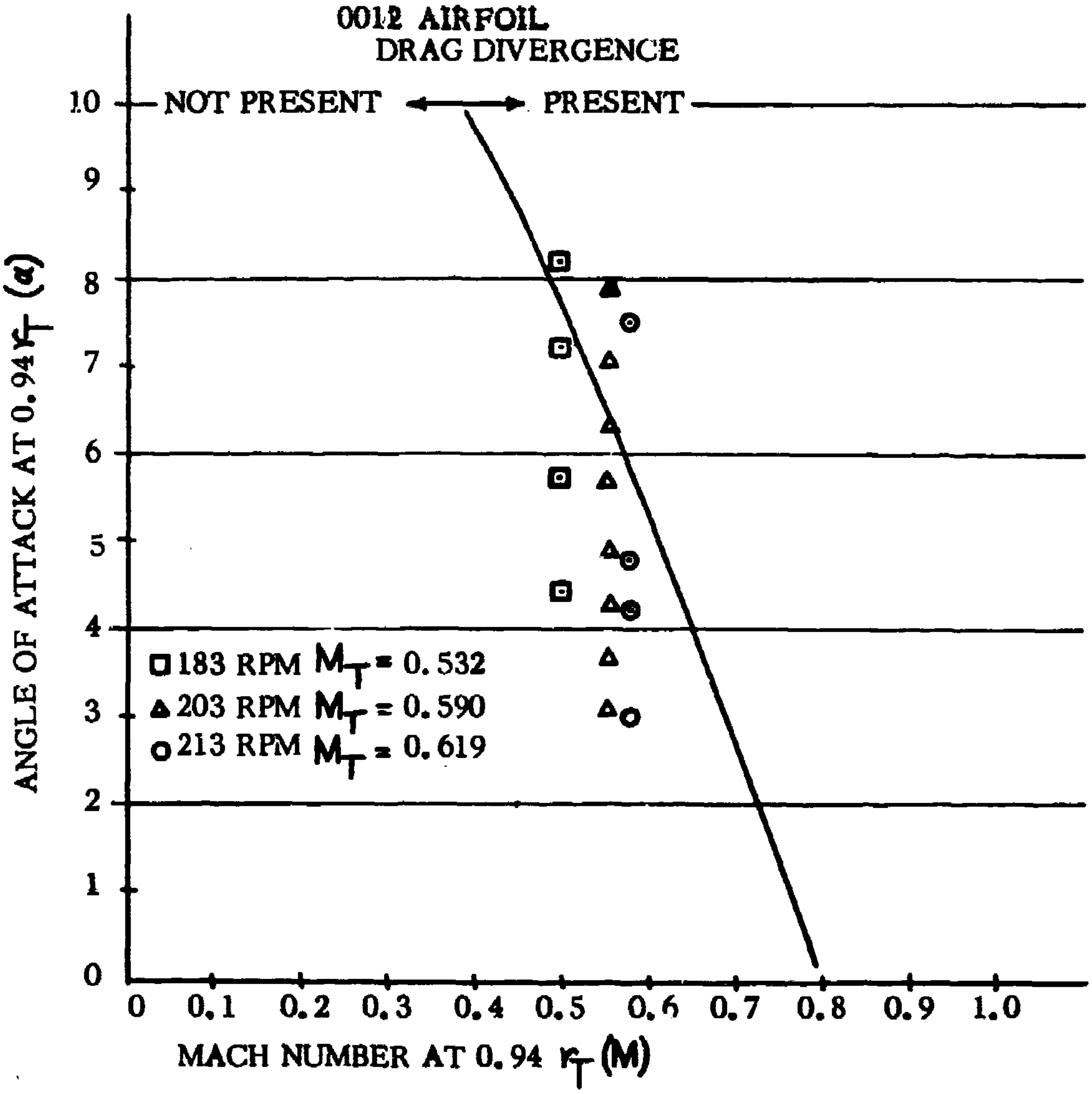

Figure 21. Drag-Divergence Curve for the CH-3C

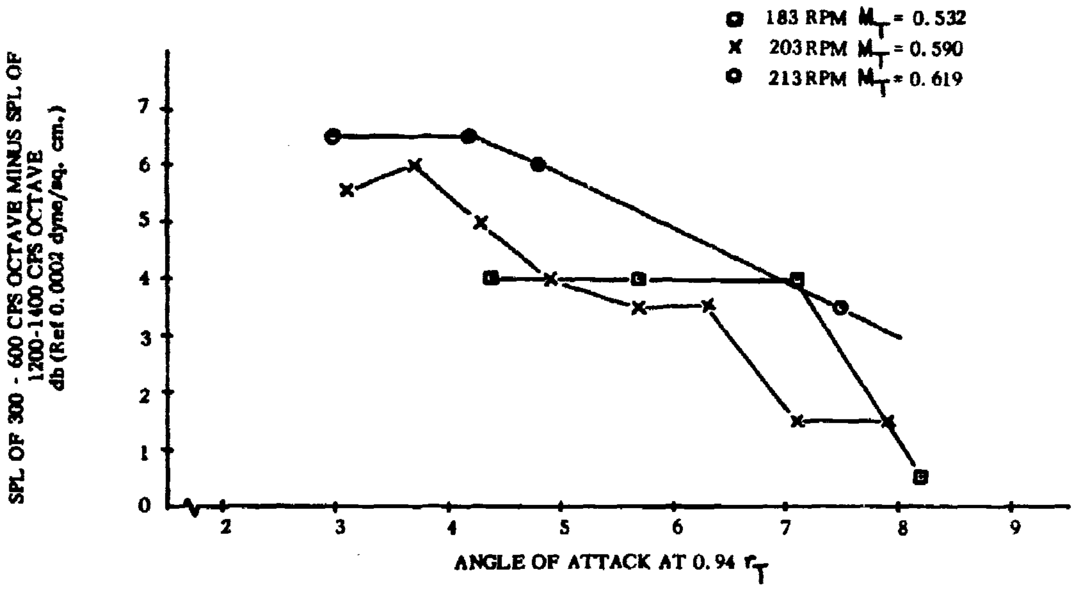

Figure 22. Onset of Drag-Divergence

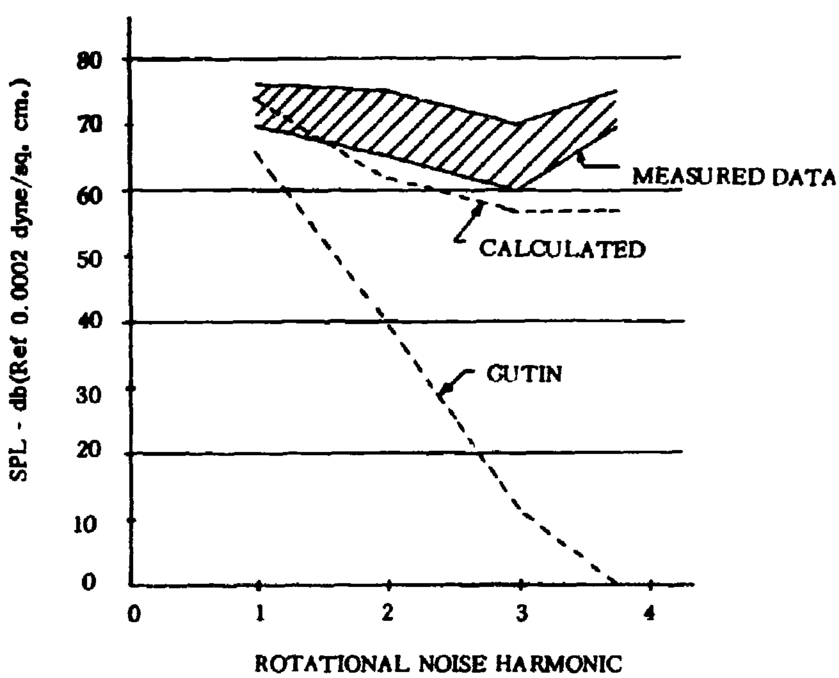

Figure 23. Calculated and Measured Levels - Hover

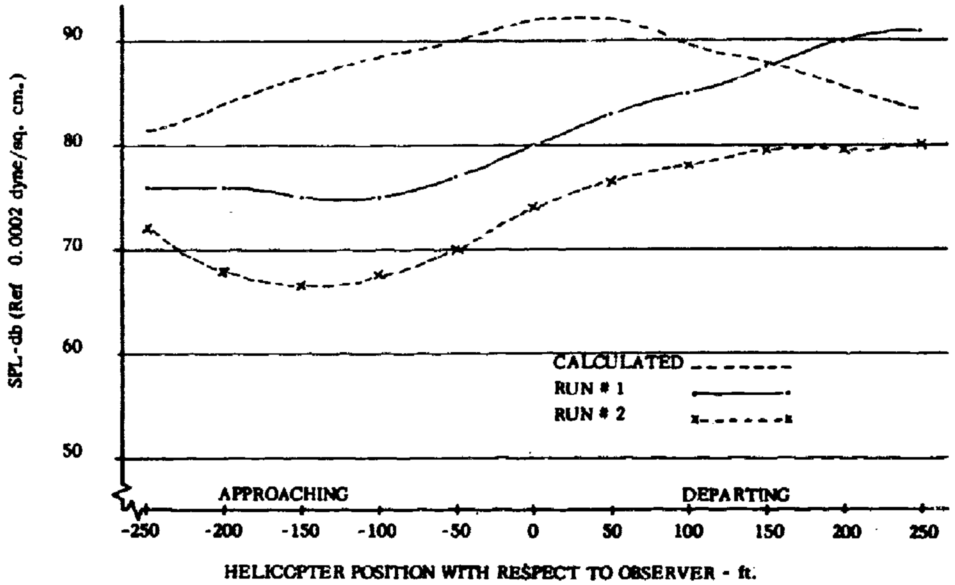

Figure 24 a. Calculated and Measured Levels - 40-Knots - First Harmonic

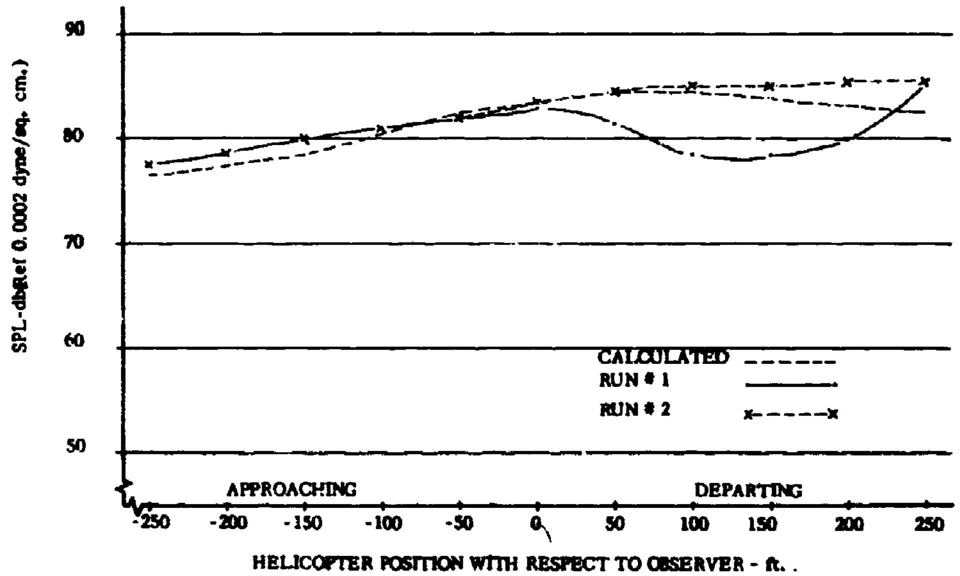

Figure 24 b. Calculated and Measured Levels - 40-Knots - Second Harmonic

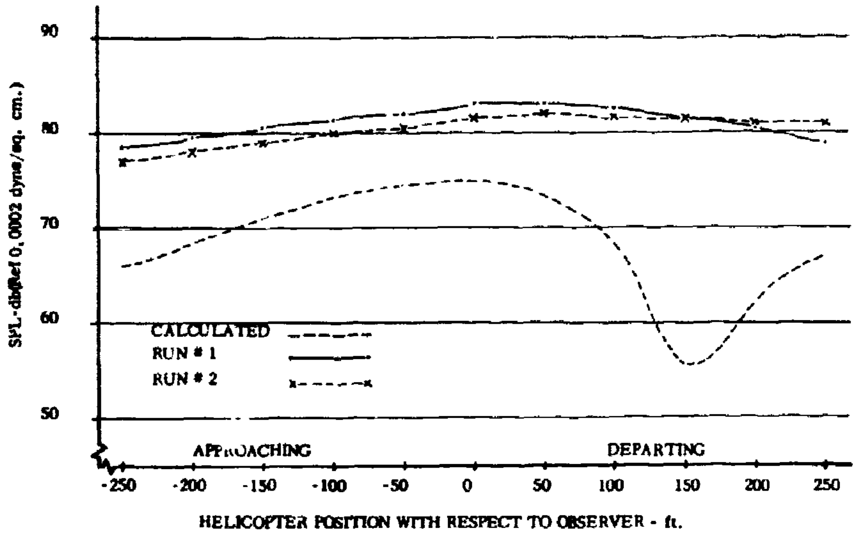

Figure 24 c. Calculated and Measured Levels - 40-Knots - Third Harmonic

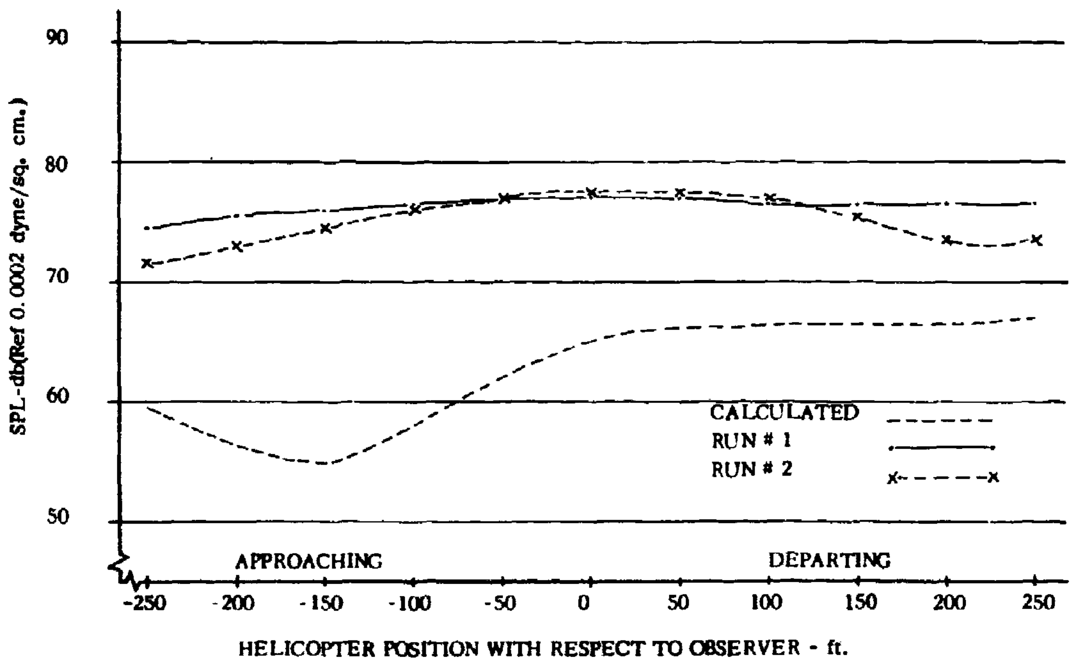

Figure 24 d. Calculated and Measured Levels - 40-Knots - Fourth Harmonic

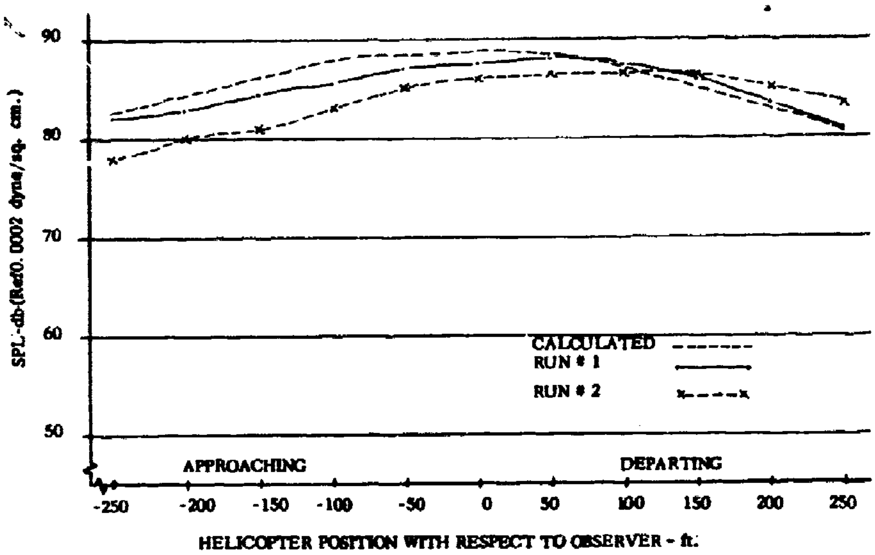

Figure 25 a. Calculated and Measured Levels - 80-Knots - First Harmonic

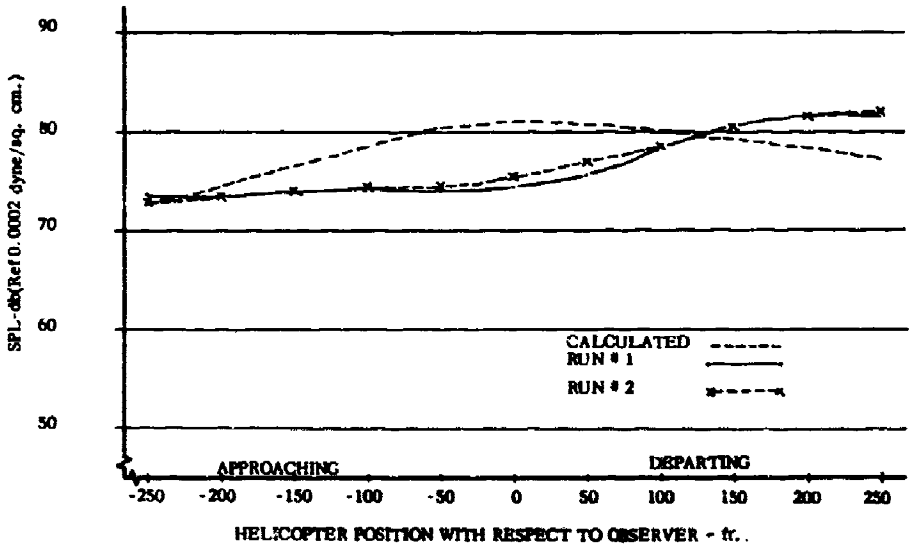

Figure 25 b. Calculated and Measured Levels - 80-Knots - Second Harmonic

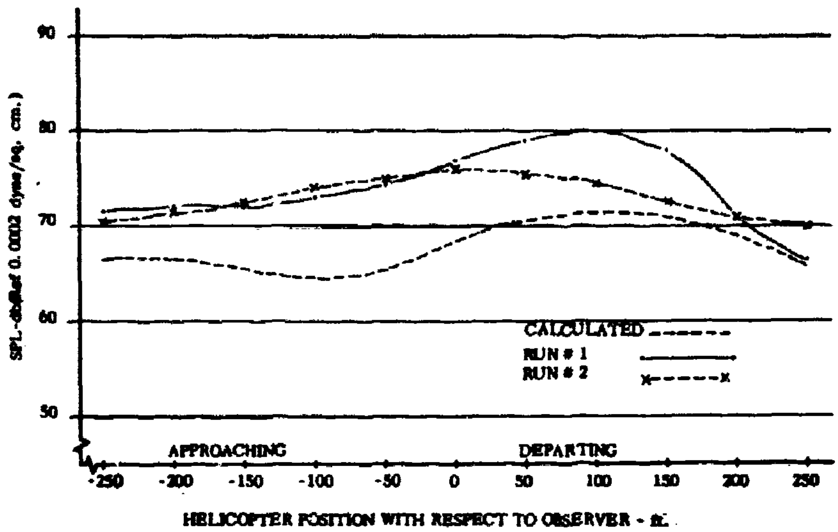

Figure 25 c. Calculated and Measured Levels - 80-Knots - Third Harmonic

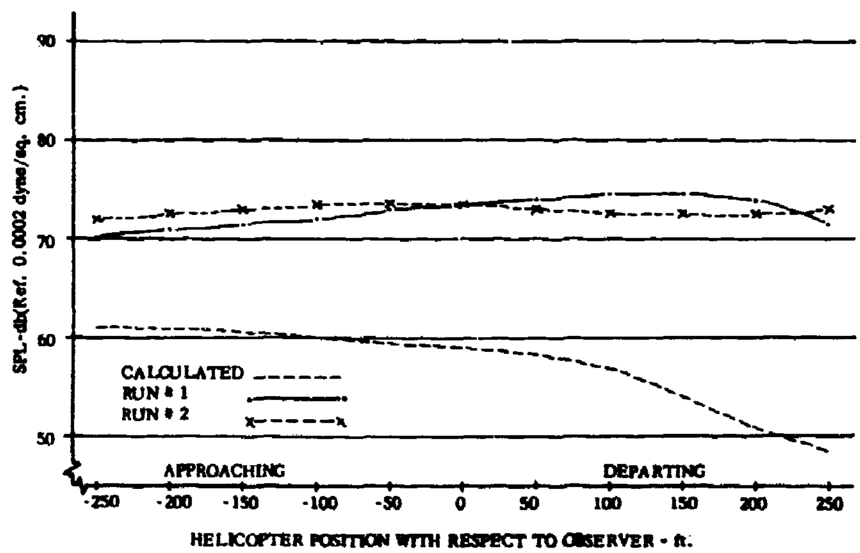

Figure 25 d. Calculated and Measured Levels - 80-Knots - Fourth Harmonic

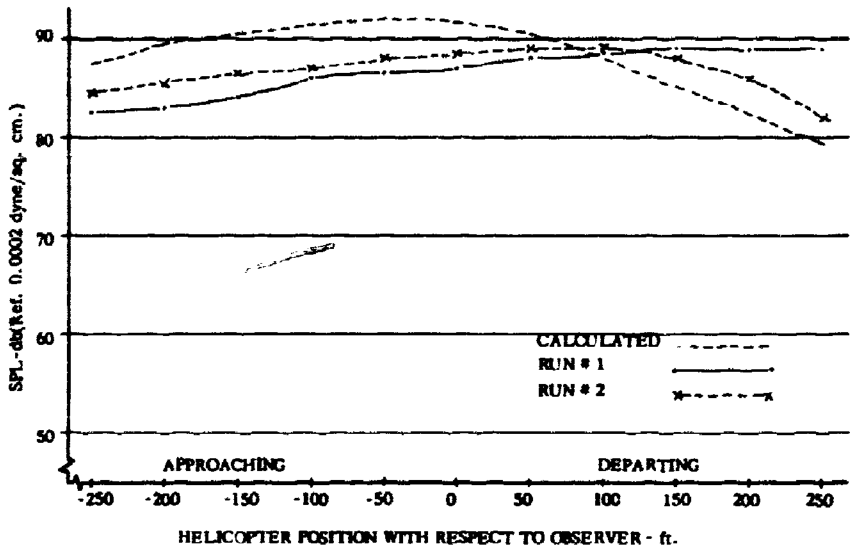

Figure 26 a. Calculated and Measured Levels - 110-Knots - First Harmonic

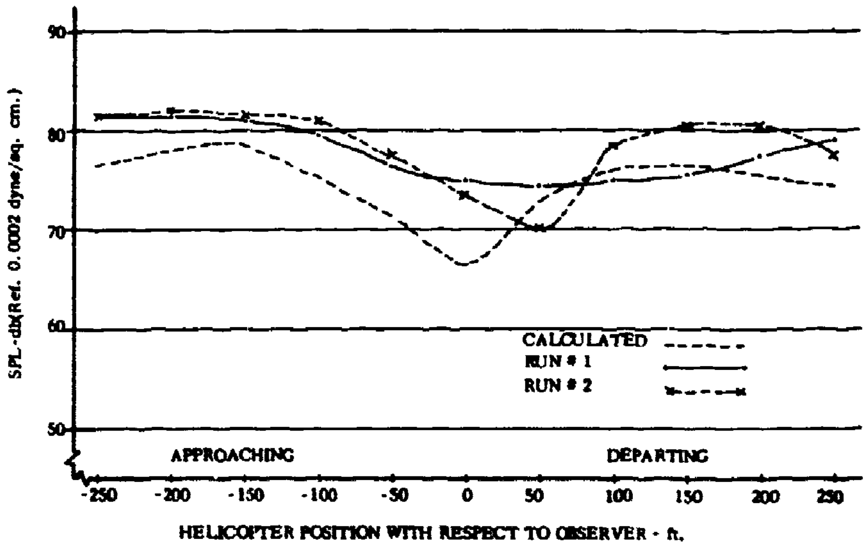

Figure 26 b. Calculated and Measured Levels - 110-Knots - Second Harmonic

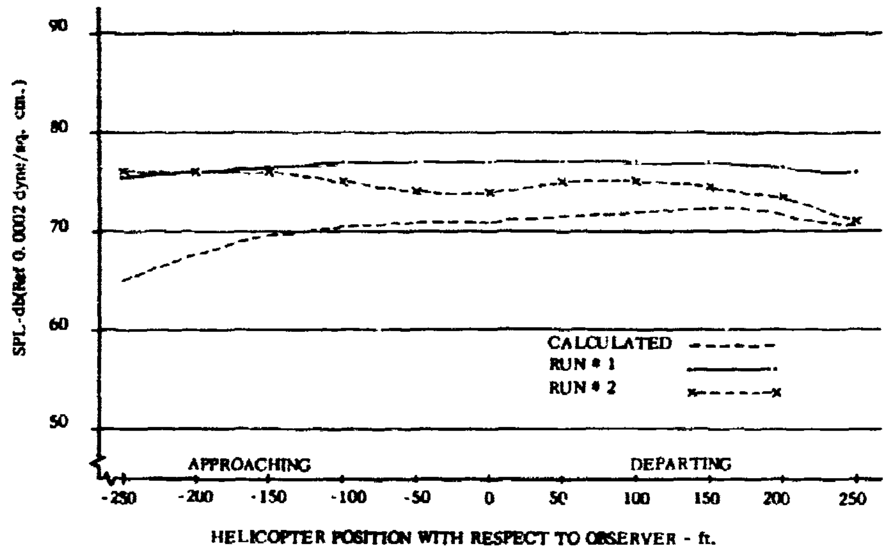

Figure 26 c. Calculated and Measured Levels - 110-Knots - Third Harmonic

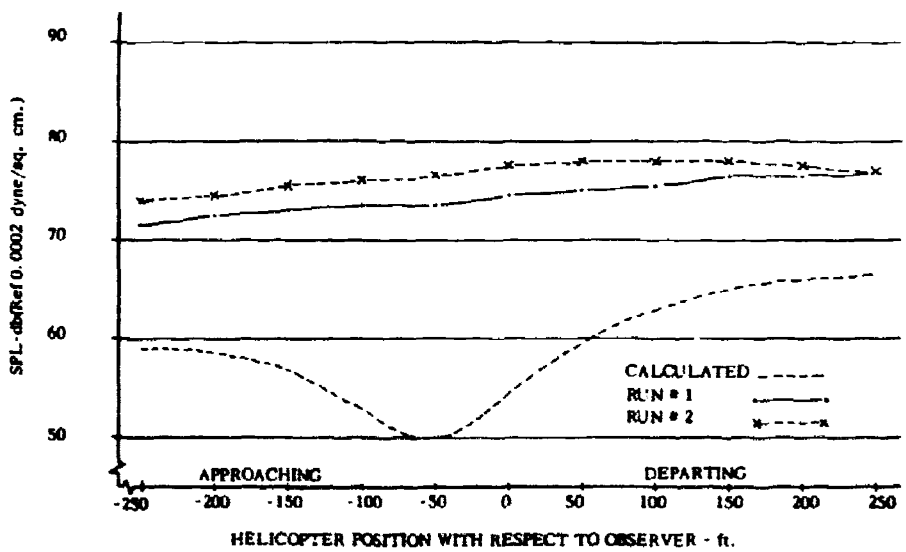

Figure 26 d. Calculated and Measured Levels - 110-Knots - Fourth Harmonic

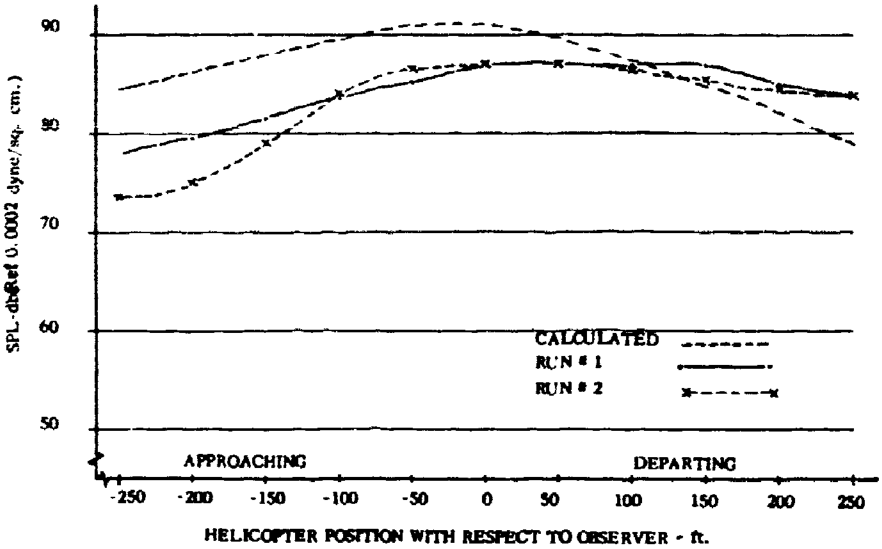

Figure 27a. Calculated and Measured Levels - 70-Knot Cyclic Pullout - First Harmonic

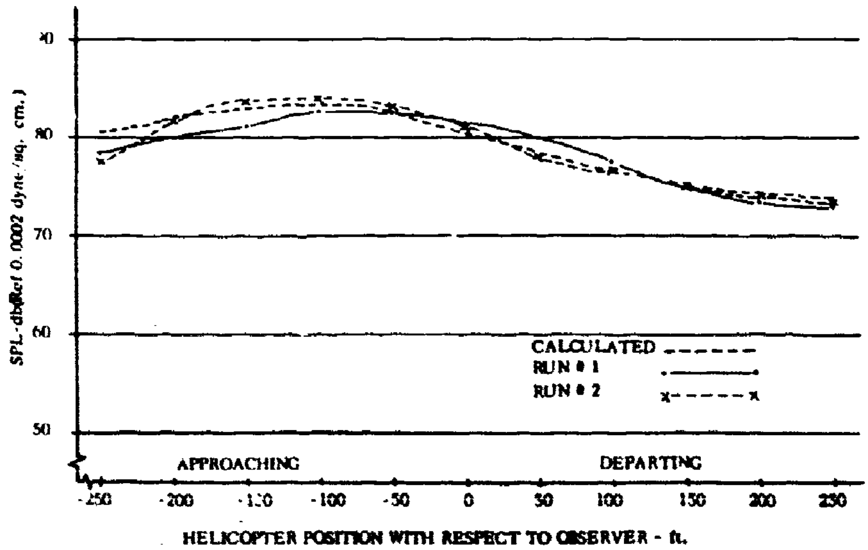

Figure 27b. Calculated and Measured Levels - 70-Knot Cyclic Pullout - Second Harmonic

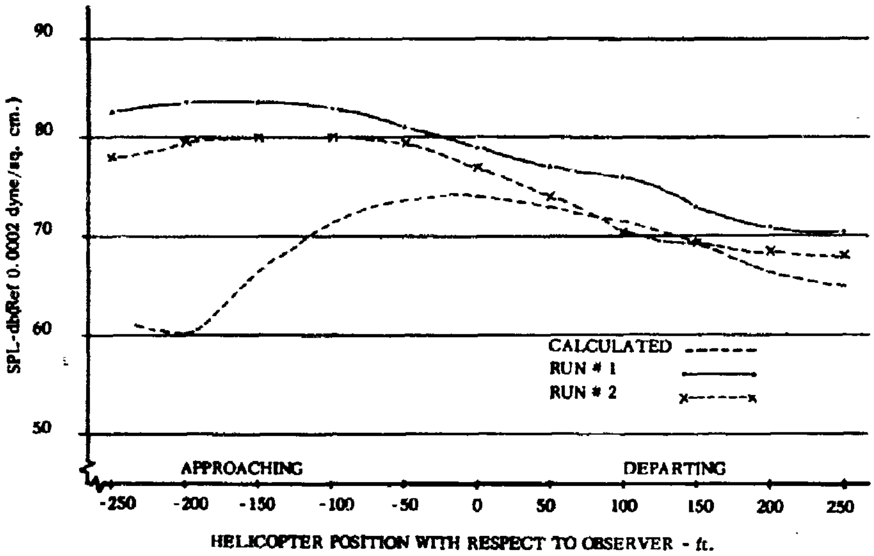

Figure 27c. Calculated and Measured Levels - 70-Knot Cyclic Pullout - Third Harmonic

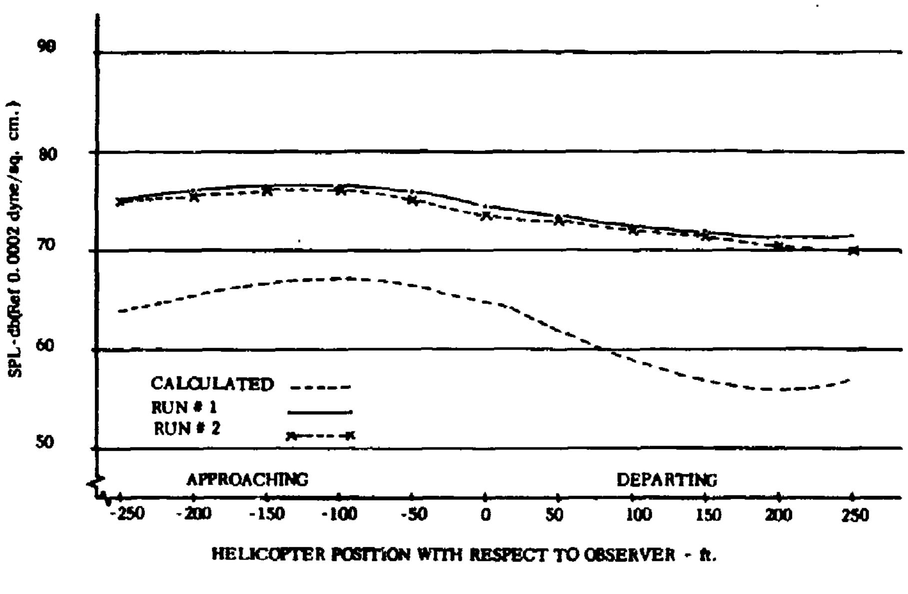

Figure 27d. Calculated and Measured Levels - 70-Knot Cyclic Pullout - Fourth Harmonic

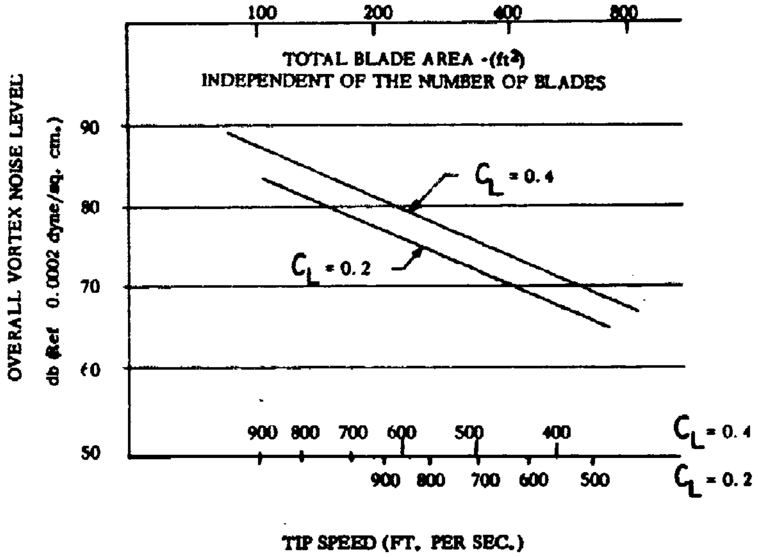

Figure 28. Calculated Noise Levels at 300 Feet, 20,000 Pounds Thrust, 5 Blades

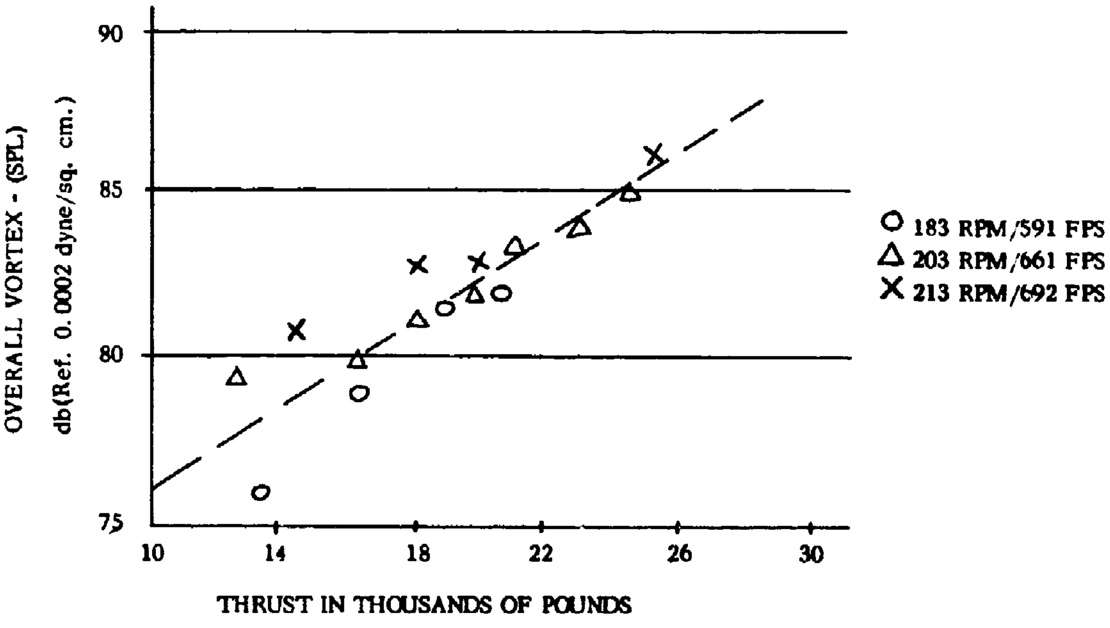

Figure 29. Sound Pressure Levels versus Thrust for 3 Tip Speeds, CH-3C

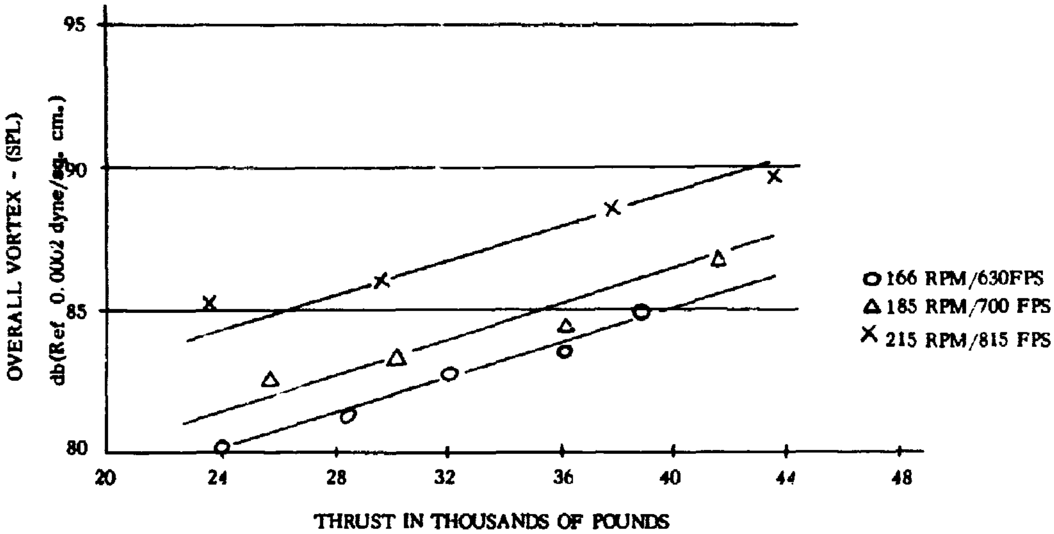

Figure 30. Sound Pressure Levels versus Thrust for 3 Tip Speeds, CH-53A

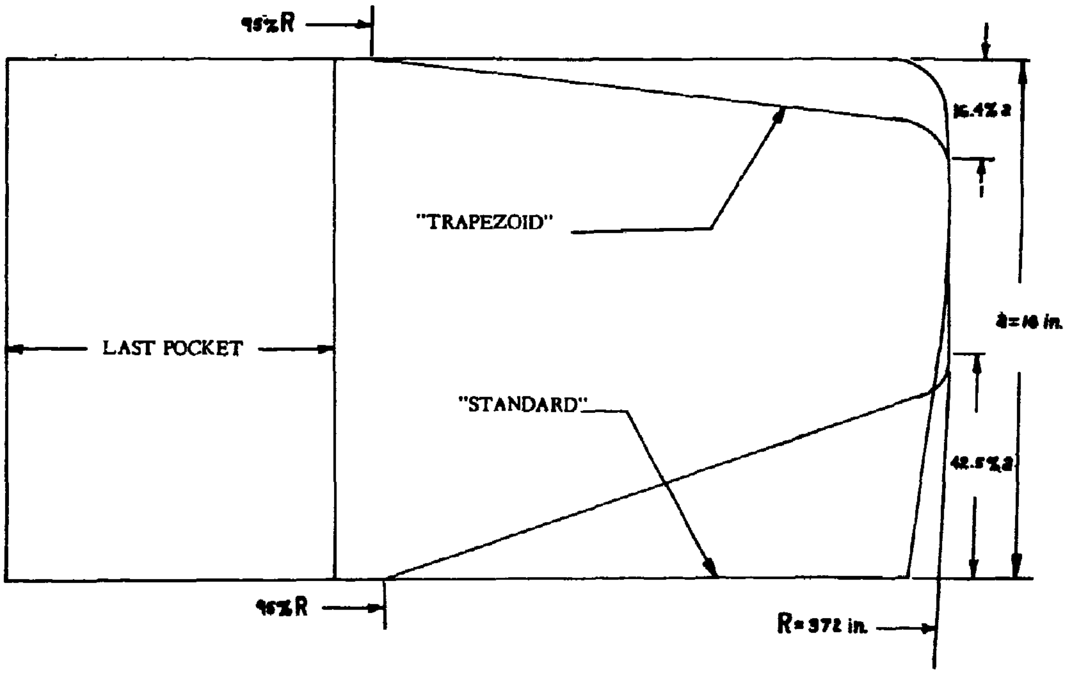

Figure 31. Trapezoidal and Square Tip Planforms

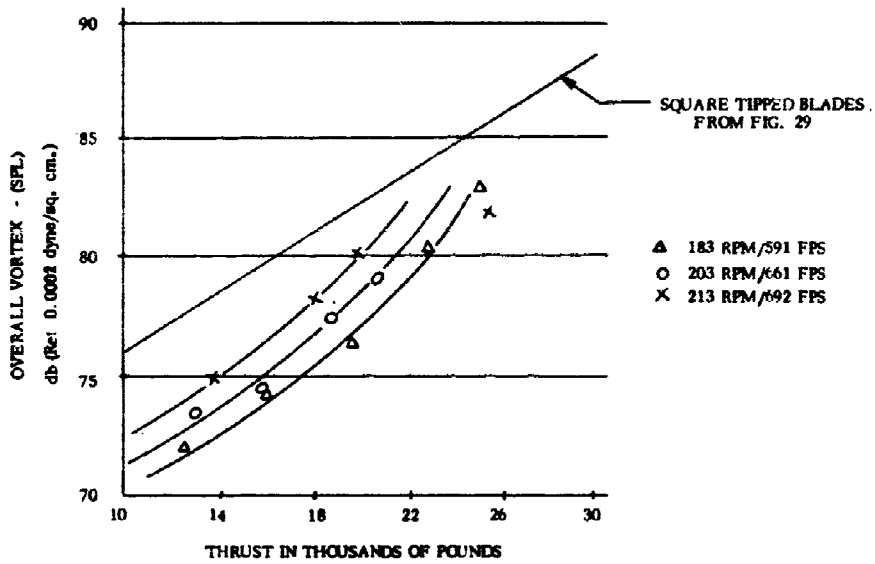

Figure 32. Sound Pressure Level versus Thrust - Trapezoidal Tips

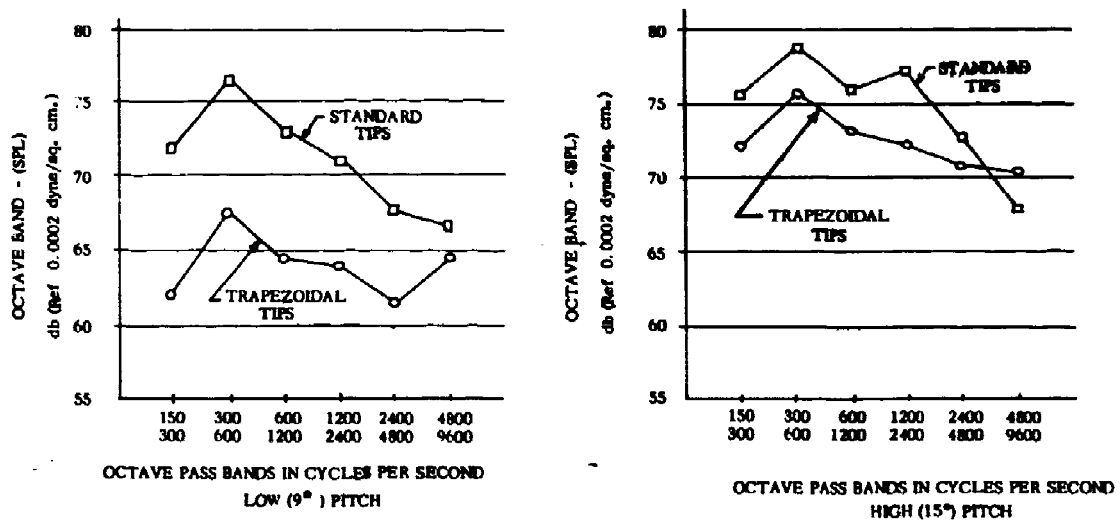

Figure 33. Octave Band Levels for Low and High Pitch (CH-3C)

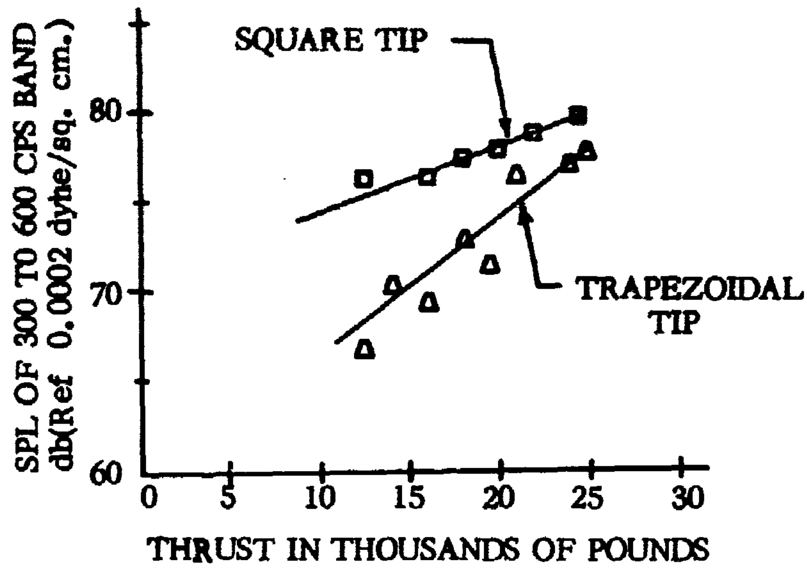

Figure 34. Comparison of Level at Strouhal Frequency of Square and Trapezoidal Tips @ 203 RPM

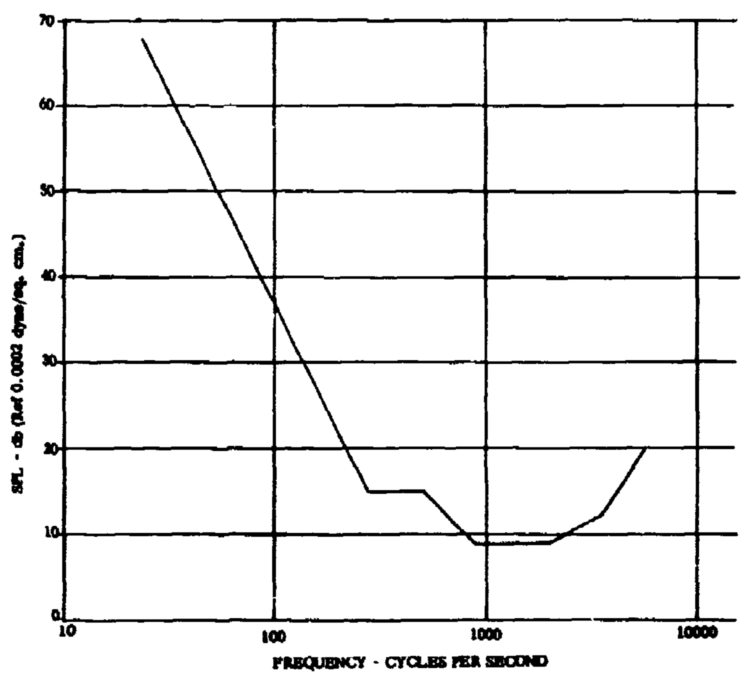

Figure 35. Detection Level Criteria for Aircraft - Spectrum Level

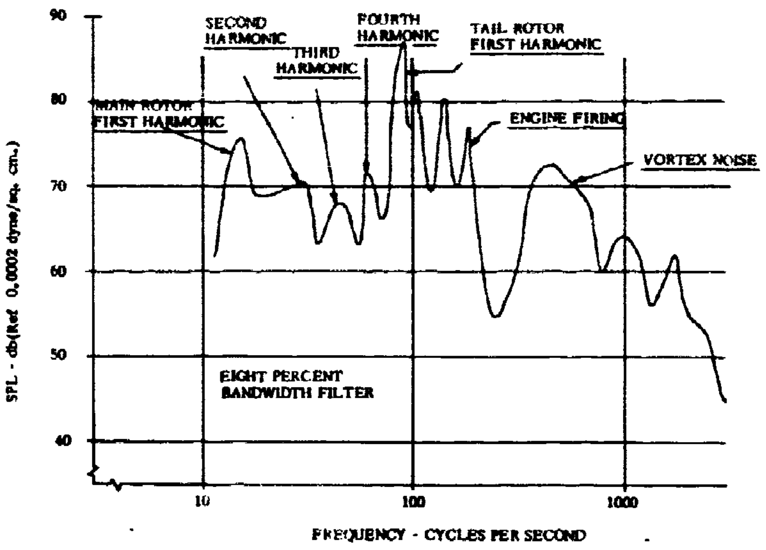

Figure 36. An S-58 Helicopter Noise Spectrum at Hover

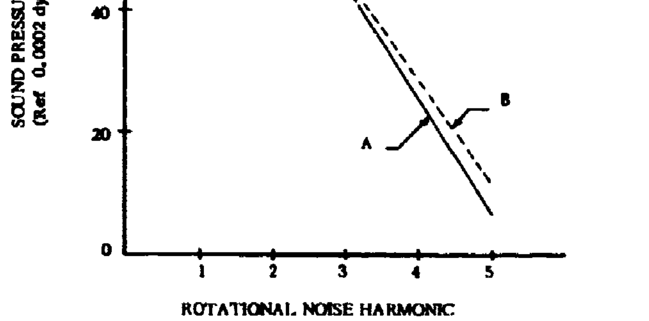

Figure 37. Effect of Blade Loading Distribution on Noise Harmonic Level

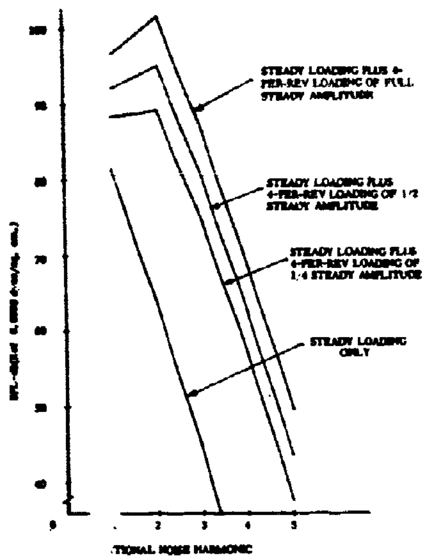

Figure 38. Effect of 4-per-rev Blade Loading on Harmonic Noise Levels

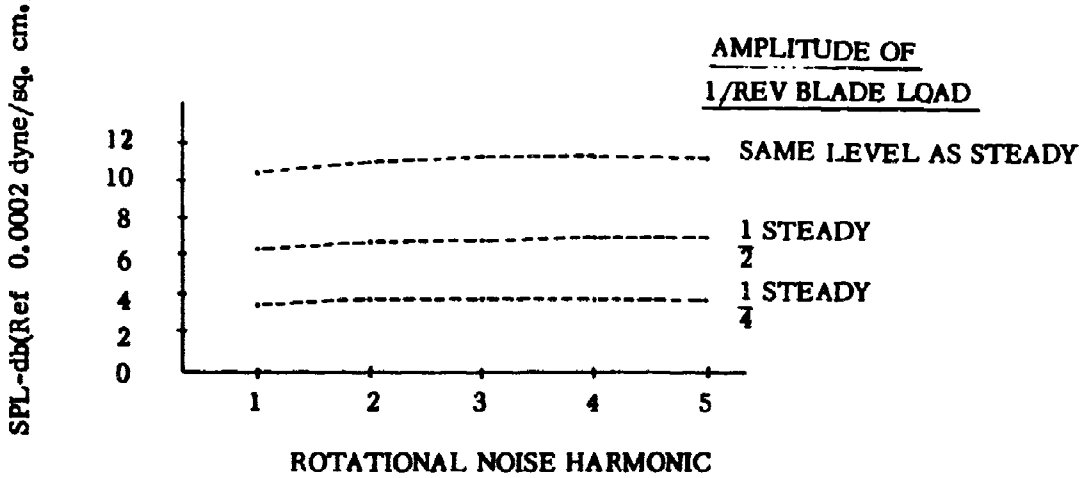

Figure 39. Effect of 1-per-rev Blade Loading on Rotational Noise Harmonics

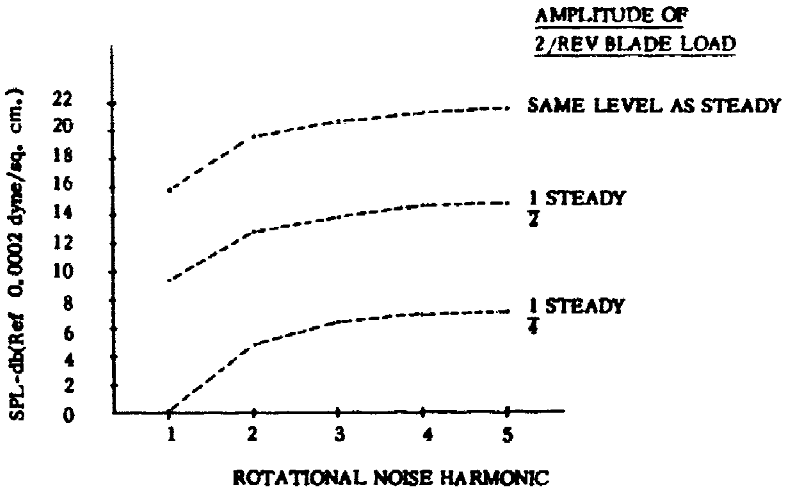

Figure 40. Effect of 2-per-rev Blade Loading on Rotational Noise Harmonics

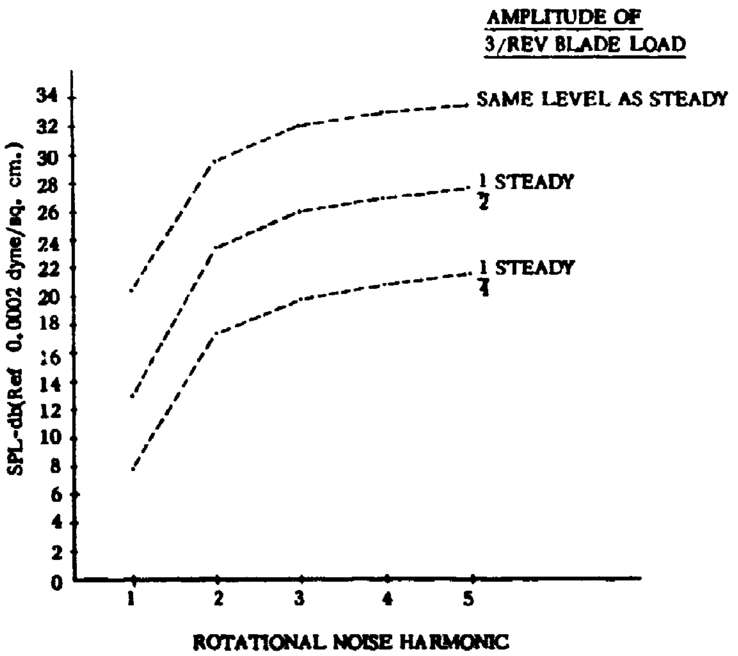

Figure 41. Effect of 3-per-rev Blade Loading on Rotational Noise Harmonics

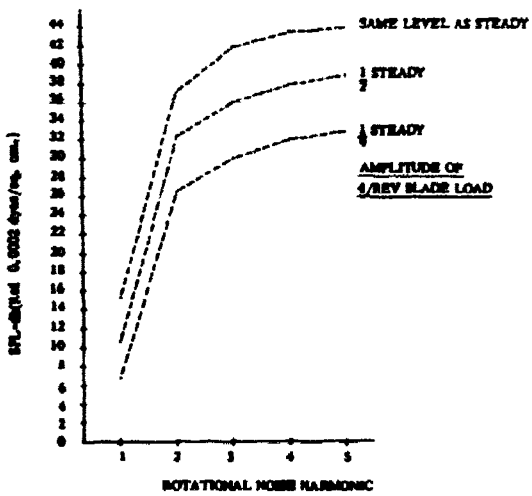

Figure 42. Effect of 4-per-rev Blade Loading on Rotational Noise Harmonics

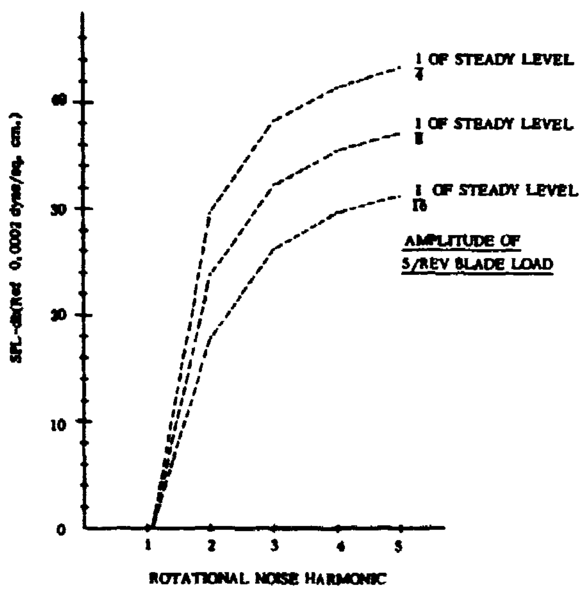

Figure 43. Effect of 5-per-rev Blade Loading on Rotational Noise Harmonics

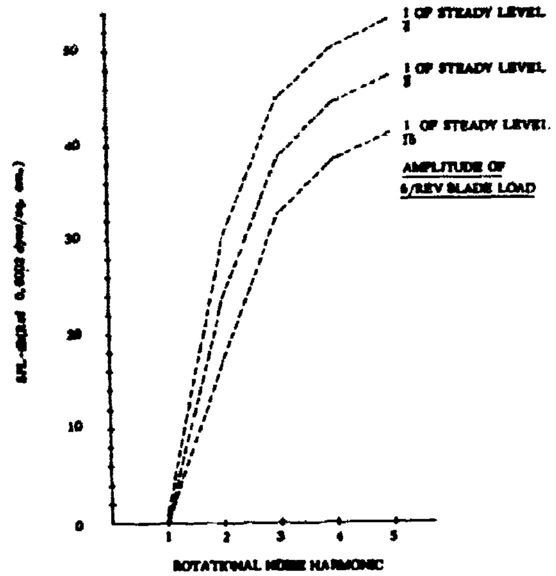

Figure 44. Effect of 6-per-rev Blade Loading on Rotational Noise Harmonics

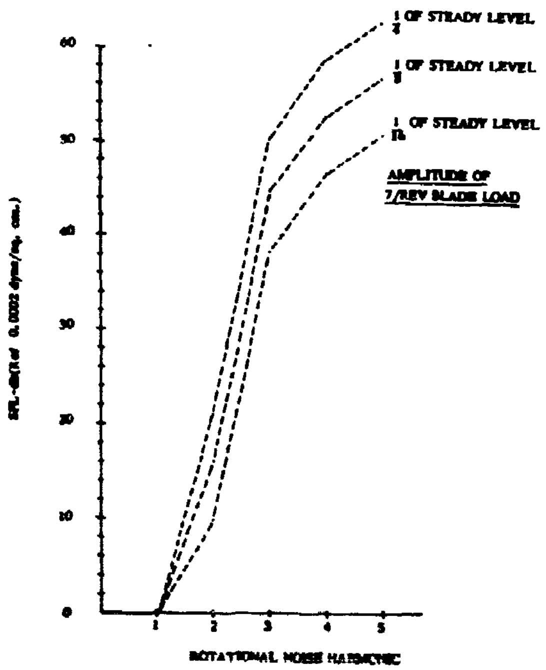

Figure 45. Effect of 7-per-rev Blade Loading on Rotational Noise Harmonics

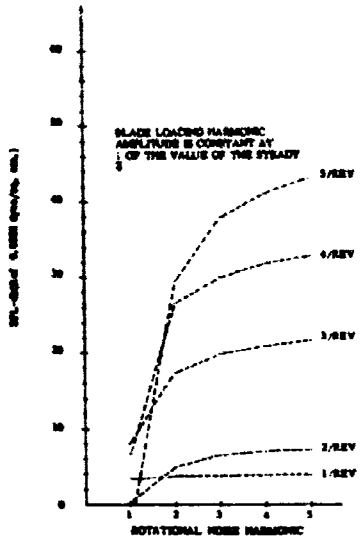

Figure 46. Influence of the 1st to the 5th Blade Loading Harmonics on Rotational Noise Harmonics

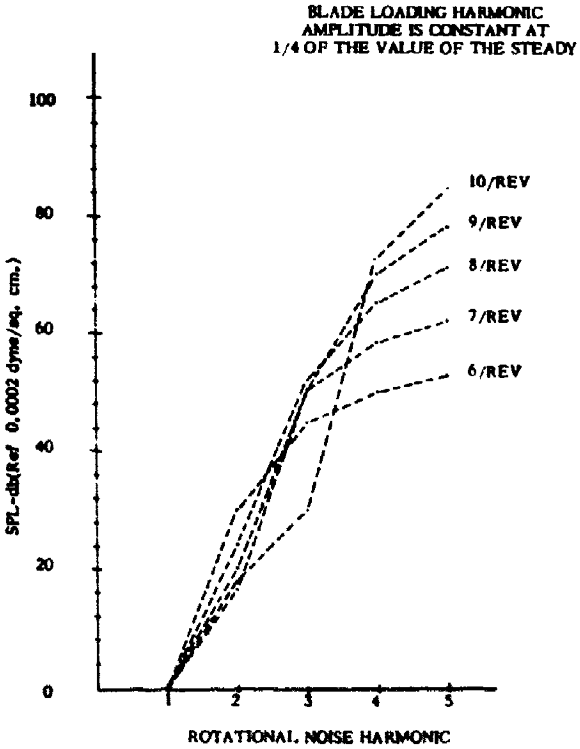

Figure 47. Influence of the 6th to the 10th Blade Loading Harmonics on Rotational Noise Harmonics

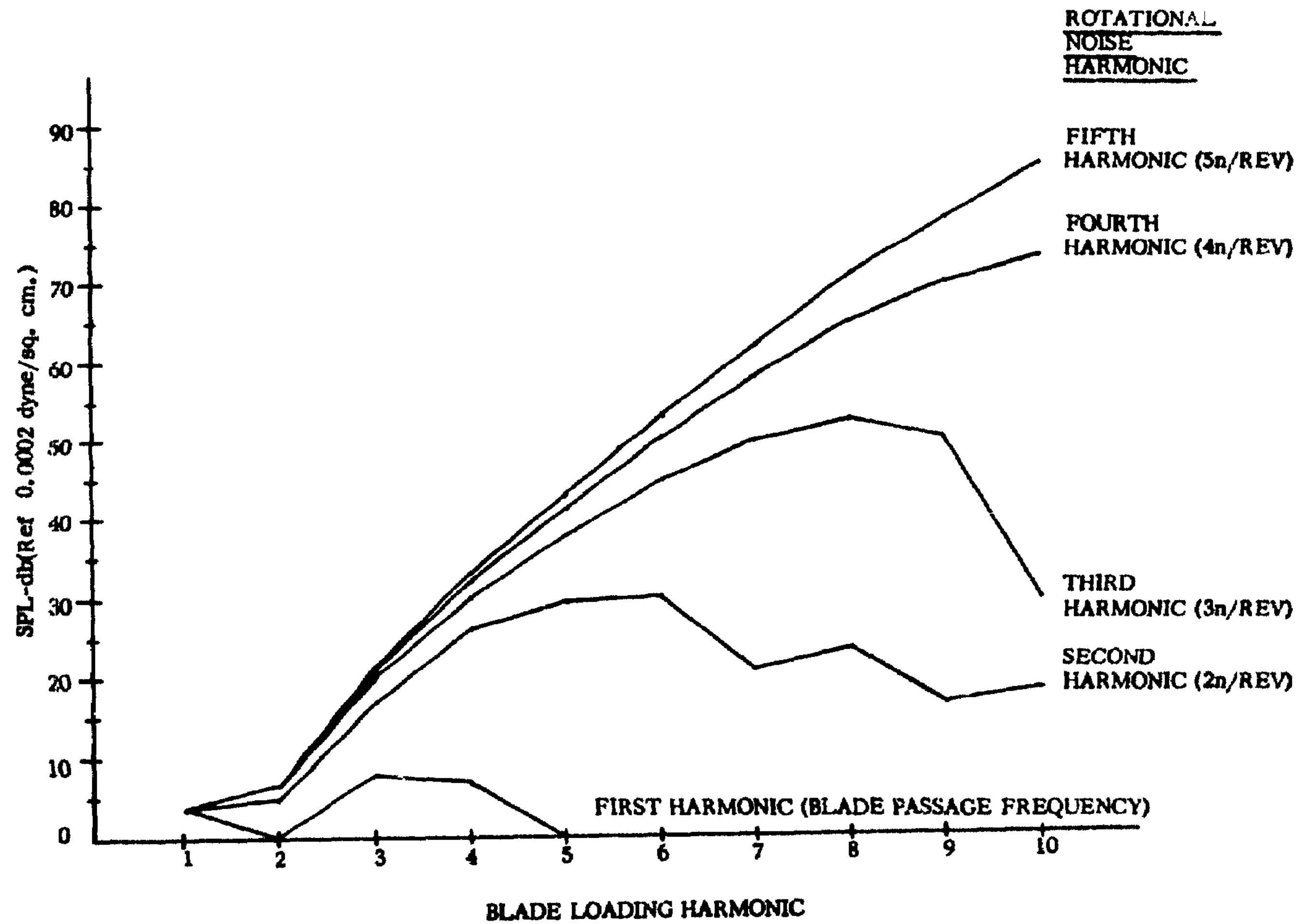

Figure 48. Additional Noise at the First to the Fifth Noise Harmonic Frequencies Due to the Introduction of 1-per-rev to 10-per-rev Harmonic Blade Loadings of One Quarter the Amplitude of the Steady Component

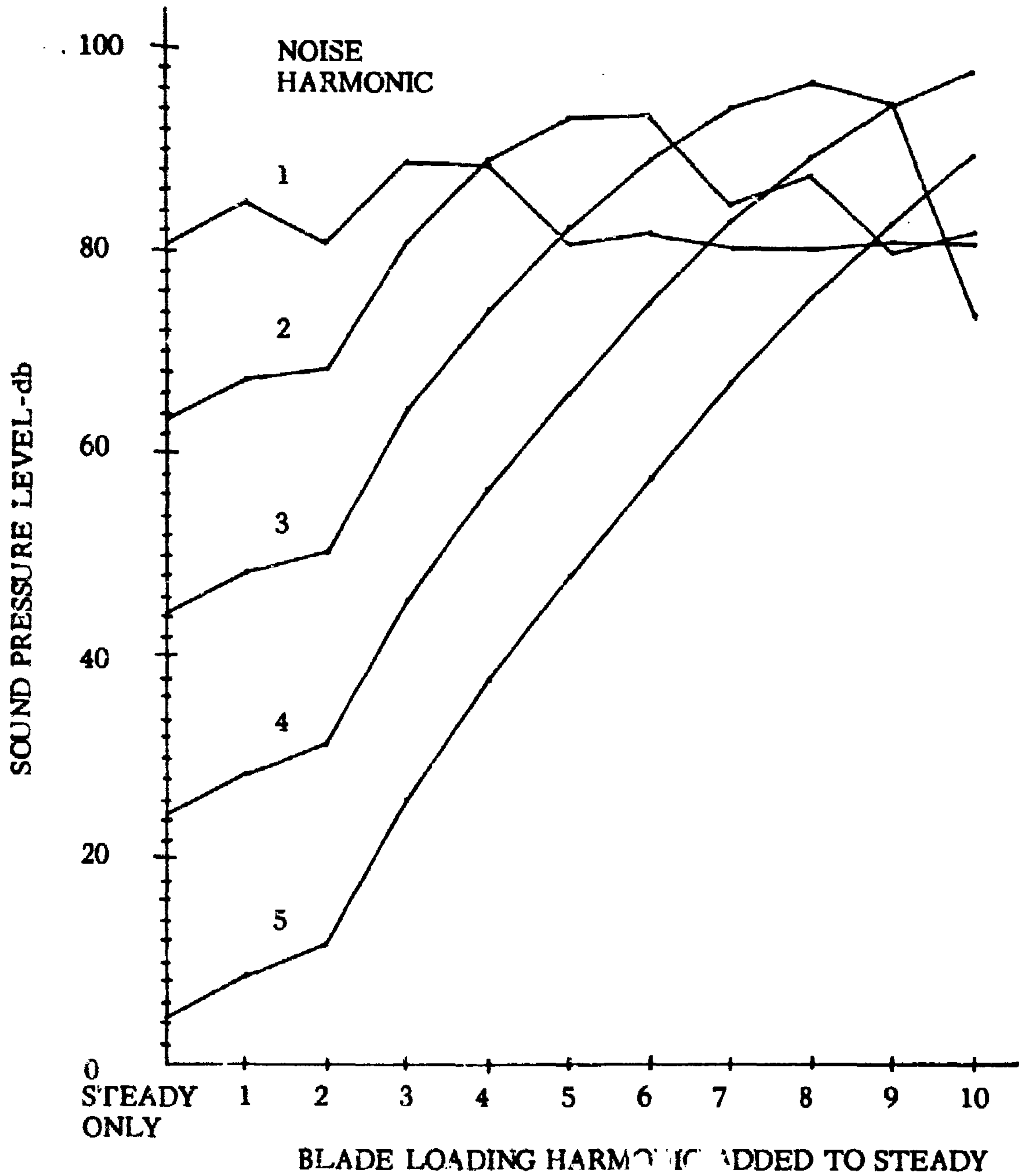

Figure 49. Sound Level Caused by a Rotor w[illegible] [illegible]eady Loading Plus a Harmonic Blade Loading of One Quarter the Amplitude of the Steady

CONCLUSIONS

It has been shown that single rotor overall vortex noise level for square tipped blades with uniform inflow can be calculated with excellent accuracy by the use of a simple formula developed in this study. The standard vortex noise spectrum is used for the unstalled condition, and another spectrum has been developed for use where stall is present. This stall spectrum contains higher levels in the upper frequencies. A reduction in rotor tip speed or thrust, or an increase in blade area (at constant thrust and tip speed) will reduce the overall vortex noise level. Vortex noise level is highly dependent on tip shape, and substantial reductions may be attained by proper design.

The solution derived for rotational noise may be used to calculate any number of harmonics in either the near or the far field under uniform or nonuniform conditions. Only single rotor systems, however, may be considered using the present solution. The only limitation to the number of harmonics that may be calculated appears to be the availability of accurate harmonic blade loading data. Harmonic blade loadings contribute significantly to the fundamental rotational harmonic and for all practical purposes completely determine detectability levels. Low-frequency rotational noise may be reduced by lowering blade loading and rotor speed. High harmonic rotational noise may be reduced by reducing the local stall and drag divergence tendencies of blades and by altering aeroelastic characteristics to minimize harmonic airloads.

Blade slap is a phenomenon which affects both rotational and vortex noise spectra and is generated by rapid changes of flow separation which occur during stall or drag-divergence conditions. Blade tip design is extremely important in attenuating blade slap. The trapezoidal shaped blade tip used in the present study produced significant reductions in blade slap noise level.

RECOMMENDATIONS FOR FURTHER STUDY

1. Conduct an analysis - test correlation program to evaluate the accuracy of the rotor noise analysis using the harmonic airload results of the NH-3A (S-61F) airload measurement program.

2. Undertake further development of existing aeroelastic-aerodynamic programs to extend their capabilities for predicting harmonic blade airloads to higher harmonics.

3. Perform a noise/performance/aeroelastic trade-off on an existing helicopter to define an optimum low-noise configuration. Modify a ship to this configuration for verification of results and for demonstration purposes.

4. Define the relationships between blade slap and the degree of stall, the extent of compressible drag-divergence, and tip vortex characteristics.

BIBLIOGRAPHY

1. Arnoldi, R. A., Propeller Noise Caused by Blade Thickness, United Aircraft Corporation Research Department, Report R-0896-1, East Hartford, Connecticut, January 10, 1956.

2. Bell Helicopter Company, A Study of the Origin and Means of Reducing Helicopter Noise, TCREC Technical Report 62-73, U. S. Army Transportation Research Command*, Fort Eustis, Virginia, November 1962.

3. Carmichael, D., and Mull, H., Recommended Design Trends for Quiet Tail Rotors, Sikorsky Aircraft Report SER-50307, Stratford, Connecticut, September 1962.

4. Curle, N., The Influence of Solid Boundaries Upon Aerodynamic Sound, Proceedings of the Royal Society, A, 231, London, England, 1955.

5. Davidson, I. M., and Hargest, T. J., "Helicopter Noise", Journal of the Royal Aeronautical Society, Volume 69, May 1965.

6. Fletcher, Harvey, and Munson, W. A., Loudness, Its Definition, Measurement, and Calculation, Journal of the Acoustical Society of America, Volume V, October 1933.

7. Garrick, I. E., and Watkins, Charles E., A Theoretical Study of the Effect of Forward Speed on the Free Space Sound-Pressure Field Around Propellers, NACA Report 1198, Langley Field, Virginia, 1954.

8. Gerstenberger, Walter, and Wood, Edward R., Analysis of Helicopter Aeroelastic Characteristics in High Speed Flight, AIAA Journal, Volume 1, Number 10, October 1963.

9. Gessow, Alfred, and Myers, Gerry C., Jr., Aerodynamics of the Helicopter, First Printing, The Macmillan Company, New York, 1952.

10. Gustafson, F. B., and Myers, G. C., Jr., Stalling of Helicopter Blades, NACA TM 1083, Washington, D. C., 1946.

* Now U. S. Army Aviation Materiel Laboratories.

11. Gutin, L., On the Sound Field of a Rotating Propeller, NACA TM 1195, Washington, D. C., October 1948.

12. Hicks, Chester W., and Hubbard, Harvey H., Comparison of Sound Emission From Two-Blade, Four-Blade, and Seven-Blade Propellers, NACA Technical Note 1354, Washington, D. C., July 1947.

13. Hubbard, Harvey H., and Maglieri, Domenic J., An Investigation of Some Phenomena Relating to Aural Detection of Airplanes, NACA Technical Note 4337, Washington, D. C., September 1958.

14. Hubbard, Harvey H., and Regier, Arthur A., Free Space Oscillating Pressures Near the Tips of Rotating Propellers, NACA Report 996, Washington, D. C., 1950.

15. Hubbard, Harvey H., and Regier, Arthur A., Propeller Loudness Charts for Light Airplanes, NACA Technical Note 1358 Washington, D. C., July 1947.

16. Hubbard, Harvey H., Propeller-Noise Charts for Transport Airplanes, NACA Technical Note 2968, Washington, D. C., June 1953.

17. Ingard, Uno, Sound Radiation from a Propeller in a Nonuniform Medium, Pratt & Whitney Aircraft, East Hartford, Connecticut, January 1964.

18. Lamb, H., Hydrodynamics, Sixth Edition, Cambridge University Press, London, England, 1932.

19. Lighthill, M. J., Sound Generated Aerodynamically, Proceedings of the Royal Society, A 211, London, England, 1952.

20. Loewy, R. G., Aural Detection of Helicopters in Tactical Situations, Part II, Institute for Defense Analysis Research Paper P-25, AD 409535, Alexandria, Virginia, May 1963.

21. Miller, R. H., Rotor Blade Harmonic Air Loading, IAS Paper No. 62-82, January 1962.

22. Mull, H. R., External Noise Characteristics of Two Commercial Transport Helicopters, United Acoustic Consultants Report R-642 and Addendum, Wilton, Connecticut, January 23, 1964.

23. Oestreicher, Hans L., "Field of a Spatially Extended Moving Sound Source", Journal of the Acoustical Society of America, Volume 29, Number 11, New York, N. Y., November 1957.

24. Piziali, R., and DuWaldt, F., A Method for Computing Rotary Wing Airload Distribution in Forward Flight, TREC Technical Report 62-44, U. S. Army Transportation Research Command, Fort Eustis, Virginia, July 1962.

25. Piziali, R., and DuWaldt, F., Computation of Rotary Wing Harmonic Airloads and Comparison with Experimental Results, American Helicopter Society, New York, New York, May 1962.

26. Powell, Alan, "Theory of Vortex Sound", The Journal of the Acoustical Society of America, Volume 36, Number 1, January 1964.

27. Roberts, John P., and Beranek, Leo L., Experiments in External Noise Reduction of a Small Pusher-Type Amphibian Airplane, Washington, D. C. NACA TM 2727, July 1952.

28. Roshko, Anatol, Experiments on the Flow Past a Circular Cylinder at Very High Reynolds Number, Journal of Fluid Mechanics, Volume 10, Part 3, May 1961.

29. Scheiman, James, A Tabulation of Helicopter Rotor-Blade Differential Pressures, Stresses, and Motions as Measured in Flight, NASA TM X-952, Langley Station, Hampton, Virginia, March 1964.

30. van de Vooren, A. I., and Zandbergen, P. J., Noise Field of a Rotating Propeller in Forward Flight, AIAA Journal, Volume 1 No. 7, July 1963.

31. Watkins, Charles E., and Durling, Barbara J., A Method for Calculation of Free-Space Sound Pressures Near a Propeller in Flight Including Considerations of a Chordwise Blade Loading, NACA TM 3809, Washington, D. C., 1956.

32. Wood, E. R., and Hilzinger, K. D., A Method for Determining the Fully Coupled Aeroelastic Response of Helicopter Rotor Blades, Presented at the American Helicopter Society Nineteenth Annual National Forum, Washington, D. C., May 1 - 4, 1963.

33. Yudin, E. Y., On the Vortex Sound From Rotating Rods, NACA TM No. 1136, Washington, D. C., March 1947.

34. Zandbergen, P. J., and van der Walle, F., On the Calculation of the Propeller Noise Field Around Aircraft, National Aero and Astronautical Research Institute, Amsterdam, Netherlands, NLR TM G-23, 1962.

Items 3 and 17 are not to be considered as subject data required to be furnished under this contract but are merely references that can be made available to the government on a limited rights basis.

DISTRIBUTION

US Army Materiel Command	5
US Army Aviation Materiel Command	6
US Army Aviation Materiel Laboratories	23
US Army Limited War Laboratory	1
US Army Human Engineering Laboratories	1
US Army Research Office-Durham	1
US Army Test and Evaluation Command	1
Plastics Technical Evaluation Center	1
US Army Medical R&D Command	1
US Army Combat Developments Command, Fort Belvoir	2
US Army Combat Developments Command Transportation Agency	1
US Army Combat Developments Command Experimentation Command	3
US Army War College	1
US Army Command and General Staff College	1
US Army Aviation School	1
US Army Tank-Automotive Center	2
US Army Electronics Command	2
US Army Aviation Test Activity, Edwards AFB	2
Air Force Flight Test Center, Edwards AFB	2
US Army Field Office, AFSC, Andrews AFB	1
Systems Engineering Group (RTD), Wright-Patterson AFB	1
Air Force Flight Dynamics Laboratory, Wright-Patterson AFB	1
Naval Air Systems Command	5
Chief of Naval Research	3
US Naval Research Laboratory	1
Marine Corps Liaison Officer, US Army Transportation School	1
Testing and Development Division, US Coast Guard	1
Manned Spacecraft Center, NASA	1
NASA Scientific and Technical Information Facility	2
NAFEC Library (FAA)	2
US Army Aviation Human Research Unit	2
US Army Board for Aviation Accident Research	1

Bureau of Safety, Civil Aeronautics Board	2
US Naval Aviation Safety Center, Norfolk	1
Federal Aviation Agency, Washington, D. C.	2
CAMI Library, FAA	1
Defense Documentation Center	20

APPENDIX I

SAMPLE CALCULATION OF VORTEX SOUND LEVELS

The vortex noise levels are easily calculated by use of equation 6 and the vortex sound spectra in Figure 1.

Using the CH-3C blade system operating at 203 rpm and producing a thrust of 19,000 pounds for our calculations, the system parameters listed in Table III are used.

Equation 6 is used to obtain the SPL at 300 feet.

$$SPL = 10 \log \frac{6.1 \times 10^{-27} A_B (V_{0.7})^6}{10^{-16}} + 20 \log \frac{C_L}{0.4}$$

From Table III

$$A_B = 217$$

Since for this configuration the drag is small compared to the lift (C_D=0.077), it is assumed that the lift is approximately equal to the thrust.

Then $$C_L = \frac{2T}{\rho A_B (V_{.7})^2}$$ (Reference 16)

Substituting the given values

$$C_L = \frac{(19{,}000)^2}{(0.002378)(217)(463)^2}$$

$$C_L = 0.35$$

Substituting these values in equation 6,

$$SPL = 10 \log \frac{6.1 \times 10^{-27} (217)(463)^6}{10^{-16}} + 20 \log \frac{0.35}{0.4}$$

$$SPL = 10 \log 1.3 \times 10^8 + 20 \log 0.875$$

$$SPL = 81.2 - 0.4$$

$$SPL = 80.8 \text{ @ } 300 \text{ feet}$$

To correct to distances of other than 300 feet from the rotor, utilize the expression

$$\Delta SPL = 20 \log \frac{300}{R}$$

In this case we wish to obtain the level at 225 feet to compare with measured data.

$$\Delta SPL = 20 \log \frac{300}{225}$$

$$\Delta SPL = 2.6 \text{ db}$$

Applying this correction to the level at 300 feet, we obtain

$$SPL = 80.8 + 2.6 \text{ or } 83.4 \text{ @ } 225 \text{ feet}$$

Since the operating range is below stall on the drag-divergence curve of Figure 21, the spectrum of Figure 19 should be used. With a calculated overall vortex level of 83 db at 225 feet, the spectrum is then predicted to be as follows:

Octave Band (CPS)	SPL (db Ref. 0.0002 dyne/sq. cm.)
150-300	75.0
300-600	79.0
600-1200	75.0
1200-2400	74.5
2400-4800	70.5
4800-9600	66.0

The measured values for this condition were:

150-300	75.0
300-600	78.0
600-1200	74.0
1200-2400	74.5
2400-4800	70.5
4800-9600	66.0

The overall level for the measured noise can be obtained by combining the octave band levels logarithmically. To obtain the overall SPL from octave band levels, first determine the intensity ratios of the individual octaves.

$$SPL_1 = 10 \log \frac{I_1}{I_0} \qquad \frac{I_1}{I_0} = 10^{\left(\frac{SPL_1}{10}\right)}$$

$$SPL_2 = 10 \log \frac{I_2}{I_0} \qquad \frac{I_2}{I_0} = 10^{\left(\frac{SPL_2}{10}\right)}$$

Sum the intensity ratios to obtain the overall intensity ratio.

$$\frac{I_T}{I_0} = \frac{I_1}{I_0} + \frac{I_2}{I_0} + \cdots$$

Convert to overall SPL.

$$SPL = 10 \log \frac{I_T}{I_0}$$

The results are summarized below:

Octave Band (CPS)	SPL (db) Measured	SPL (db) Calculated
Overall	82.0	83.0
150-300	75.0	75.0
300-600	78.0	79.0
600-1200	74.0	75.0
1200-2400	74.5	74.5
2400-4800	70.5	70.5
4800-9600	66.0	66.0

APPENDIX II

VORTEX NOISE TEST INSTRUMENTATION

A block diagram of the instrumentation used in the test program is presented in Figure 50. The acoustic signal was picked up with a low impedance moving-coil microphone. The microphone was coupled to a General Radio 1551-C Sound Level Meter which served as a calibrated pre-amplifier and decade attenuator. The output of the sound level meter was recorded on a Nagra III B tape recorder. The overall system was calibrated electrically prior to each series of measurements.

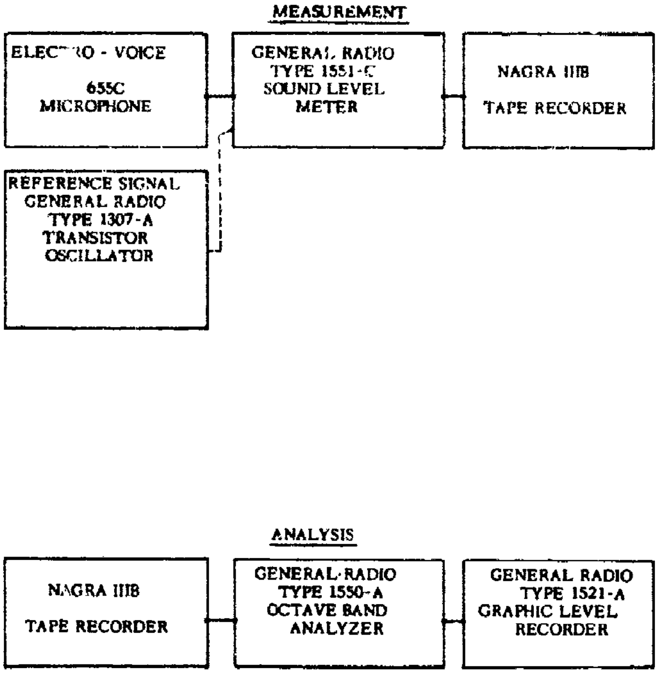

Figure 50. Vortex Noise Test Instrumentation

The recorded data was played back through an octave band analyzer. The octave band levels were recorded with a graphic level recorder. Because of the rapidly changing position of the rotating source and the proximity of the microphone with respect to the source, each of the octave bands showed short time variations or modulation. In addition, there were longer time variations that were attributed to changing wind conditions. These time variations were averaged out by graphically recording the levels of the individual octaves and noting the midpoint of the spread. The modulation was found to be higher at the lower end of the spectrum than at the high-frequency end of the spectrum.

The time-averaged data was then corrected for system response and the octave band levels were tabulated. The overall vortex noise level was computed by summing the corrected levels in the individual octaves from the 150-300 cps band to the 4800-9600 cps band.

APPENDIX III

CALCULATION OF PARTIAL DERIVATIVES

Calculate $\frac{\partial S}{\partial x}$ knowing

$$S^2 = R^2 + r^2 - 2rR\cos\sigma(\cos\theta\cos\psi + \sin\theta\sin\psi) \qquad (29)$$

From Figure 3

$$R^2 = x^2 + y^2 + z^2 \ , \ \cos\theta = \frac{x}{-R\cos\sigma} \ , \ \sin\theta = \frac{y}{R\cos\sigma}$$

Therefore, write

$$S^2 = x^2 + y^2 + z^2 + r^2 - 2r\cos\sigma\frac{x^2+y^2+z^2}{(x^2+y^2+z^2)\cos\sigma}(-x\cos\psi + y\sin\psi) \qquad (30)$$

which reduces to

$$S^2 = x^2 + y^2 + z^2 + r^2 - 2r(-x\cos\psi + y\sin\psi) \qquad (31)$$

Taking the partial with respect to x

$$S\frac{\partial S}{\partial x} = x + r\cos\psi \qquad (32)$$

but noting that $x = -R\cos\sigma\cos\theta$ this reduces to

$$\frac{\partial S}{\partial x} = \frac{-R}{S}\cos\sigma\cos\theta + \frac{r}{S}\cos\psi \qquad (33a)$$

Similarly, for the y and z directions

$$\frac{\partial S}{\partial y} = \frac{R}{S}\cos\sigma\sin\theta - \frac{r}{S}\sin\psi \qquad (33b)$$

$$\frac{\partial S}{\partial z} = \frac{R}{S}\sin\sigma \qquad (33c)$$

It is desirable to eliminate the second term of Equations (33a) and (33b) in order to simplify the solution. From the ratio of magnitudes of the two terms it appears that this elimination may be valid if the field point distance R is one diameter or more.

Equation (33) then becomes

$$\frac{\partial S}{\partial x} = \frac{-R}{S} \cos\sigma \cos\theta$$

$$\frac{\partial S}{\partial y} = \frac{R}{S} \cos\sigma \sin\theta$$

$$\frac{\partial S}{\partial z} = \frac{R}{S} \sin\sigma$$

APPENDIX IV

APPROXIMATION OF CHORDWISE PRESSURE DISTRIBUTION AS A STEP FUNCTION PLUS SCALE SHIFT

The Fourier series expansion of the initial blade passage time history in the rotor disk (Figure 5) is

$$\Delta P(r,\psi,t) = \sum_{m=1}^{\infty} A_m \cos mn\Omega t + B_m \sin mn\Omega t$$

where

$$A_m = \frac{n\Omega}{\pi} \int_{\psi/\Omega}^{\psi/\Omega + 2\pi/n\Omega} \Delta P(r,\psi,t) \cos mn\Omega t \, dt \tag{34a}$$

$$B_m = \frac{n\Omega}{\pi} \int_{\psi/\Omega}^{\psi/\Omega + 2\pi/n\Omega} \Delta P(r,\psi,t) \sin mn\Omega t \, dt \tag{34b}$$

By shifting the time scale by ψ/Ω the pressure pulse appears as in Figure 51. The corresponding mathematical representation is

$$\Delta P(r,\psi,t) = \sum_{m=1}^{\infty} a_m \cos(mn\Omega t - mn\psi) + b_m \sin(mn\Omega t - mn\psi)$$

with

$$a_m = \frac{n\Omega}{\pi} \int_{0}^{2\pi/n\Omega} \Delta P(r,\psi,T + \psi/\Omega) \cos mn\Omega T \, dT \tag{35a}$$

$$b_m = \frac{n\Omega}{\pi} \int_{0}^{2\pi/n\Omega} \Delta P(r,\psi,T + \psi/\Omega) \sin mn\Omega T \, dT \tag{35b}$$

where

$$T = t - \psi/\Omega$$

As an approximation to the function of Figure 51, a step function will be used as shown in Figure 52. The amplitude of this step function is

$$\overline{\Delta P} = \int_{0}^{a/\Omega r} \frac{\Delta P(r,\psi,t)}{a/\Omega r} \, dt \tag{36}$$

An additional scale shift of $a/2\Omega r$ permits expansion of the function of Figure 52 as a cosine series and gives

$$\Delta P(r,\psi,t) = \sum_{m=1}^{\infty} a_m \cos\left(mn\Omega t - mn\psi - \frac{man}{2r}\right) \tag{37}$$

where

$$a_m = \frac{2}{m\pi} \sin \frac{man}{2r} \; \overline{\Delta P}$$

which corresponds to the function of Figure 6.

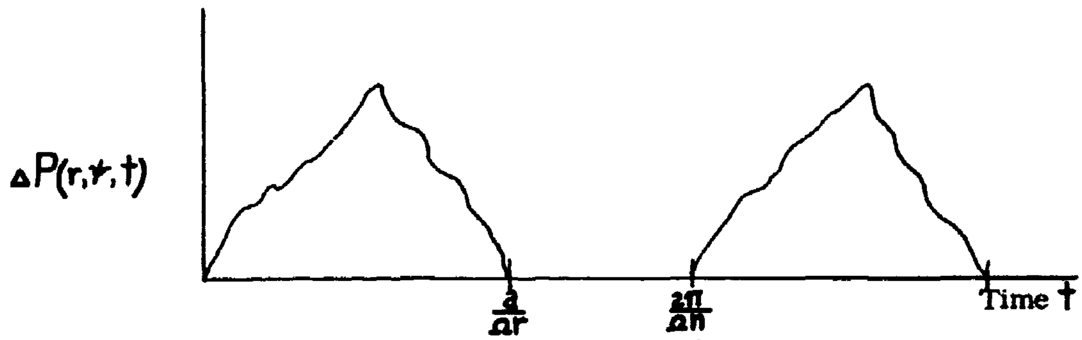

Figure 51. Time History of Blade Passage Over $r\,dr\,d\psi$ After Time Shift

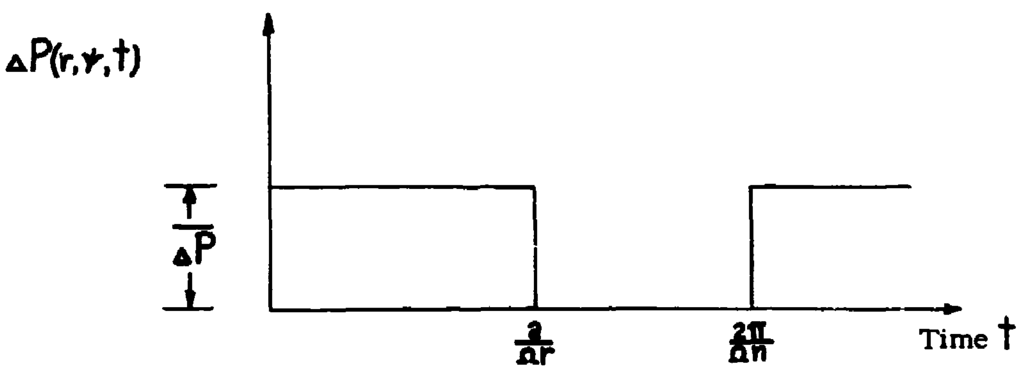

Figure 52. Step Function Approximation

APPENDIX V

DEFINITION OF BLADE PITCH ANGLE

Blade angle β is controlled by collective pitch, cyclic pitch, and twist. With the coordinate system of Figure 2, the following is true:

longitudinal cyclic pitch angle = $\beta_1 \cos\psi$

lateral cyclic pitch angle = $\overline{\beta}_1 \sin\psi$

where β_1 and $\overline{\beta}_1$ are the longitudinal and lateral cyclic pitch magnitudes, respectively. The effect of negative blade twist is accounted for as follows:

pitch angle change due to twist = $-\gamma(r - r_0)$

where

γ is the twist rate

r_0 is the blade radial station at which twist begins.

The expression for pitch angle resulting from twist is based on the assumption that the collective pitch angle is measured at the blade root. Combining the effects of cyclic pitch, twist effect, and β_0 the collective pitch angle, the true blade pitch angle is obtained.

$$\beta = \beta_0 - \gamma(r - r_0) + \beta_1 \cos\psi + \overline{\beta}_1 \sin\psi$$

APPENDIX VI

DESCRIPTION OF PROGRAM FOR CALCULATING ROTATIONAL NOISE

A program has been developed to facilitate the calculation of rotor rotational noise from equation 26 of this report. This is a Fortran IV program intended for use on the IBM 7094/44 D. C. S. As explained previously, the solution represents sound pressure at a point for rotational noise at the mth harmonic of blade passage. The solution may be used for calculating the rms sound pressure at any point in the near or far field outside one diameter from the rotor. The solution's accuracy decreases with increasing rotor system translational speed up to Mach 0.3 which is the practical limit for accuracy.

Method and Subprograms

The method used repeatedly evaluates the basic sound pressure equation given in the analysis. This includes a double integration. One integration is around the rotor disk with the sample points (azimuth angles) chosen at constant intervals. Subroutine SIMCOR, which used Simpsons (1/3) Rule with correction term was chosen to perform this integration. The other integration is along the radius where sample radial stations are unevenly spaced, hence, requiring the use of subroutine AVQUAD. This is a method whereby several intervals are approximated by "averaged quadratics" and integrated analytically. The flow diagram is shown in Figure 53.

Running time can be approximated at 20 sec. plus 5 sec. per field point. 5,000 units of output is sufficient unless several causes are run with all output options on. The deck setup is as follows:

```
$ DCID           with facility accounting information

$ EXECUTE        IBJOB

$ IBJOB          MAP

            Binary Deck      Rotational Noise

            Binary Deck      SIMCOR

            Binary Deck      AVQUAD

7/8 END OF JOB

   DATA
```

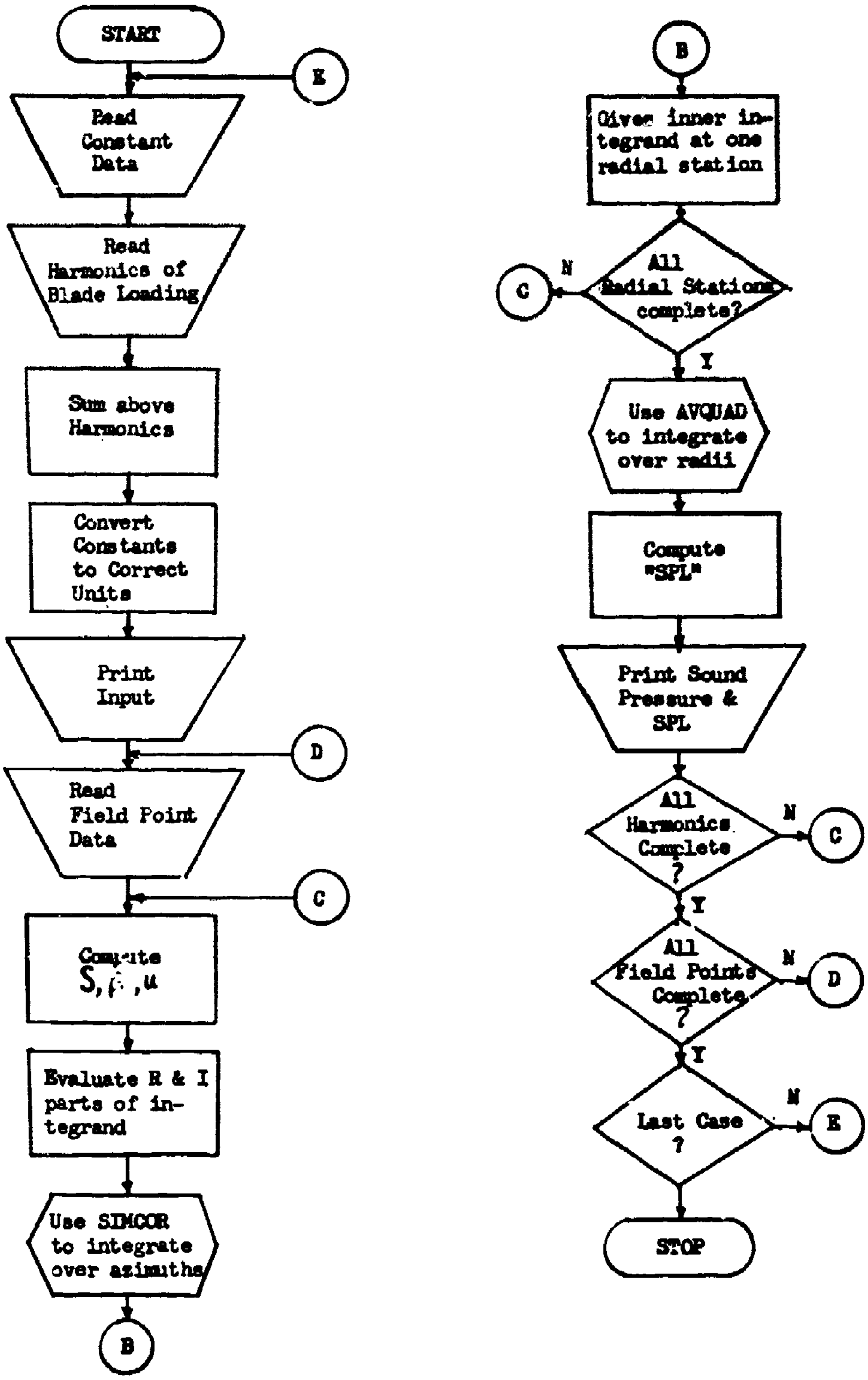

Figure 53. Computer Flow Diagram

7/8 END OF JOB

$ IBSYS

$ PAUSE

$ PAUSE

Program Parameters

The parameters which must be known to use the program and their units are listed below:

n	Number of rotor blades
Ω	Angular velocity of rotor, revolutions per minute
a	Blade chord, inches
c	Velocity of sound, feet per second
R_0	Radius at start of blade twist, inches
β_0	Collective (steady) pitch angle, degrees
β_1	Cosine component of cyclic pitch (longitudinal), degrees
$\overline{\beta_1}$	Sine component of cyclic pitch (lateral), degrees
γ	Blade twist rate, degrees per inch
L_0	Steady blade section loading for one radial station, pounds per inch
L_m	Cosine component of the mth harmonic of blade section loading for one radial station, pounds per inch
M_m	Sine component of the mth harmonic of blade section loading for one radial station, pounds per inch
R	Distance from center of rotor to point at which noise level is to be calculated, feet

θ Angle in rotor plane between longitudinal axis of helicopter (0 degrees at tail) and point at which level is to be calculated, positive in direction of rotor rotation, degrees

σ Angle in plane of rotor axis between rotor plane and point at which level is to be calculated, positive in direction of rotor thrust, degrees

Figures 2 and 3 show system parameters.

Input Format

The input format, which is to be used for every case is described below. The input format is shown on the coding form in Figure 54. A sample case is shown in Figure 55.

Card 1: Title Card

Col. 1 - 1, Col. 2 - any desired title

Card 2: Basic Constants

Col. 2 - end code = 0 last case; = 1 case(s) follow

Col. 3 & 4 - (right adjusted) number of field points

Col. 5-12* - n

Col. 13-20* - Ω

Col. 21-28* - a

Col. 29-36* - c

Col. 37-44* - R_o

Col. 45-52* - β_o

Col. 53-60* - β_1

Col. 61-68* - $\overline{\beta_1}$

Col. 69-76* - γ

*Must have decimal point.

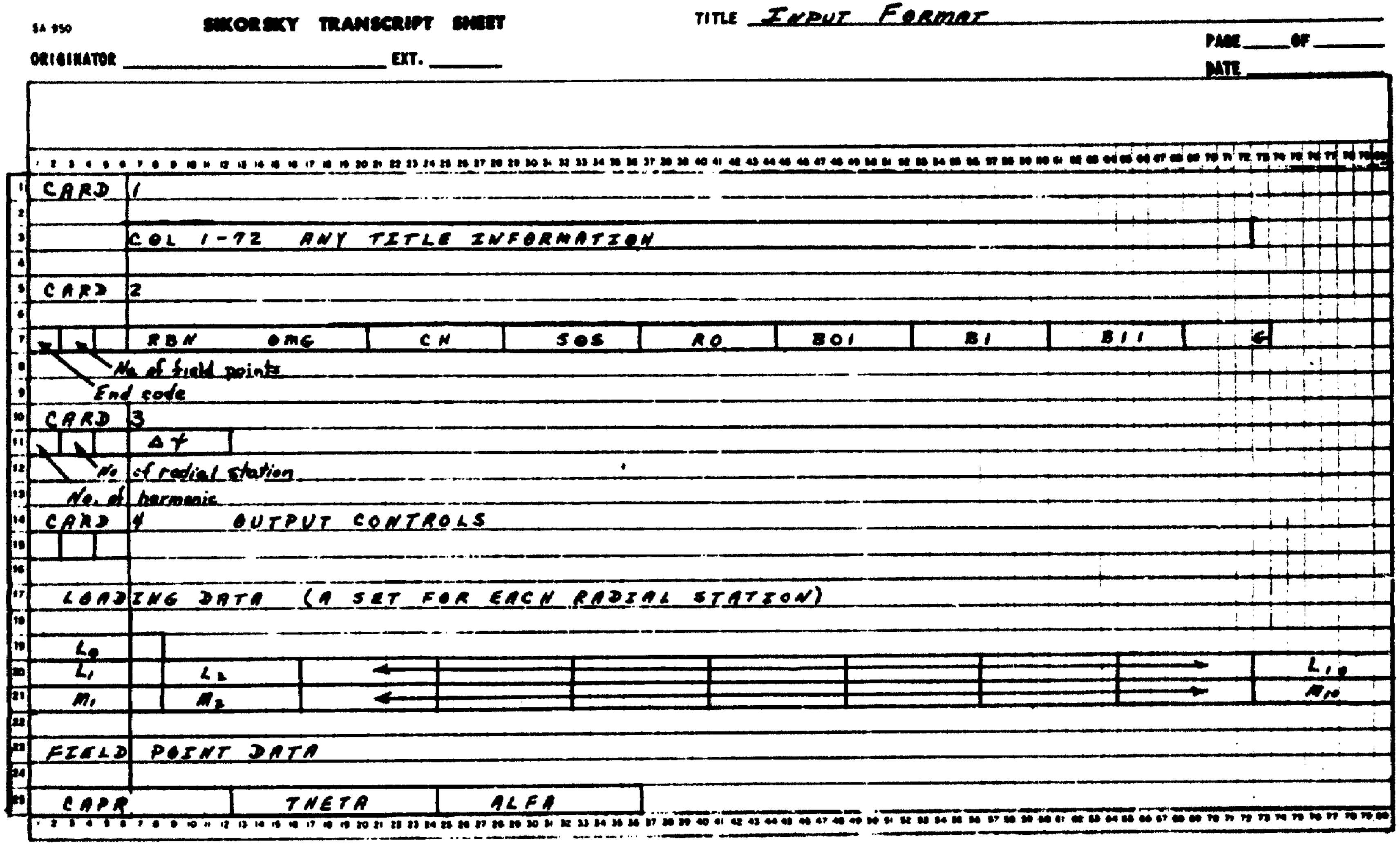

Figure 54. Input Format

SA 950 **SIKORSKY TRANSCRIPT SHEET** TITLE *Rotor Noise Prediction*

ORIGINATOR ______ EXT. ______ PAGE 1 OF 2

DATE ______

1	1 80 KNOT CRUISE DATA 5 58 NASA TM X 952 TABLE 13									
2	0 1 4.0	214.0	16.0	1126.0	50.0	13.08	2.21	-5.28	0.024	
3	4 8 2.0									
4	000000									
5	84.0	134.5	185.0	262.0	286.0	302.0	319.0	336.0		
6										
7	2.175									
8	-1.949	.643	-.322	-.070	-.048	.061	-.024	.025	.063	.027
9	2.157	-.730	.414	.026	-.074	.080	-.039	-.011	-.034	-.019
10										
11	6.341									
12	-2.083	1.373	-.082	-.033	-.014	-.002	-.055	-.094	-.081	-.093
13	3.209	-.608	.380	-.171	-.162	-.140	-.080	-.079	-.105	-.083
14										
15	9.111									
16	-1.512	2.028	.252	-.018	.123	.162	-.011	.044	.000	-.012
17	3.186	-.115	.599	.017	-.198	-.100	-.007	-.037	.051	-.053
18										
19	17.475									
20	-.217	3.331	1.153	.237	.028	.206	.289	-.215	-.111	.104
21	-.516	1.147	.677	-.573	-.337	-.008	.123	-.026	-.160	.162
22										
23	18.889									
24	1.820	3.068	2.156	.663	-.177	.339	-.060	.126	.083	-.419
25	-2.687	.370	.047	-.303	1.188	.106	.301	-.395	-.220	.178

Figure 55 a. Sample Input Sheet

SA 950

SIKORSKY TRANSCRIPT SHEET

TITLE *Rotor Noise Prediction*

ORIGINATOR ______ EXT. ______

PAGE 2 OF 2

DATE ______

1	19.036									
2	3.158	2.307	1.894	1.064	-.130	.181	-.160	-.056	.064	-.041
3	-3.888	.159	-.122	.028	-1.180	-.277	.415	.036	-.214	-.041
4										
5	19.556									
6	3.608	1.616	1.622	1.242	-.128	.190	.007	-.334	-.038	.503
7	-3.201	-.013	-.415	.512	-.772	-.758	.395	.553	-.369	-.349
8										
9	0.0									
10	0.0	0.0	0.0	0.0	0.0	0.0	0.0	0.0	0.0	0.0
11	0.0	0.0	0.0	0.0	0.0	0.0	0.0	0.0	0.0	0.0
12										
13	320.0		90.0		-37.0					
14										
15										
16										
17										
18										
19										
20										
21										
22										
23										
24										
25										

Figure 55 b. Sample Input Sheet (Cont.)

Card 3: Control Constants

Col. 1 & 2 - number of harmonics of rotational noise desired ($1 \leq N \leq 10$) (right adjusted)

Col. 4 - number of radial stations ($4 \leq N \leq 8$)

Col. 5-12 - angular increment of integration, degree (with decimal point)

(NOTE: $(360/\Delta\Psi)$ = even integer, $\Delta\Psi \geq \frac{1}{2}$ degree

Card 4: Output Controls

= 00 intermediate output not desired

= 99 intermediate output desired

Col. 1 & 2 - controls printout of input and radial integration

Col. 3 & 4 - controls printout of azimuthal integrations

Col. 5 & 6 - controls printout of S, β, u (from equation 26 of the report)

Card 5: Radial blade stations in fields of 9, inches*

For each radial station:

L_0 in Col. 1-8* on first card

L_1 - L_{10} in fields of 8* on second card

M_1 - M_{10} in fields of 8* on third card

For each field point:

One card with three parameters in fields of twelve, R, θ, σ, in that order (decimal points required).

*All fields specified must contain points.

Notes Regarding the Input Format

A case (Card 2, Col. 2) is a complete set of input data with a number of harmonics, fields points, etc. A new case would require a new title, a new set of basic constants, etc.

The number of field points here (Card 2, Col. 3 & 4) must agree with the number of cards describing the individual field points which are the last set of input cards.

The number of rotational noise harmonics desired (Card 3, Col. 1 & 2) partially determines the program running time.

The number of radial stations (Card 3, Col. 4) is arbitrary and is dependent on the number of stations at which blade loading is available. Evenly spaced stations over the length of the blade are desirable because the program interpolates between points. When the program is run at Sikorsky Aircraft, the last station is at the blade tip and the loading is zero at this position.

The angular increment of integration (Card 3, Col. 5-12) must be small to obtain a valid solution. If only one harmonic of rotational noise is to be calculated, an increment as large as 15 degrees may be used. When 10 harmonics of rotational noise are to be calculated,a maximum increment of 2 degrees is tolerable. Slightly increased accuracy may be gained by further reducing the increment, however, computer running time is increased accordingly.

The intermediate data printout which is determined by the output control card (Card 4) was used primarily for debugging the program. The normal printout includes the station number and radius, azimuth number and angle, section loading for each radial and azimuth position, field point coordinates, sound pressure and sound pressure level. The intermediate output adds a great deal of volume to the output and is not ordinarily required.

The number of radial blade stations (Card 5) must correspond to that specified in Card 3, Col. 4.

Description of Sample Case

The data for the sample 80-knot flyby case was taken from NASA TM X-952, "A Tabulation of Helicopter Rotor Blade Differential Pressures, Stresses, and Motions as Measured in Flight". The ship used was an H-34 (Sikorsky S-58) helicopter. Rotational noise was calculated for 5 harmonics of rotational noise from the main rotor at 11 field points.

The blade root pitch (β_0 , β_1 , $\bar{\beta}_1$) was taken from the pitch motion portion of Table 13(c) of the referenced NASA report. The harmonic loading for 7 blade stations was taken from Table 13(d) of the same report and the tip was considered the eighth station with zero loading assumed. The sample input and output for this case is shown in Figures 55 and 56, respectively.

80 KNOT CRUISE DATA S 58 NASA TM X 952 TABLE 13

B01 0.130000E 02 B1 0.221000E 01 B11 -0.528000E 01 CHORD 0.160000E 02 OMEGA 0.214000E 03 BLADES 4.

RADIUS AT START OF TWIST 0.500000E 02

BLADE SECTION LOADING

RADIUS / AZIMUTH		1 0.840000E 02	2 0.134500E 03	3 0.185000E 03	4 0.252000E 03	5 0.286000E 03	6 0.302000E 03	7 0.319000E 03	8 0.336000E 03
1	0.	0.601000E 00	0.517700E 01	0.101870E 02	0.222800E 02	0.264280E 02	0.273170E 02	0.276440E 02	0.
2	2.0	0.642918E 00	0.513755E 01	0.102737E 02	0.222088E 02	0.260848E 02	0.269272E 02	0.272413E 02	0.
3	4.0	0.680249E 00	0.513344E 01	0.103392E 02	0.220957E 02	0.257280E 02	0.264998E 02	0.267695E 02	0.
4	6.0	0.718226E 00	0.516894E 01	0.103870E 02	0.219448E 02	0.253609E 02	0.260445E 02	0.262533E 02	0.
5	8.0	0.754513E 00	0.524466E 01	0.104206E 02	0.217616E 02	0.249819E 02	0.255697E 02	0.257182E 02	0.
6	10.0	0.798796E 00	0.535762E 01	0.104435E 02	0.215521E 02	0.245888E 02	0.250623E 02	0.251875E 02	-0.
7	12.0	0.852369E 00	0.550179E 01	0.104589E 02	0.213228E 02	0.241768E 02	0.245871E 02	0.246802E 02	-0.
8	14.0	0.917756E 00	0.566874E 01	0.104696E 02	0.210808E 02	0.237415E 02	0.240873E 02	0.242087E 02	-0.
9	16.0	0.996413E 00	0.584860E 01	0.104780E 02	0.208325E 02	0.232803E 02	0.235844E 02	0.237776E 02	-0.
10	18.0	0.108854E 01	0.603105E 01	0.104858E 02	0.205841E 02	0.227930E 02	0.230787E 02	0.233836E 02	-0.
11	20.0	0.119304E 01	0.620633E 01	0.104944E 02	0.203405E 02	0.222826E 02	0.225698E 02	0.230167E 02	-0.
12	22.0	0.130756E 01	0.636608E 01	0.105047E 02	0.201053E 02	0.217555E 02	0.220574E 02	0.226618E 02	-0.
13	24.0	0.142876E 01	0.650406E 01	0.105170E 02	0.198804E 02	0.212208E 02	0.215412E 02	0.223610E 02	-0.
14	26.0	0.155255E 01	0.661656E 01	0.105315E 02	0.196662E 02	0.206899E 02	0.210224E 02	0.219168E 02	-0.
15	28.0	0.167454E 01	0.670254E 01	0.105480E 02	0.194616E 02	0.201746E 02	0.205031E 02	0.214948E 02	0.
16	30.0	0.179040E 01	0.676353E 01	0.105661E 02	0.192644E 02	0.196864E 02	0.199868E 02	0.210264E 02	0.
17	32.0	0.189631E 01	0.680316E 01	0.105852E 02	0.190713E 02	0.192346E 02	0.194785E 02	0.205102E 02	0.
18	34.0	0.198925E 01	0.682665E 01	0.106042E 02	0.188791E 02	0.188257E 02	0.189641E 02	0.199534E 02	0.
19	36.0	0.206735E 01	0.684007E 01	0.106219E 02	0.186845E 02	0.184622E 02	0.185102E 02	0.193709E 02	0.
20	38.0	0.212994E 01	0.684960E 01	0.106369E 02	0.184849E 02	0.181423E 02	0.180632E 02	0.187845E 02	0.
21	40.0	0.217765E 01	0.686080E 01	0.106473E 02	0.182786E 02	0.178606E 02	0.176491E 02	0.182201E 02	0.
22	42.0	0.221227E 01	0.687809E 01	0.106513E 02	0.180651E 02	0.176081E 02	0.172725E 02	0.177049E 02	0.
23	44.0	0.223657E 01	0.690427E 01	0.106466E 02	0.178448E 02	0.173741E 02	0.169359E 02	0.172639E 02	0.
24	46.0	0.225393E 01	0.694035E 01	0.106311E 02	0.176193E 02	0.171467E 02	0.166399E 02	0.169167E 02	-0.
25	48.0	0.226807E 01	0.698561E 01	0.106028E 02	0.173905E 02	0.169152E 02	0.163822E 02	0.166744E 02	-0.
26	50.0	0.228258E 01	0.703776E 01	0.105600E 02	0.171607E 02	0.166703E 02	0.161582E 02	0.165378E 02	-0.
27	52.0	0.230066E 01	0.709338E 01	0.105015E 02	0.169315E 02	0.164064E 02	0.159608E 02	0.164968E 02	-0.
28	54.0	0.232477E 01	0.714838E 01	0.104268E 02	0.167042E 02	0.161212E 02	0.157813E 02	0.165305E 02	-0.
29	56.0	0.235644E 01	0.719863E 01	0.103363E 02	0.164785E 02	0.158163E 02	0.156098E 02	0.166091E 02	-0.
30	58.0	0.239616E 01	0.724040E 01	0.102313E 02	0.162532E 02	0.154968E 02	0.154360E 02	0.166971E 02	-0.
31	60.0	0.244341E 01	0.727091E 01	0.101141E 02	0.160257E 02	0.151706E 02	0.152503E 02	0.167570E 02	-0.
32	62.0	0.249678E 01	0.728861E 01	0.998802E 01	0.157927E 02	0.148468E 02	0.150447E 02	0.167535E 02	-0.
33	64.0	0.255419E 01	0.729342E 01	0.985708E 01	0.155502E 02	0.145350E 02	0.148134E 02	0.166577E 02	0.
34	66.0	0.261314E 01	0.728668E 01	0.972591E 01	0.152947E 02	0.142433E 02	0.145534E 02	0.164512E 02	0.
35	68.0	0.267107E 01	0.727106E 01	0.959945E 01	0.150234E 02	0.139778E 02	0.142654E 02	0.161282E 02	0.
36	70.0	0.272565E 01	0.725025E 01	0.948265E 01	0.147353E 02	0.137415E 02	0.139535E 02	0.156977E 02	0.
37	72.0	0.277510E 01	0.722864E 01	0.938007E 01	0.144318E 02	0.135341E 02	0.136251E 02	0.151829E 02	0.
38	74.0	0.281835E 01	0.721082E 01	0.929568E 01	0.141169E 02	0.133523E 02	0.132909E 02	0.146194E 02	0.
39	76.0	0.285527E 01	0.720124E 01	0.923253E 01	0.137974E 02	0.131904E 02	0.129637E 02	0.140525E 02	0.
40	78.0	0.288664E 01	0.720381E 01	0.919264E 01	0.134830E 02	0.130415E 02	0.126581E 02	0.135328E 02	0.
41	80.0	0.291415E 01	0.722159E 01	0.917690E 01	0.131853E 02	0.128993E 02	0.123890E 02	0.131108E 02	0.
42	82.0	0.294026E 01	0.725667E 01	0.918511E 01	0.129174E 02	0.127590E 02	0.121708E 02	0.128321E 02	-0.
43	84.0	0.296794E 01	0.731006E 01	0.921614E 01	0.126926E 02	0.126189E 02	0.120165E 02	0.127320E 02	-0.
44	86.0	0.300049E 01	0.738176E 01	0.926816E 01	0.125234E 02	0.124815E 02	0.119363E 02	0.128320E 02	-0.
45	88.0	0.304117E 01	0.747091E 01	0.933890E 01	0.124199E 02	0.123537E 02	0.119371E 02	0.131368E 02	-0.
46	90.0	0.309300E 01	0.757600E 01	0.942600E 01	0.123890E 02	0.122470E 02	0.120220E 02	0.136330E 02	-0.

Figure 56 a. Sample Output Sheet

47	92.0	0.315848E 01	0.769510E 01	0.952729E 01	0.124335E 02	0.121761E 02	0.121895E 02	0.142902E 02	-0.
48	94.0	0.323990E 01	0.782612E 01	0.964107E 01	0.125514E 02	0.121581E 02	0.124361E 02	0.150029E 02	-0.
49	96.0	0.333674E 01	0.796702E 01	0.976627E 01	0.127361E 02	0.122100E 02	0.127460E 02	0.158949E 02	-0.
50	98.0	0.349097E 01	0.811599E 01	0.990252E 01	0.129785E 02	0.123473E 02	0.131111E 02	0.167238E 02	-0.
51	100.0	0.358015E 01	0.827134E 01	0.100501E 02	0.132582E 02	0.125808E 02	0.135153E 02	0.174870E 02	0.
52	102.0	0.372397E 01	0.843193E 01	0.102099E 02	0.135643E 02	0.129158E 02	0.139384E 02	0.181270E 02	0.
53	104.0	0.387988E 01	0.859668E 01	0.103830E 02	0.138772E 02	0.133497E 02	0.143618E 02	0.185966E 02	0.
54	106.0	0.404334E 01	0.876474E 01	0.105704E 02	0.141799E 02	0.138718E 02	0.147867E 02	0.188632E 02	0.
55	108.0	0.421749E 01	0.893530E 01	0.107727E 02	0.144581E 02	0.144632E 02	0.151350E 02	0.189113E 02	0.
56	110.0	0.439344E 01	0.910749E 01	0.109900E 02	0.147009E 02	0.150979E 02	0.154513E 02	0.187432E 02	0.
57	112.0	0.457037E 01	0.928028E 01	0.112210E 02	0.149024E 02	0.157442E 02	0.157026E 02	0.183784E 02	0.
58	114.0	0.474567E 01	0.945246E 01	0.114635E 02	0.150618E 02	0.163677E 02	0.158800E 02	0.178522E 02	0.
59	116.0	0.491702E 01	0.962263E 01	0.117139E 02	0.151837E 02	0.169338E 02	0.159783E 02	0.172094E 02	0.
60	118.0	0.508243E 01	0.978926E 01	0.119677E 02	0.152779E 02	0.174108E 02	0.159968E 02	0.165028E 02	-0.
61	120.0	0.524025E 01	0.995081E 01	0.122190E 02	0.153962E 02	0.177724E 02	0.159381E 02	0.157850E 02	-0.
62	122.0	0.538914E 01	0.101050E 02	0.124617E 02	0.154352E 02	0.180013E 02	0.158098E 02	0.151088E 02	-0.
63	124.0	0.552805E 01	0.102531E 02	0.126894E 02	0.155305E 02	0.180895E 02	0.156219E 02	0.145092E 02	-0.
64	126.0	0.565609E 01	0.103917E 02	0.128961E 02	0.156369E 02	0.180397E 02	0.153874E 02	0.140234E 02	-0.
65	128.0	0.577258E 01	0.105212E 02	0.130765E 02	0.158264E 02	0.178653E 02	0.151208E 02	0.136648E 02	-0.
66	130.0	0.587693E 01	0.106415E 02	0.132267E 02	0.160468E 02	0.175885E 02	0.148377E 02	0.134429E 02	-0.
67	132.0	0.596867E 01	0.107531E 02	0.133446E 02	0.163207E 02	0.172391E 02	0.145536E 02	0.133427E 02	-0.
68	134.0	0.604739E 01	0.108568E 02	0.134298E 02	0.166452E 02	0.168910E 02	0.142832E 02	0.133489E 02	-0.
69	136.0	0.611282E 01	0.109526E 02	0.134838E 02	0.170118E 02	0.164595E 02	0.140396E 02	0.134285E 02	0.
70	138.0	0.616481E 01	0.110419E 02	0.135099E 02	0.174074E 02	0.160981E 02	0.138341E 02	0.135575E 02	0.
71	140.0	0.620338E 01	0.111250E 02	0.135131E 02	0.178156E 02	0.157958E 02	0.136749E 02	0.137040E 02	0.
72	142.0	0.622876E 01	0.112017E 02	0.134990E 02	0.182178E 02	0.155744E 02	0.135680E 02	0.138421E 02	0.
73	144.0	0.624139E 01	0.112715E 02	0.134741E 02	0.185955E 02	0.154473E 02	0.135161E 02	0.139524E 02	0.
74	146.0	0.624198E 01	0.113352E 02	0.134448E 02	0.189318E 02	0.154186E 02	0.135199E 02	0.140245E 02	0.
75	148.0	0.623134E 01	0.113849E 02	0.134161E 02	0.192131E 02	0.154841E 02	0.135762E 02	0.140569E 02	0.
76	150.0	0.621080E 01	0.114245E 02	0.133929E 02	0.194306E 02	0.156316E 02	0.136822E 02	0.140564E 02	0.
77	152.0	0.618091E 01	0.114492E 02	0.133776E 02	0.195807E 02	0.158437E 02	0.138321E 02	0.140381E 02	0.
78	154.0	0.614348E 01	0.114563E 02	0.133713E 02	0.196654E 02	0.160997E 02	0.140198E 02	0.140205E 02	-0.
79	156.0	0.609949E 01	0.114436E 02	0.133727E 02	0.196921E 02	0.163781E 02	0.142389E 02	0.140246E 02	-0.
80	158.0	0.604996E 01	0.114089E 02	0.133793E 02	0.196728E 02	0.166595E 02	0.144828E 02	0.140703E 02	-0.
81	160.0	0.599571E 01	0.113512E 02	0.133865E 02	0.196223E 02	0.169282E 02	0.147460E 02	0.141737E 02	-0.
82	162.0	0.593729E 01	0.112700E 02	0.133892E 02	0.195574E 02	0.171739E 02	0.150233E 02	0.143450E 02	-0.
83	164.0	0.587491E 01	0.111660E 02	0.133814E 02	0.194944E 02	0.173922E 02	0.153107E 02	0.145872E 02	-0.
84	166.0	0.580845E 01	0.110408E 02	0.133579E 02	0.194480E 02	0.175844E 02	0.156047E 02	0.148955E 02	-0.
85	168.0	0.573745E 01	0.108969E 02	0.133122E 02	0.194297E 02	0.177567E 02	0.159029E 02	0.152584E 02	-0.
86	170.0	0.566118E 01	0.107371E 02	0.132417E 02	0.194480E 02	0.179186E 02	0.162032E 02	0.156988E 02	-0.
87	172.0	0.557857E 01	0.105648E 02	0.131435E 02	0.195018E 02	0.180812E 02	0.165037E 02	0.160753E 02	0.
88	174.0	0.548853E 01	0.103831E 02	0.130167E 02	0.195924E 02	0.182550E 02	0.168025E 02	0.164886E 02	0.
89	176.0	0.538975E 01	0.101949E 02	0.128624E 02	0.197120E 02	0.184481E 02	0.170975E 02	0.168720E 02	0.
90	178.0	0.528098E 01	0.100024E 02	0.126832E 02	0.198508E 02	0.186646E 02	0.173860E 02	0.172143E 02	0.
91	180.0	0.516100E 01	0.980700E 01	0.124830E 02	0.199960E 02	0.189040E 02	0.176650E 02	0.175020E 02	0.
92	182.0	0.502877E 01	0.960907E 01	0.122887E 02	0.201351E 02	0.191606E 02	0.179308E 02	0.177295E 02	0.
93	184.0	0.488346E 01	0.940814E 01	0.120396E 02	0.202558E 02	0.194244E 02	0.181795E 02	0.178978E 02	0.
94	186.0	0.472450E 01	0.920296E 01	0.118070E 02	0.203475E 02	0.196821E 02	0.184073E 02	0.180137E 02	0.
95	188.0	0.455164E 01	0.899181E 01	0.115736E 02	0.204030E 02	0.199185E 02	0.186106E 02	0.180886E 02	0.
96	190.0	0.436497E 01	0.877275E 01	0.113435E 02	0.204184E 02	0.201190E 02	0.187865E 02	0.181366E 02	-0.
97	192.0	0.416495E 01	0.854404E 01	0.111192E 02	0.203937E 02	0.202711E 02	0.189331E 02	0.181728E 02	-0.
98	194.0	0.395241E 01	0.830448E 01	0.109024E 02	0.203323E 02	0.203663E 02	0.190500E 02	0.182109E 02	-0.
99	196.0	0.372857E 01	0.805368E 01	0.106930E 02	0.202407E 02	0.204016E 02	0.191381E 02	0.182619E 02	-0.
100	198.0	0.349506E 01	0.779227E 01	0.104902E 02	0.201273E 02	0.203794E 02	0.192000E 02	0.183327E 02	-0.
101	200.0	0.325386E 01	0.752199E 01	0.102921E 02	0.200013E 02	0.203083E 02	0.192400E 02	0.184253E 02	-0.
102	202.0	0.300731E 01	0.724560E 01	0.100962E 02	0.198719E 02	0.202016E 02	0.192652E 02	0.185375E 02	-0.
103	204.0	0.275803E 01	0.696672E 01	0.989998E 01	0.197470E 02	0.200762E 02	0.192758E 02	0.186630E 02	-0.
104	206.0	0.250899E 01	0.668949E 01	0.970105E 01	0.196324E 02	0.199503E 02	0.192844E 02	0.187930E 02	-0.
105	208.0	0.226304E 01	0.641821E 01	0.949745E 01	0.195316E 02	0.198418E 02	0.192952E 02	0.189176E 02	0.
106	210.0	0.202346E 01	0.615688E 01	0.928800E 01	0.194453E 02	0.197655E 02	0.193137E 02	0.190276E 02	0.

Figure 56 b. Sample Output Sheet (Cont.)

107	212.0	0.179324E 01	0.590881E 01	0.967234E 01	0.193719E 02	0.197319E 02	0.193441E 02	0.191158E 02	0.
108	214.0	0.157518E 01	0.567630E 01	0.885098E 01	0.193081E 02	0.197456E 02	0.193890E 02	0.191783E 02	0.
109	216.0	0.137179E 01	0.546036E 01	0.862521E 01	0.192495E 02	0.198048E 02	0.194490E 02	0.192152E 02	0.
110	218.0	0.118504E 01	0.526066E 01	0.839690E 01	0.191912E 02	0.199018E 02	0.195230E 02	0.192304E 02	0.
111	220.0	0.101632E 01	0.507553E 01	0.816825E 01	0.191295E 02	0.200235E 02	0.196079E 02	0.192312E 02	0.
112	222.0	0.866332E 00	0.490227E 01	0.794156E 01	0.190616E 02	0.201539E 02	0.196996E 02	0.192270E 02	0.
113	224.0	0.735002E 00	0.473739E 01	0.771892E 01	0.189870E 02	0.202754E 02	0.197932E 02	0.192284E 02	0.
114	226.0	0.621527E 00	0.457713E 01	0.750202E 01	0.189068E 02	0.203719E 02	0.198635E 02	0.192451E 02	-0.
115	228.0	0.524405E 00	0.441789E 01	0.729198E 01	0.188243E 02	0.204305E 02	0.199663E 02	0.192846E 02	-0.
116	230.0	0.441549E 00	0.425669E 01	0.708930E 01	0.187441E 02	0.204436E 02	0.200383E 02	0.193510E 02	-0.
117	232.0	0.376443E 00	0.409180E 01	0.689387E 01	0.186715E 02	0.204102E 02	0.200983E 02	0.194445E 02	-0.
118	234.0	0.308343E 00	0.392197E 01	0.670507E 01	0.186114E 02	0.203363E 02	0.201472E 02	0.195610E 02	-0.
119	236.0	0.252490E 00	0.374858E 01	0.652199E 01	0.185676E 02	0.202345E 02	0.201851E 02	0.196926E 02	-0.
120	238.0	0.200337E 00	0.357356E 01	0.634359E 01	0.185418E 02	0.201223E 02	0.202267E 02	0.198298E 02	-0.
121	240.0	0.145751E 00	0.340019E 01	0.616897E 01	0.185328E 02	0.200206E 02	0.202699E 02	0.199610E 02	-0.
122	242.0	0.991844E-01	0.323250E 01	0.599759E 01	0.185364E 02	0.199507E 02	0.203262E 02	0.200760E 02	-0.
123	244.0	0.477858E-01	0.307484E 01	0.582938E 01	0.185454E 02	0.199318E 02	0.204040E 02	0.201674E 02	0.
124	246.0	-0.455011E-02	0.293131E 01	0.566490E 01	0.185496E 02	0.199780E 02	0.205112E 02	0.202315E 02	0.
125	248.0	-0.572108E-01	0.280531E 01	0.550529E 01	0.185372E 02	0.200964E 02	0.2[illegible]38E 02	0.202700E 02	0.
126	250.0	-0.108965E 00	0.269907E 01	0.535223E 01	0.184954E 02	0.202855E 02	0.20[illegible]56E 02	0.202898E 02	0.
127	252.0	-0.158126E 00	0.261336E 01	0.520776E 01	0.184118E 02	0.205344E 02	0.210566E 02	0.203028E 02	0.
128	254.0	-0.202760E 00	0.254737E 01	0.507408E 01	0.182760E 02	0.208236E 02	0.213132E 02	0.203246E 02	0.
129	256.0	-0.240926E 00	0.249875E 01	0.495330E 01	0.180804E 02	0.211261E 02	0.215981E 02	0.203728E 02	0.
130	258.0	-0.270916E 00	0.246389E 01	0.484719E 01	0.178216E 02	0.214103E 02	0.218998E 02	0.204644E 02	0.
131	260.0	-0.291467E 00	0.243826E 01	0.475695E 01	0.175007E 02	0.216426E 02	0.222041E 02	0.206137E 02	0.
132	262.0	-0.301933E 00	0.241698E 01	0.468304E 01	0.171239E 02	0.217908E 02	0.224943E 02	0.208297E 02	-0.
133	264.0	-0.302383E 00	0.239537E 01	0.462512E 01	0.167018E 02	0.218280E 02	0.227527E 02	0.211146E 02	-0.
134	266.0	-0.293628E 00	0.236953E 01	0.458200E 01	0.162491E 02	0.217349E 02	0.229619E 02	0.214619E 02	-0.
135	268.0	-0.277157E 00	0.233677E 01	0.455179E 01	0.157833E 02	0.215024E 02	0.231060E 02	0.218570E 02	-0.
136	270.0	-0.255000E 00	0.229600E 01	0.453200E 01	0.153230E 02	0.211330E 02	0.231720E 02	0.222770E 02	-0.
137	272.0	-0.229530E 00	0.224783E 01	0.451983E 01	0.148670E 02	0.206409E 02	0.231510E 02	0.226932E 02	-0.
138	274.0	-0.203217E 00	0.219456E 01	0.451239E 01	0.144923E 02	0.200508E 02	0.230388E 02	0.230730E 02	-0.
139	276.0	-0.178372E 00	0.213984E 01	0.450701E 01	0.141526E 02	0.193962E 02	0.228369E 02	0.233834E 02	-0.
140	278.0	-0.156859E 00	0.208833E 01	0.450147E 01	0.138777E 02	0.187160E 02	0.225517E 02	0.235943E 02	-0.
141	280.0	-0.140101E 00	0.204501E 01	0.449420E 01	0.136724E 02	0.180514E 02	0.221950E 02	0.236814E 02	0.
142	282.0	-0.128537E 00	0.201464E 01	0.448438E 01	0.135366E 02	0.174422E 02	0.217830E 02	0.236297E 02	0.
143	284.0	-0.121974E 00	0.200109E 01	0.447203E 01	0.134654E 02	0.169229E 02	0.213351E 02	0.234351E 02	0.
144	286.0	-0.119426E 00	0.200682E 01	0.445795E 01	0.134499E 02	0.165202E 02	0.208726E 02	0.231054E 02	0.
145	288.0	-0.119279E 00	0.203251E 01	0.444358E 01	0.134782E 02	0.162508E 02	0.204178E 02	0.226604E 02	0.
146	290.0	-0.119502E 00	0.207691E 01	0.443085E 01	0.135372E 02	0.161202E 02	0.199920E 02	0.221303E 02	0.
147	292.0	-0.117902E 00	0.213669E 01	0.442194E 01	0.136135E 02	0.161230E 02	0.196148E 02	0.215533E 02	0.
148	294.0	-0.112412E 00	0.220779E 01	0.441909E 01	0.136951E 02	0.162442E 02	0.193027E 02	0.209722E 02	0.
149	296.0	-0.101371E 00	0.228391E 01	0.442437E 01	0.137726E 02	0.164612E 02	0.190681E 02	0.204312E 02	0.
150	298.0	-0.837671E-01	0.235922E 01	0.443953E 01	0.138399E 02	0.167468E 02	0.189198E 02	0.199713E 02	-0.
151	300.0	-0.594068E-01	0.242809E 01	0.446589E 01	0.138953E 02	0.170724E 02	0.188617E 02	0.196270E 02	-0.
152	302.0	-0.290003E-01	0.248606E 01	0.450433E 01	0.139407E 02	0.174114E 02	0.188940E 02	0.194236E 02	-0.
153	304.0	0.585976E-02	0.253046E 01	0.455529E 01	0.139820E 02	0.177421E 02	0.190134E 02	0.193748E 02	-0.
154	306.0	0.422255E-01	0.256098E 01	0.461890E 01	0.140281E 02	0.180497E 02	0.192138E 02	0.194824E 02	-0.
155	308.0	0.790131E-01	0.257972E 01	0.469512E 01	0.140897E 02	0.183277E 02	0.194870E 02	0.197364E 02	-0.
156	310.0	0.111298E 00	0.259131E 01	0.478386E 01	0.141784E 02	0.185784E 02	0.198241E 02	0.201167E 02	-0.
157	312.0	0.136651E 00	0.260246E 01	0.488518E 01	0.143054E 02	0.188119E 02	0.202154E 02	0.205955E 02	-0.
158	314.0	0.152485E 00	0.262139E 01	0.499938E 01	0.144803E 02	0.190444E 02	0.206520E 02	0.211409E 02	-0.
159	316.0	0.156967E 00	0.265699E 01	0.512708E 01	0.147102E 02	0.192961E 02	0.211257E 02	0.217197E 02	0.
160	318.0	0.149271E 00	0.271788E 01	0.526922E 01	0.149990E 02	0.195880E 02	0.216290E 02	0.223014E 02	0.
161	320.0	0.129725E 00	0.281142E 01	0.542699E 01	0.153470E 02	0.199392E 02	0.221559E 02	0.228606E 02	0.
162	322.0	0.998531E-01	0.294279E 01	0.560171E 01	0.157510E 02	0.203643E 02	0.227006E 02	0.233794E 02	0.
163	324.0	0.622902E-01	0.311427E 01	0.579462E 01	0.162046E 02	0.208712E 02	0.232582E 02	0.238480E 02	0.
164	326.0	0.205789E-01	0.332478E 01	0.600666E 01	0.166984E 02	0.214594E 02	0.238234E 02	0.242653E 02	0.
165	328.0	-0.211328E-01	0.356971E 01	0.623823E 01	0.172215E 02	0.221201E 02	0.243904E 02	0.246373E 02	0.
166	330.0	-0.384624E-01	0.384112E 01	0.648900E 01	0.177617E 02	0.228365E 02	0.249533E 02	0.249754E 02	0.

Figure 56 c. Sample Output Sheet (Cont.)

167	332.0	-0.871984E-01	0.412832E 01	0.675774E 01	0.183065E 02	0.235849E 02	0.255040E 02	0.252941E 02	0.
168	334.0	-0.103696E 00	0.441864E 01	0.704221E 01	0.188441E 02	0.243372E 02	0.260339E 02	0.256075E 02	-0.
169	336.0	-0.169222E 00	0.469855E 01	0.733917E 01	0.193635E 02	0.250633E 02	0.265333E 02	0.259274E 02	-0.
170	338.0	-0.902144E-01	0.495479E 01	0.764446E 01	0.198555E 02	0.257335E 02	0.269919E 02	0.262605E 02	-0.
171	340.0	-0.584245E-01	0.517558E 01	0.795317E 01	0.203125E 02	0.263216E 02	0.273989E 02	0.266074E 02	-0.
172	342.0	-0.109311E-01	0.535167E 01	0.825993E 01	0.207286E 02	0.268067E 02	0.277442E 02	0.269614E 02	-0.
173	344.0	0.455824E-01	0.547721E 01	0.855914E 01	0.210998E 02	0.271746E 02	0.280187E 02	0.273094E 02	-0.
174	346.0	0.121070E 00	0.555025E 01	0.884537E 01	0.214231E 02	0.274190E 02	0.282150E 02	0.276329E 02	-0.
175	348.0	0.158466E 00	0.557298E 01	0.911364E 01	0.216967E 02	0.275414E 02	0.283280E 02	0.279104E 02	-0.
176	350.0	0.278082E 00	0.555151E 01	0.935976E 01	0.219198E 02	0.275496E 02	0.283554E 02	0.281197E 02	-0.
177	352.0	0.356039E 00	0.549531E 01	0.958053E 01	0.220919E 02	0.274573E 02	0.282975E 02	0.282409E 02	0.
178	354.0	0.429056E 00	0.541636E 01	0.977388E 01	0.222132E 02	0.272812E 02	0.281579E 02	0.282585E 02	0.
179	356.0	0.494793E 00	0.532806E 01	0.993900E 01	0.222842E 02	0.270396E 02	0.279423E 02	0.281639E 02	0.
180	358.0	0.552074E 00	0.524405E 01	0.100762E 02	0.223059E 02	0.267501E 02	0.276588E 02	0.279566E 02	0.
181	360.0	0.601000E 00	0.517700E 01	0.101870E 02	0.222800E 02	0.264280E 02	0.273170E 02	0.276440E 02	0.

Figure 56 d. Sample Output Sheet (Cont.)

80 KNOT CRUISE DATA S 58 NASA TM X 952 TABLE 13

FIELD POINT RADIUS 0.320000E 03 AZIMUTH 0.900000E 02 ELEVATION -0.370000E 02

HARMONIC	SOUND PRESSURE	SPL
1	0.83927852E-04	0.892301626E 02
2	0.347295541E-04	0.815660216E 02
3	0.767529942E-05	0.684539941E 02
4	0.288920146E-05	0.599675966E 02

Figure 56 e. Sample Output Sheet (Cont.)

APPENDIX VII

SAMPLE CALCULATION-ASSUMED RELATIONSHIP BETWEEN BLADE LOADING, THRUST AND TORQUE

Referring to Figure 7, which shows an end view of a rotor blade, and replacing $\vec{g}_m$ with the steady force $\vec{F}$, note that

$$L = \frac{\vec{F}}{\Delta r}$$

where Δr is a spanwise element of blade. The in-plane force is then

$$F_i = L \Delta r \sin\beta$$

and the out-of-plane force is

$$F_o = L \Delta r \cos\beta$$

Thrust and torque are defined by

$$T = F_o n = nL \Delta r \cos\beta$$

$$Q = F_i r n = rnL \Delta r \sin\beta$$

From the relationships we find

$$\beta = \tan^{-1} \frac{Q}{rT}$$

$$L = \frac{T}{n \Delta r \cos\beta}$$

The values selected for the example are

$Q = 7.79 \times 10^5$ pound-inches
T = 11,300 pounds
r = 269 inches
n = 4 blades
Δr = 7 inches

which give

β = 14.35 degrees
L = 417 pounds per inch

APPENDIX VIII

ROTATIONAL NOISE TEST INSTRUMENTATION

A block diagram of the instrumentation used in the Phase II test is presented in Figure 53. Measurements were made with a one-half-inch condenser microphone and the signal fed into the line input of a Nagra IIIB tape recorder. The 400-cps beeper signal used for a time reference was fed into the recorder through its microphone input and was generated by a General Radio transistorized oscillator. Overall levels were adjusted to avoid overloading the recorder. Data was recorded at hover, 40-knot, 80-knot, and 110-knot cruise, and 70-knot cyclic pullout. A recording was made with rotor system stopped and engine running to determine the extent of engine noise interference in the rotor noise frequency range of interest.

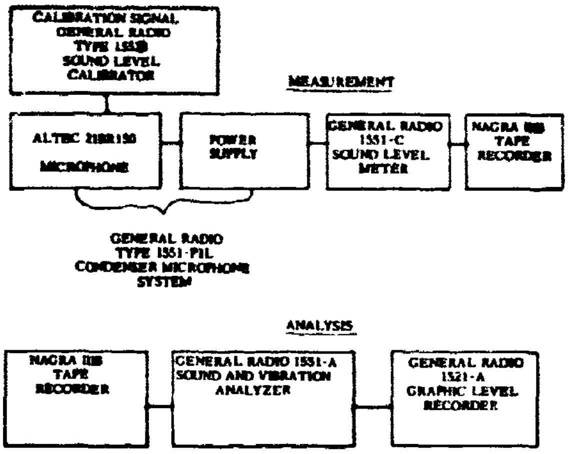

Figure 57. Rotational Noise Test Instrumentation

All noise records were analyzed twice. First, one-third-octave bandwidth plots of noise level versus frequency were made to determine the frequency of the main rotor blade passage and to evaluate masking noise. Second, plots were made of noise level versus time at the individual rotor harmonic frequencies as determined by the spectrum plots.

Frequency analysis of the records with the engine running and stopped rotor system showed that engine spikes appeared from 79 cps upward. The tail rotor fundamental blade passage frequency of the S-58 helicopter appears at 85 cps for the rotor speed used in the test. The fifth harmonic of the main rotor is at 75 cps and is masked by engine noise. For this reason, only the first four harmonics of the rotational noise were analyzed. This data is presented in the section entitled "Correlation of Measured and Calculated Rotational Noise".

APPENDIX IX

ROTOR SYSTEM PARAMETERS AND LOADS FOR PHASE III STUDY

The S-58 rotor system in the hover condition is used as the basis for the Phase III study of the effects of harmonic blade loading. The pertinent rotor system parameters are:

Number of blades	4
Blade radius, feet	28
Blade twist, degrees	-8
Blade chord, feet	1.367

Selected operating parameters are:

Rotor speed, rpm	210
Blade pitch angle at root, degrees	19.6
Thrust, pounds	11,300
Loaded radial increment, inches	7.0

Eight-tenths of the tip radius (r = 269 inches) is selected as the effective blade radius. The pitch angle β, corrected from the root angle for blade twist is 14.35 degrees.

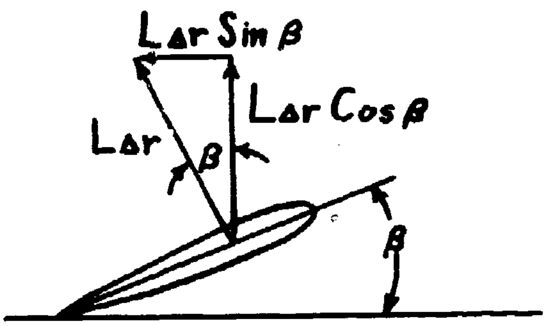

Figure 58. Blade Aerodynamic Loading

From Figure 58,

L = blade section loading, pounds per inch
r = loaded blade incremental radius, inches
β = blade pitch angle, degrees
n = number of blades

Total thrust $T = nL\,\Delta r\cos\beta$

or, solving for L,

$$L = \frac{T}{n\,\Delta r\cos\beta} = \frac{11{,}300}{4 \times 7 \times \cos 14.35°} = 417 \text{ pounds per in.}$$

This 417 pounds-per-inch blade loading is used as the steady component of all Phase III calculations. Harmonic loading levels are fractions of this figure.

Unclassified
Security Classification

DOCUMENT CONTROL DATA - R&D

(Security classification of title, body of abstract and indexing annotation must be entered when the overall report is classified)

1. ORIGINATING ACTIVITY (Corporate author) Sikorsky Aircraft Division of United Aircraft Corporation Stratford, Connecticut	2a. REPORT SECURITY CLASSIFICATION Unclassified 2b. GROUP

3. REPORT TITLE

Helicopter Rotor Noise Generation and Propagation

4. DESCRIPTIVE NOTES (Type of report and inclusive dates)

Final Report

5. AUTHOR(S) (Last name, first name, initial)

Schlegel, Ronald G., King, Robert J., Mull, Harold R.

6. REPORT DATE	7a. TOTAL NO. OF PAGES	7b. NO. OF REFS
October 1966	115	34

8a. CONTRACT OR GRANT NO. DA 44-177-AMC-141(T) b. PROJECT NO. Task 1P121401A14801 c. d.	9a. ORIGINATOR'S REPORT NUMBER(S) USAAVLABS Technical Report 66-4 9b. OTHER REPORT NO(S) (Any other numbers that may be assigned this report)

10. AVAILABILITY/LIMITATION NOTICES

Distribution of this document is unlimited.

11. SUPPLEMENTARY NOTES	12. SPONSORING MILITARY ACTIVITY
	US Army Aviation Materiel Laboratories Fort Eustis, Virginia

13. ABSTRACT

An improved method is presented for calculating rotor system overall vortex noise and frequency spectra for stalled and unstalled rotors. Correlation of measured and predicted vortex noise was evaluated using two rotor systems operating over a wide range of speeds and thrusts. Correlation was found to be excellent. Blade tip planform studies revealed significant vortex noise reductions with tapered tips.

A new procedure is also derived for calculating near and far field rotor rotational noise with nonuniform inflow. The method extends the standard steady load method by including the effects of harmonic airloads. Correlation studies were conducted using an H-34 helicopter. Agreement between low frequency measured and predicted noise was good. However, correlation with high harmonic rotational noise was poor. This is probably due to inadequate definition of high harmonic airloads.

Presented results establish the importance of high harmonic rotational noise for detectability and loudness, and further work is recommended to more accurately define high harmonic blade loading. Since an airload measurement program is being conducted on the NH-3A, it is recommended that a correlation program be conducted to more fully evaluate the accuracy of the presented noise analysis program using the NH-3A airload results.

This study was performed for single rotor systems only, and in its present form is not directly applicable to systems with multiple rotors in juxtaposition.

DD FORM 1 JAN 64 1473

Unclassified
Security Classification

Unclassified

Security Classification

14. KEY WORDS	LINK A		LINK B		LINK C	
	ROLE	WT	ROLE	WT	ROLE	WT
Noise Helicopter Rotor Noise						

INSTRUCTIONS

1. ORIGINATING ACTIVITY: Enter the name and address of the contractor, subcontractor, grantee, Department of Defense activity or other organization *(corporate author)* issuing the report.

2*a*. REPORT SECURITY CLASSIFICATION: Enter the overall security classification of the report. Indicate whether "Restricted Data" is included. Marking is to be in accordance with appropriate security regulations.

2*b*. GROUP: Automatic downgrading is specified in DoD Directive 5200.10 and Armed Forces Industrial Manual. Enter the group number. Also, when applicable, show that optional markings have been used for Group 3 and Group 4 as authorized.

3. REPORT TITLE: Enter the complete report title in all capital letters. Titles in all cases should be unclassified. If a meaningful title cannot be selected without classification, show title classification in all capitals in parenthesis immediately following the title.

4. DESCRIPTIVE NOTES: If appropriate, enter the type of report, e.g., interim, progress, summary, annual, or final. Give the inclusive dates when a specific reporting period is covered.

5. AUTHOR(S): Enter the name(s) of author(s) as shown on or in the report. Enter last name, first name, middle initial. If military, show rank and branch of service. The name of the principal author is an absolute minimum requirement.

6. REPORT DATE: Enter the date of the report as day, month, year; or month, year. If more than one date appears on the report, use date of publication.

7*a*. TOTAL NUMBER OF PAGES: The total page count should follow normal pagination procedures, i.e., enter the number of pages containing information.

7*b*. NUMBER OF REFERENCES: Enter the total number of references cited in the report.

8*a*. CONTRACT OR GRANT NUMBER: If appropriate, enter the applicable number of the contract or grant under which the report was written.

8*b*, 8*c*, & 8*d*. PROJECT NUMBER: Enter the appropriate military department identification, such as project number, subproject number, system numbers, task number, etc.

9*a*. ORIGINATOR'S REPORT NUMBER(S): Enter the official report number by which the document will be identified and controlled by the originating activity. This number must be unique to this report.

9*b*. OTHER REPORT NUMBER(S): If the report has been assigned any other report numbers *(either by the originator or by the sponsor)*, also enter this number(s).

10. AVAILABILITY/LIMITATION-NOTICES: Enter any limitations on further dissemination of the report, other than those imposed by security classification, using standard statements such as:

(1) "Qualified requesters may obtain copies of this report from DDC."

(2) "Foreign announcement and dissemination of this report by DDC is not authorized."

(3) "U. S. Government agencies may obtain copies of this report directly from DDC. Other qualified DDC users shall request through
_______________________________."

(4) "U. S. military agencies may obtain copies of this report directly from DDC. Other qualified users shall request through
_______________________________."

(5) "All distribution of this report is controlled. Qualified DDC users shall request through
_______________________________."

If the report has been furnished to the Office of Technical Services, Department of Commerce, for sale to the public, indicate this fact and enter the price, if known.

11. SUPPLEMENTARY NOTES: Use for additional explanatory notes.

12. SPONSORING MILITARY ACTIVITY: Enter the name of the departmental project office or laboratory sponsoring *(paying for)* the research and development. Include address.

13. ABSTRACT: Enter an abstract giving a brief and factual summary of the document indicative of the report, even though it may also appear elsewhere in the body of the technical report. If additional space is required, a continuation sheet shall be attached.

It is highly desirable that the abstract of classified reports be unclassified. Each paragraph of the abstract shall end with an indication of the military security classification of the information in the paragraph, represented as *(TS), (S), (C), or (U)*.

There is no limitation on the length of the abstract. However, the suggested length is from 150 to 225 words.

14. KEY WORDS: Key words are technically meaningful terms or short phrases that characterize a report and may be used as index entries for cataloging the report. Key words must be selected so that no security classification is required. Identifiers, such as equipment model designation, trade name, military project code name, geographic location, may be used as key words but will be followed by an indication of technical context. The assignment of links, rules, and weights is optional.

Unclassified

Security Classification